Pontifícia Universidade Católica
do Rio de Janeiro

Eliana Paola Marín Castaño

Linking the rheology of W/O crude emulsions with the droplet agreggation process

Tese de Doutorado

Thesis presented to the Programa de Pós-graduação em Engenharia Mecânica of PUC-Rio in partial fulfillment of the requirements for the degree of Doutor em Engenharia Mecânica.

Advisor: Prof. Paulo R. de Souza Mendes
Departamento de Engenharia Mecânica da PUC-Rio

Rio de Janeiro
March 2020

Pontifícia Universidade Católica
do Rio de Janeiro

Eliana Paola Marín Castaño

Linking the rheology of W/O crude emulsions with the droplet agreggation process

Thesis presented to the Programa de Pós-graduação em Engenharia Mecânica of PUC-Rio in partial fulfillment of the requirements for the degree of Doutor em Engenharia Mecânica. Approved by the Examination Committee.

Prof. Paulo R. de Souza Mendes
Advisor
Departamento de Engenharia Mecânica da PUC-Rio

Marcia Cristina Khalil De Oliveira
Centro de pesquisa e desenvolvimento - CENPES (RJ)

Prof. Frederico Wanderley Tavares
Programa de Engenharia Química (PEQ) - COPPE/UFRJ (RJ)

Profa. Aurora Pérez Gramatges
Departamento de Química da PUC-Rio

Prof. Marcio da Silveira Carvalho
Departamento de Engenharia Mecânica da PUC-Rio

Rio de Janeiro, March 31st, 2020

Eliana Paola Marín Castaño

Graduated in Chemical Engineering at National University of Colombia (Manizales) in 2011 and obtained her M.Sc. Degree in Material, Chemical Process and Metallurgy Engineering from Pontifical Catholic University of Rio de Janeiro (PUC - Rio) in 2015

Bibliographic data

Marín Castaño, Eliana Paola

Linking the rheology of W/O crude emulsions with the droplet agreggation process/ Eliana Paola Marín Castaño; Advisor: Prof. Paulo R. de Souza Mendes. - Rio de Janiero: PUC-Rio, Departamento de Engenharia Mecânica, 2020.

v., 108 f.: il.; 30 cm

1. Tese (doutorado) – Pontifícia Universidade Católica do Rio de Janeiro, Departamento de Engenharia Mecânica.

Inclui referências bibliográficas.

1. Engenharia Mecânica - Teses. 2. Reologia de emulsões. 3. Emulsões A/O a partir de óleo cru. 3. Transição de Fases. 4. Agregação de clusters. I. Mendes, Paulo Roberto de Souza. II. Pontifícia Universidade Católica do Rio de Janeiro. Departamento de Engenharia Mecânica. III. Título.

CDD:621

Acknowledgements

Firstly, I would like to thank my advisor, Professor Paulo Roberto de Souza Mendes, for his support and trust during all these past four years. I feel huge respect and admiration for his academic life.

Thanks to CNPq and PETROBRAS for having granted me a scholarship and the financial support that made it possible to conduct this research.

Secondly, I would like to express my special gratitude to the GReo group, which I am so happy to be a part of. To Professor Monica for maintaining the unit in the group and for her rheology knowledge. In particular, I would like to thank the "Emulsified Group" (Daniel, João, Tati, Patricia and Ricardo) for all the academic discussion and mostly for helping me understand better the emulsion world. A special gratitude to my "boss" and friend Ricardo for his support during these last years, trying to clear my thoughts and to be present in this academic path always by my side. Thanks, Alexandre, for your technical support, always working on improving our ideas in the best possible way. I would like to thank Elias, Behbood and Roberta for your knowledge that many times I explored. Finally, but not less important, I would like to show my gratitude for all the beer time of the group, for the so talkative nights full of fun.

Thirdly, to Erika and Daniel, thanks for helping me with the English. Also, thanks to Ricardo, Daniel and Julian for the discussion of results and suggestions, which helped me build up this document.

Fourthly, I would like to thank my parents, you are my motivation and my happiness. Thanks also to my sister (Dudu) and brother (Tetor) for your emotional and financial support. I love you so much. I am blessed to have you as my family. Special gratitude to Julian, for being my partner in both life and academic related subjects, always challenging me and transmitting his love for science. To my friends, Isabel and Tiphane, thanks for always being there for me when I needed you.

Abstract

Marín Castaño, Eliana Paola; de Souza Mendes, Paulo R (Advisor). **Linking the rheology of W/O crude emulsions with the droplet agreggation process**. Rio de Janeiro, 2020. 108p. Tese de Doutorado - Departamento de Engenharia Mecânica, Pontifícia Universidade Católica do Rio de Janeiro.

This research focused on studying the rheology of W/O emulsions formed by different crude oils, with special attention to their behavior when subjected to Brownian and hydrodynamic forces. At a microscale level, particle-particle and particle-medium interactions, both of which are involved in the phenomenon of aggregation, define the emulsion's rheological behavior due to the complex structures created by the droplets as their concentration rises. An experimental study was performed in order to visualize the emulsions characteristics according to its disperse phase concentration and the shear rate applied, verifying the existence of both coalescence and flocculation phenomena during shearing. The modeling of interactions between droplets allowed the prediction of the emulsion's behavior by colloidal thermodynamics. With it, a methodology to fit the experimental data that included both the shear rate and disperse phase concentration parameters was proposed. This work emphasizes the importance of studying emulsion systems at a micro-scale level in order to obtain a better comprehension of the formation and breakage processes of complex and random aggregate structures. This allows the prediction of the emulsion's rheological behavior, and the proposition of a phenomenological model to best describe it.

Keywords

Emulsion rheology; W/O Crude emulsion; Phase transition; Clustering aggregation.

Resumo

Marín Castaño, Eliana Paola; de Souza Mendes, Paulo R. **Ligando a reologia de emulsões A/O a partir de óleo cru com o processo de agregação de gotas.**. Rio de Janeiro, 2020. 108p. Tese de Doutorado - Departamento de Engenharia Mecânica, Pontifícia Universidade Católica do Rio de Janeiro.

Esta pesquisa focou-se no estudo da reologia de emulsões A/O preparadas com diferentes óleos crus, dando atenção especial ao seu comportamento quando sujeitas a forças brownianas e hidrodinâmicas. Em uma microescala, as interações partícula-partícula e partícula-meio, ambas envolvidas no fenômeno de agregação, definem o comportamento reológico da emulsão devido às complexas estruturas criadas pelas gotículas quando sua concentração aumenta. Um estudo experimental foi realizado para visualizar as características da emulsão de acordo com sua concentração de fase dispersa e a taxa de cisalhamento aplicada, verificando-se a existência de tanto o fenômeno de coalescência quanto o de floculação durante o cisalhamento. A modelagem das interações entre as gotículas permitiu a previsão do comportamento da emulsão a partir da termodinâmica de coloides. Com isso, uma metodologia que ajustasse os dados experimentais incluindo parâmetros da taxa de cisalhamento e da concentração da fase dispersa foi proposto. Essa metodologia foi então aplicada a algumas equações reológicas comuns, encontradas na literatura. Este trabalho enfatiza a importância do estudo de emulsões em escala micro a fim de obter uma melhor compreensão dos processos de formação e quebra das complexas estruturas randômicas de agregados. Isso permite prever seu comportamento reológico e propor um modelo fenomenológico que o descreva.

Palavras-Chave

Reologia de emulsões; Emulsão A/O a partir de óleo cru; Transição de Fases; Agregação de clusters.

Contents

List of Figures

List of Table

1
Introduction

Emulsions have long been of great interest to scientific community because of their huge applicability in many industries [94]. In the petroleum industry, for example, emulsions are recurrently encountered throughout the production time of crude oil [27, 29, 101, 119]. Crude oil is found in reservoirs along with water or brine and in the process of oil removal, water is often coproduced [101]. However, additional water also has been introduced into the reservoir to help the process of extraction into crude salts remotion or as steam to improve the fractionation [101]. W/O emulsions are formed readily when water and oil flow with high turbulence through nozzles and piping used during the oil production. A problem caused by the formation of water-in-crude oil emulsions is the increment of the crude oil apparent viscosity, impacting, consequently, the oil production [29]. These emulsions increase pumping and transportation expenses, they might damage pipes, pumps, production equipment, and distillation columns, and they can poison downstream refinery catalysts [5, 108]. The flow assurance field includes the understanding of the emulsion behavior to develop models and theories from different fields of science as, for instance, thermodynamics, rheology, math and statistics.

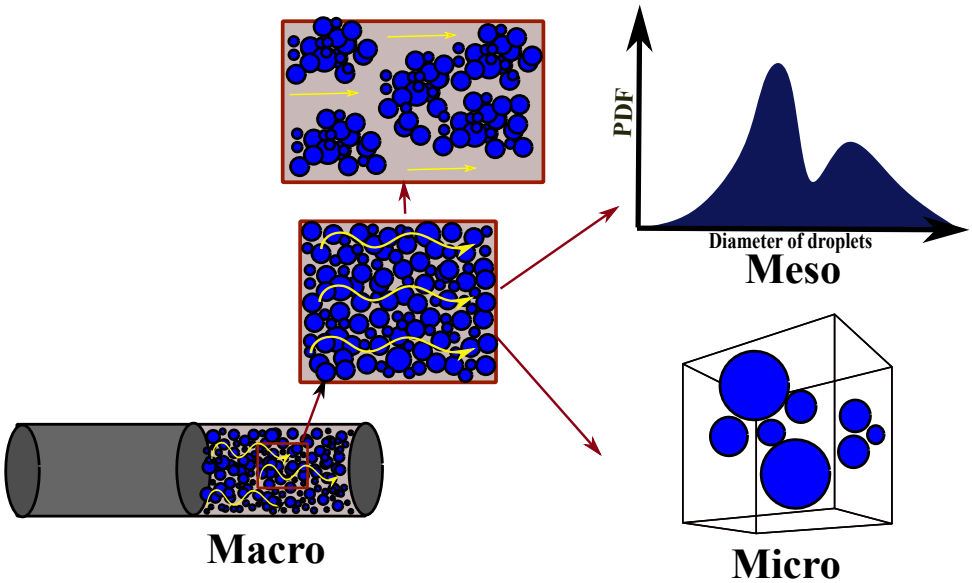

Figure 1.1: Schematic multiscale description of colloid system: Macroscale, Mesoscale and Microscale

There is a wide range of models and theories that have been proposed to understand the behavior of colloids from the macroscale to the microscale. The schematic description of model-scales is shown in Figure **1.1**. The research of colloids starts from the macroscale view. Mainly, macroscale studies are made by empirical developments models or by hybrids between empirical and theoretical approaches. These approaches have several limits to applications. For the mesoscale models, some statistic approaches have been used to try to predict the behavior of structures of colloid systems. Some models that can be found in the literature are percolation, moment method, fractal model and Ree-Eyring theory [20, 32, 37, 88]. Recently, micro-scale models have appeared. They try to describe the phenomena of flocculation and aggregation due to the interactions between the particles with huge detail. However, due to the difficulty in their modeling and computational cost associated, the microscale is not usually used.

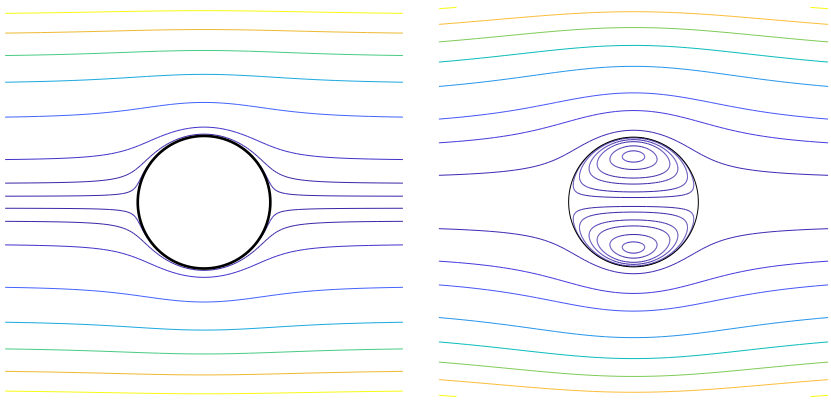

(a) Around to a hard-sphere (b) Around to a droplet

Figure 1.2: Streamline around suspended particles and emulsion droplet based by model proposed by [31]

As an idea of this model's computational cost, one can imagine the theory developed for the flow around a hard-sphere applied to model the flow around a simple drop of an emulsion. Two models are already widely studied [31]. In the Figures **1.2**a and **1.2**b, the streamlines around the hard-sphere and a droplet can be seen, respectively. It is observed that inside the droplet there are also a streamline due to the movement of fluid inside the droplet. The equation for this flow around the droplet implicates the solution of twice the number of equations than the flow around hard-sphere. Now, if we want to describe this flow when the concentration of the dispersed phase increases, it is imperative to include the particle-particle interaction to predict their rheological behavior. Then, this theory initially applied to one droplet is not longer valid because it violates the main

supposition that one particle does not interact to another. Therefore, the need for a complex mathematical model and efficient calculation arises, which is impossible to do presently due to computational limitations.

All in all, the principal goal of this work is the study of W/O emulsions from a microscale point of view searching to understand the phenomena involved in this process. For that, models in macro were improved and a mesoscale model based on a statistic approach was proposed. The document was divided into four chapters: Chapter 2 introduces a background about the leading concepts of emulsions and a literature review is also presented. Later, in Chapter 3, the experimental methodology is described and the rheological experimental results for W/O emulsions for two different crude oils is shown. Flocculation and coalescence phenomena are also analyzed. In Chapter 4, the thermodynamic approach is related to the rheology by state-behavior theory applied to colloidal systems. Chapter 5 presents the algorithm proposed to predict the viscosity behavior at a concentration and shear rate. The results of the experimental data fitting with three different equations were analyzed by comparing their residual errors. The statistical model proposed to describe the emulsion behavior due to the interactions and formation of the structure of aggregate is subsequently introduced. A brief introduction is presented at the beginning of each chapter, along with a brief conclusion at the end.

2
Background and Literature review

In this chapter, initially, some general concepts related to the W/O emulsion and its stability are presented. Concepts associated with particle-particle and particle-medium interactions due to their importance in the discussion of the results in the next chapters are detailed. The most influential factors that affect emulsion rheology were described. Besides, a complete background review of the main equation and principles concerning emulsion rheology was done. A table with the equations in chronological order was elaborated. Also, depending on their formulation, the applicability range of concentration and shear rate, polydispersity, whether the shear rate effect and interface deformability were or not included, the rheology equations were classified.

2.1
Emulsion

A suspension is a mixture formed by two-phases that are insoluble or immiscible. One of these phases is dispersed within the other in small particles. If the particles are in a size range between 1 nm and 1 μm, the system is called a colloidal system. An emulsion is a suspension between two liquids, one dispersed (drops) in another [76]. Emulsions are classified as a colloidal system. Specifically, an emulsion needs a third component to maintain these immiscible liquids suspended. This third component is called an emulsifier or surfactant. The surfactant is the main responsible for the emulsion formation and its stability [107]. The emulsification process requires external mechanical energy to break up the bulk liquid into smaller droplets increasing the interfacial contact area. This process is not thermodynamically spontaneous [107]. The droplet size is proportional to the stirring energy, so to achieve smaller size droplets (the biggest area), larger stirring energy is required [39]. As a result of the mixing, oil droplets in water (oil-in-water - O/W) or water droplets in oil (water-in-oil - W/O) can be obtained [52, 76, 98].

The emulsion properties and stability are essentially governed by the same basic suspension principles [108]. Adding one liquid to another modifies the physical properties of the continuous phase, e.g., its appearance, texture, density, and viscosity [76]. These properties are determined by the system's

chemical nature, such as the oil chemical composition, phase solubility and water ionic composition. Some important emulsion properties are: dispersed phase concentration (φ), droplets size (d_p), density relation between the phases (σ_r), viscosity of continuous phase (μ_o) and interfacial tension (γ). Using conventional analytical instruments and standardized methodologies, these properties can be determined and evaluated [122].

Emulsion stability refers to the emulsion's ability to resist changes in its physicochemical properties over time [108]. The emulsion stability is influenced by its chemical composition as well as by the processing conditions. Some emulsion properties that allow measuring its stability are: dispersed concentration, droplets size, physicochemical interactions, and rheological behavior [39, 105]. Emulsion stability can be defined in term of thermodynamic or kinetic fields. Thermodynamics defines if the system is in equilibrium or not, and kinetic, the time that the system requires to return to a stable equilibrium state of minimum free energy. The interfacial free energy is proportional to the total area of contact between two phases when this energy is minimum, and the system is considered thermodynamically stable. Emulsions are considered metastable systems (or unstable) because the separate oil and water phases have lower free energy than the phases mixed as an emulsion.

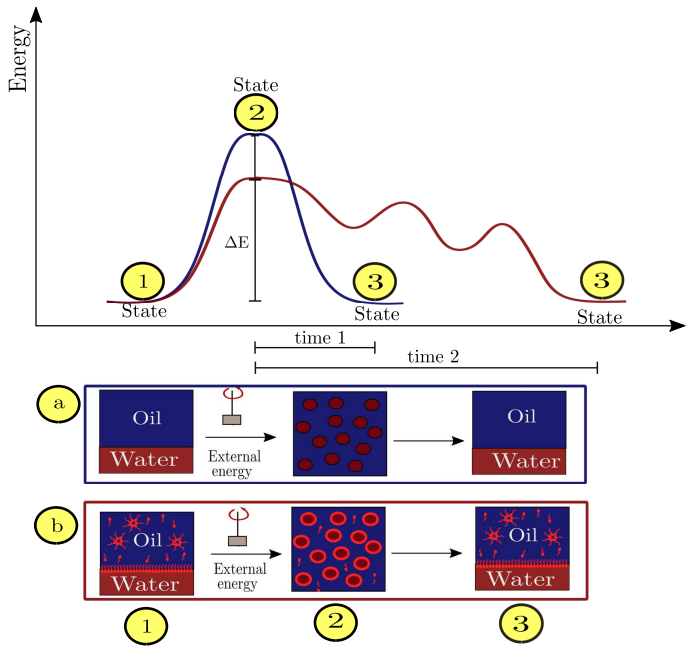

Figure 2.1: Schematic representation of the free energy path for the breakdown process for systems a) without surfactan (blue line) and b) with surfactant (red line). Adapted from [107]

Figure **2.1** represents schematically the emulsification process with (a) and without (b) surfactant. For both systems, the first point (1) starts in the

minimum free energy where the phases are separated and the the system is at its most stable configuration. To achieve the second state of maximum free energy (2), where the emulsion is produced, necessary external shear energy must be applied in order to rupture the dispersed phase into small droplets. This point is considered as a metastable state due to the system will always try to return to the state of minimum free energy, in this case, being the third point (3). The time that this process demand will be defined by the path that it uses to arrive at this third point [76, 122]. Surfactants are active agents that provide certain stability to the emulsion, creating repulsion between the droplets inhibiting their coalescence [11,52]. The surfactants help to generate energy barriers, becoming a noncontinuous process. As a result, the time to achieve the third point is increased even though the emulsion is still considered thermodynamically unstable [107]. However, the system becomes kinetically stable because the demulsification time is so long than it can be considered almost infinite.

Water-in-crude Oil emulsion

Water-in-crude oil emulsions are formed during crude oil production, transportation, and processing and they are stabilized by the presence of natural surfactants [119]. Some of these indigenous components of crude oils are: resins, asphaltenes, waxes, and inorganic particles [22,75,85,119]. Resins and asphaltenes are a major emulsion stabilizer [27, 85, 92]. These substances act as active agents adsorbing and accumulating onto the W/O interfaces, forming strong and elastic films surrounding water droplets, acting as a rigid skin on the surface of the droplets [22,75]. This formed film gives certain rheology properties to the interface, very important in the stability of crude oil emulsions [22,85]. Asphaltenes films are elastic solids, with relative immobility and an irreversible absorbency, while resin films are less dense and easily disrupted [121]. Resins are known for adsorbing more strongly than asphaltenes, due to their lower interfacial tension. Asphaltenic film properties are significantly influenced by the oil phase aromaticity, the asphaltene concentration, and its aging time, whereas resin film properties are much less influenced by those factors [27].

The molecular structure of asphaltenes varies depending on the crude oil source. They are composed of diverse macromolecules formed of monomers, nanoaggregates, and clusters [121]. Therefore, asphaltenes do not have a defined molecular structure [27, 92]. Asphaltenes are characterized by fused ring small aliphatic side chains, and polar heteroatom-containing functional groups [27,101]. The average molecular weight is roughly 750 g mol $^{-1}$ and the molecule diameter

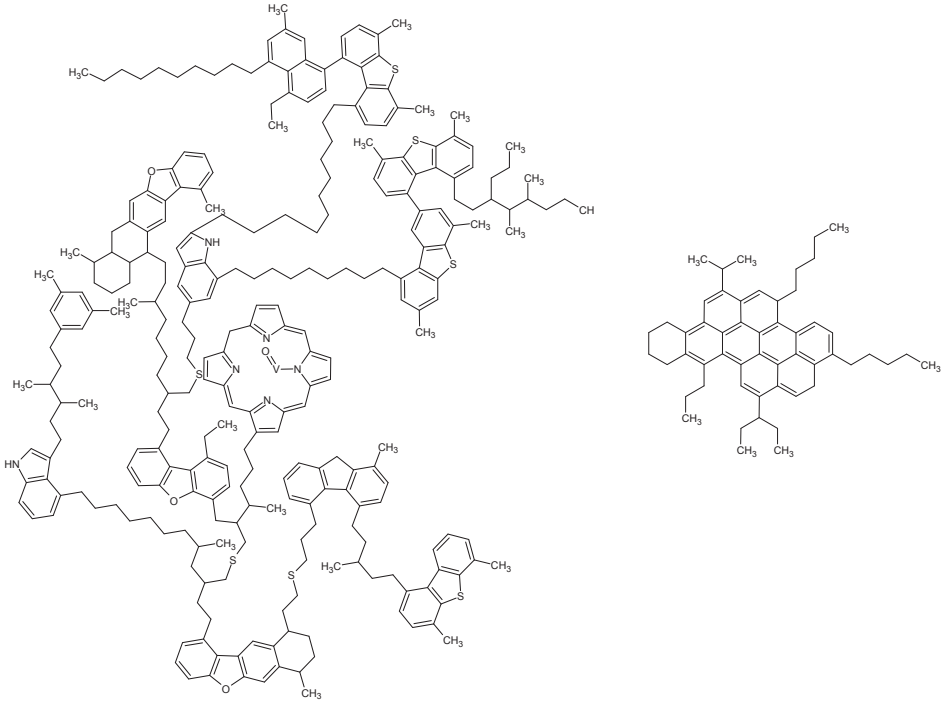

(a) Asphaltene molecule (b) Resin molecule

Figure 2.2: Schematic surfactant molecules present into water-in-crude oil emulsions interfaces. Adapted from [2]

is in a range of 10-20 A° [27]. The presence of carboxylic acid, carbonyl, phenol, pyrrole,and pyridine functional groups in asphaltenes has been observed [101]. A schematic example of asphaltenes and resin molecules is shown in Figures **2.2**a and **2.2**b, respectively.

Crude oils contain not only asphaltenes and resins but also organic acids called naphthenic acids [26]. Crude oil naphthenic acids are a mixture of primary, secondary, and tertiary, largely cycloparrafinic, organic acids in the molecular weight range of 250-750 amu [112]. Several works at naphthenic acid studying its interfacial activity have been reported [26, 95, 112]. Naphthenic acid composition and chemical structure determine its interfacial's nature, properties, and characteristics [112].

2.2 Colloidal interactions

2.2.1 Particle-Particle

Particles suspended are constantly interacting among themselves. The interaction depends on its source, which can be via dispersion, surface, depletion, and hydrodynamic forces [41]. The dispersion (or Brownian) interactions arise

from the ubiquitous quantum mechanical effects, surface forces arise from interactions of colloidal surfaces, depletion forces arise to attractive interaction when soluble polymers are unable to entrance the space between particles, and finally, hydrodynamics interactions arise from a disturbance induced by the application of an external force to the fluid. In this section, only forces belonging to dispersion, surface and depletion interactions will be mentioned.

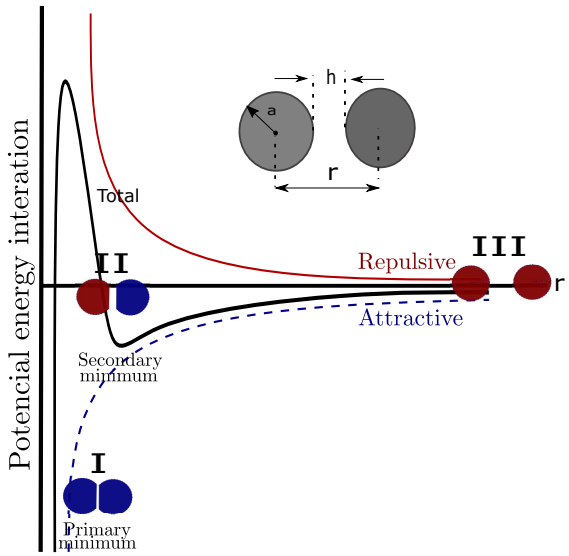

Figure 2.3: Shemetic diagram of droplet interaction Energy (DLVO Theory). Adapted from [122].

DLVO (Derjaguin-Landau-Verwey-Overbeek) theory describes quantitatively the flocculation/aggregation process of dispersed systems as a balance of forces between particles interacting through a liquid medium [122]. It estimates the total potential energies combining the attraction (Van der Waals) and repulsion (electrostatic-double layer) effects versus inter-particle distance (see Figure **2.3**) [76, 94]. The distance between the center-to-center droplet is r and the distance between droplets is h. At the first minimum (I), intense flocculation can be observed, the attraction is very strong and the repulsive energy barrier is small, and there isn't short-range repulsion. At this point, droplet coalescence can appear. In the second minimum (II), the attraction is moderately strong but there is a larger repulsive energy barrier, consequently weak flocculation may take place. The flocculated emulsion in the secondary minimum will separate more easily than those in the first minimum (I) [76, 122].

Van der Waals interactions

The electron cloud fluctuation of one atom leads to the electron cloud polarization of another [107]. As a consequence, instantaneous dipole-induced

forces are generated. These forces have an attractive character and are called London-van der Waals or dispersion forces. Colloidal particles have similar polarization effects as the atomic case. These interactions are additive, and as an approximation, a sum (or integration) of interaction energies for all molecules pairs belonging to different particles [56, 76]. Hamaker [36] developed a theory to determine these forces as an estimate equation that depends on the chemical characteristics of particles and suspending medium [41].

Depletion interactions

Interactions and stability of an emulsion can be affected by some species not adsorbed at the droplet interface [56, 76]. The species that are are unable to adsorb on the interface lead to a rise of the attractive forces between particles. Some of these species are soluble polymers, surfactants or nanoparticles [107].

Steric interactions

Steric interactions are repulsive forces that prevent particles from aggregating [107]. Nonionic surfactant absorbed on the surface give stability due to the steric repulsion generated between the hydrophilic headgroups of the amphiphile surfactant [76]. Another important steric interaction is one between the surfactant absorbed in the solvent used [56, 107]. Steric stabilization consists of covering the particles with polymers which prevents them from getting in the range of attractive forces.

2.2.2 Particle-Medium

The particle-medium interaction can be described depending on the kind motion that controls the system: Brownian or hydrodynamic. Brownian motion is defined as the random motion of suspended particles owing to the collisions between molecules belonging to the continuous phase. This phenomenon controls the motion when the system does not suffer any other external forces (shear, electric, magnetic forces, etc.) or the forces can be weak enough to affect directly its motion. In contrast, the hydrodynamic motion refers to the case when the flow is influenced by applied external forces, acting directly on its interactions and structure [41]. When a suspension is subjected to shearing, particles align with streamlines of the continuous medium. At the same time, they suffer a rotating around its mass center, dissipating more energy [45, 60].

On the other hand, particles act as hurdles that prevent the normal motion of the continuous medium. As a result, the flow's resistance is increased, consequently, its viscosity is increased too. Different mathematical formulations to describe the viscosity-increasing with the dispersed phase concentration have been reported. Some of these equations will be shown in section 2.5.

In summary, colloidal system behavior depends on the interaction nature, kind of motion and dispersed phase concentration.

Depending on how concentrated the system is, the suspension can be considered as a diluted, semidiluted or concentrated system [52]. The transition limit between each one of these regions or "matter states" will be defined by the chemical nature of the involved substances and intensity of particle-particle interactions [3, 96]. Besides, the concentration is one of the most important variables which defines the phase transition of a suspension system. Therefore, the transition between each state will be conditioned by the dispersed phase concentration. This conserves similarities with the phase transition of a pure substance [3]. From rheology and thermodynamic science, some studies analyzing the phase transition of this specific case have been developed [3, 41]. In Chapter 4, a more detailed study about this subject will be presented.

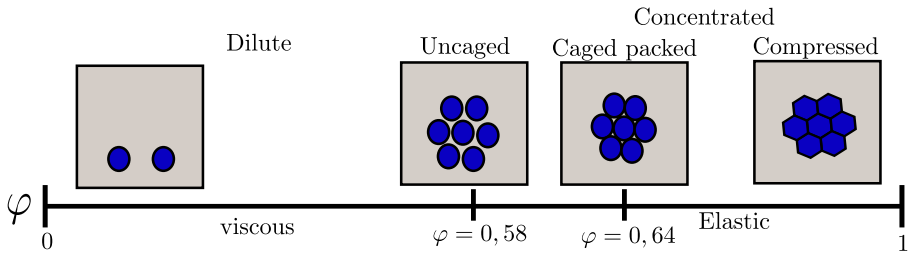

Figure 2.4: Schematic diagram of change of network structure with the volume fraction of the dispersed phase for a monodisperse emulsion. Adapted from [52].

The scheme of this phase transition is presented in Figure **2.4**. As mentioned before, the motion of the continuous phase is reduced and the interaction between the particles is boosted when the concentration of the dispersed phase (φ) increases, consequently, its viscosity will be changed too. When it is above 58% the colloid is considered as a concentrated colloid suspension. This point is called glass transition volume fraction (φ_g) [72]. Each particle becomes caught in a permanent enclosure formed by its neighbor particles. However, the particles have limited free space for motion given by the enclosure. Another important point is when the concentration achieves the maximum geometric packing fraction φ_m. Random fluid-crystal state transition can be observed [41]. In the case of hard-spheres, this value can be equal to 64% to a random close packing structure or 74% to

a face-centered crystal structure. Nevertheless, due to the deformability of the interface of the emulsion droplets, a higher maximum volume fraction than 74% is possible to achieve. As a result, systems with compressed structures and elastic rheological behavior can be seen [15, 52, 64].

2.3 Stability of emulsion

The colloidal system stability refers to the ability of the particles to remain suspended in a solution at equilibrium over time [39, 105]. The aggregation process of stored emulsions may be influenced by its characteristics and processing conditions, like concentration, size, charge, interactions, and rheology behavior [39, 42]. The mechanisms that lead to instability are schematized in Figure **2.5**.

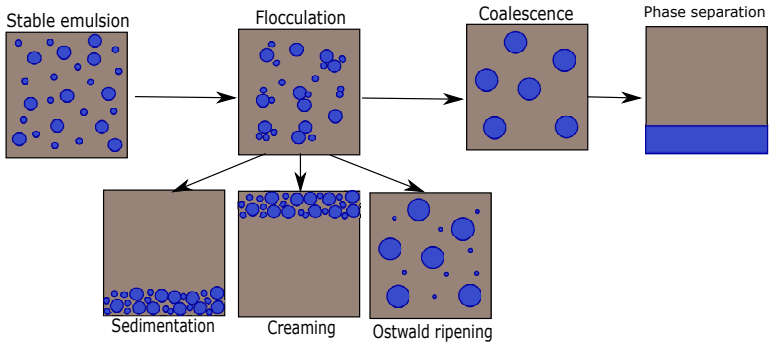

Figure 2.5: Instability mechanisms in the emulsion system. Adapted from [39].

Flocculation is the start of the emulsion instability process. Flocculation kinetics can be analyzed by the DLVO theory. When the repulsion forces are not sufficiently high to maintain the emulsion stable, van der Waals forces start to have a bigger effect on interactions between droplets. The transition between secondary to a primary minimum will depend on both Brownian and hydrodynamic interactions [76, 122]. The flocculation is considered as a weak and reversible process when the total potential energy between droplets is equal to the second minimum energy of the DLVO curve. And it is strong and irreversible when the total potential energy is equal to the first minimum. In flocculation, droplets remain separated by a layer on the surface without breaking the film [76]. The flocculation process foments the formation of aggregates, which can be structured into any kind of network depending on the characteristics of the system [3, 96].

Creaming or sedimentation are a consequence of flocculation. These processes depend on gravity forces and the difference between the dispersed and medium density. Moreover, Ostwald ripening is caused by the difference between

the small and large droplets solubility. Bigger droplets absorb smaller droplets by diffusion. Finally, coalescence is induced by thinning and disruption of the liquid film between the droplets [105]. Emulsions with a stronger energy barrier to coalescence are still amenable to flocculation.

2.4 Emulsion rheology

The rheology of emulsions maintains a close analogy with the theories applied for suspensions. The suspension rheology has been hugely studied, however, a complete understanding continues to be a challenge [6, 21, 48]. The factors that affect its rheology are amply reported in literature [6, 46, 47, 58, 64, 73]. The most important factors are volume fraction of dispersed phase, the ratio of dispersed phase viscosity to continuous phase viscosity, interfacial tension, particle-particle interaction, particle deformability, particle-size distribution function, particle shape, continuous phase rheology. Some of these factors will be detailed as following.

Concentration dependence

The concentration of the dispersed phase (φ) is the factor that has the most impact on the rheology of emulsions [105]. As previously seen, the rheology behavior of an emulsion can be changed from a simple viscous liquid to an elastic solid only by increasing its dispersed phase concentration.

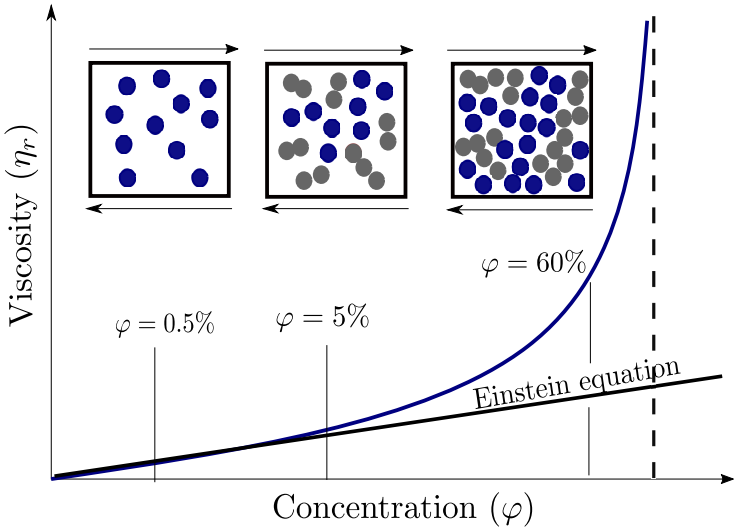

Figure 2.6: Schematic relation between the relative viscosity and the concentration of uniform hard-spheres at a constant shear rate. Blue color represents the individual spheres and the gray color represents the aggregates of spheres (flocs) that start to appear with the increase of the concentration. Adapted from [15].

The relation between the emulsion viscosity and its continuous phase is amply used as a parameter to characterize the emulsion. This viscosity is called relative viscosity (η_r). The variation of viscosity-concentration with φ has been schematized in Figure **2.6**. The curve has an exponential increase of viscosity with increasing concentration. The interactions are minimum at low concentrations. As a consequence, the viscosity is low, with values near to the viscosity of the continuous phase. With the increase in concentration, networks due to the formation of the clusters of particles are formed. At high concentrations, random complex structures can be seen. The black line is a projection of the linear equation for dilute systems. Above a certain point of concentration, the suppositions applied to diluted emulsion are no longer valid due to the increase of interactions. The viscosity tends to infinity when the concentration approaches the φ_m [15]. Above φ_g, the dispersion can be in an arrested (jammed) state and a yield-stress answer can be expected [15, 72].

Maximum packing and polydispersity

For almost all the suspensions, particle size is not uniform and the best way to describe it is with a particle size distribution. In Figure **2.7** three different viscosity values for three different size distribution functions were schematized, all of them having the same volume fraction (64%). Two of these distribution functions are monodisperse systems with two different particle sizes. One is constituted by smaller particles, and the other, by larger particle sizes. The third case is a system with a polydisperse distribution function constituted by the mix between these particle sizes. The distribution function is a result of the combination of the previous monodisperse distribution functions [66, 67] , which can be observed in Figure **2.7**. The maximum packing fraction for the monodisperse system is lower than polydisperse one owing to the better stacking scheme of the particles when there are different sizes [15]. The fine particles can occupy spaces between the coarse particles. For the hard-sphere particles case, the maximum packing of two monodisperse systems is the same, because it is an arranged geometry, and it is independent of size. However, when the system is an emulsion, the maximum packing value can differ depending on the size due to the deformation of the droplets. The deformation for the coarse emulsions is expected to be higher than those of the corresponding fine emulsions [67]. Therefore, it is expected that the fine emulsion exhibit a much higher viscosity as compared to the coarser one.

When an emulsion is composed of a mix between fine and coarse droplets, the resulting mixed emulsion exhibits viscosities even lower than the one for the coarse

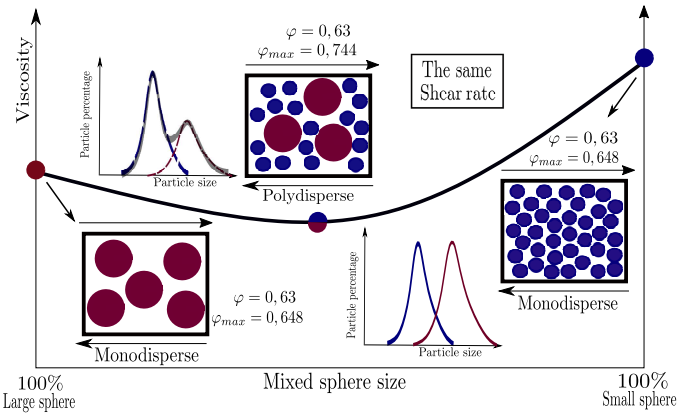

Figure 2.7: Schematic representation of the effect of polydisperse and φ_{max} in the viscosity of the suspensions with the same concentration of dispersed phase. The fine spheres and coarse spheres are represented by red and blue color, respectively. Adapted from [62, 73]).

emulsion. This is especially true at low shear stresses and at a low percentage of fine particle sizes. The viscosity will be a function of the percentage of fine droplets. The viscosity will have a minimum value of viscosity for a certain percentage of these fine droplets. Consequently, the minimum value of viscosity will be a reflex of a maximum value of φ_m due to optimal arrangement between the fine and coarse particles [66, 67].

On the other hand, highly concentrated emulsions under shear can change their distribution size due the breakage and coalescence of droplets [46]. As a result, the maximum packing value changes with the shear forces applied. Besides, even if it does not change the distribution size in the distribution size of the droplets, it is necessary to be aware of the distribution function of the aggregate droplets or clusters that can change constantly due to the shearing applied [99]. Therefore, different viscosity answers can be obtained for the same droplet size due to changes in the liquid film and trapped liquid between the aggregates when they are subjected to different shear forces [60, 81]. Therefore, the distribution of the particles changes constantly due to their dependence on the flow history and the nature of the suspension [15]. The suspension can have a different value of φ_m for each system and each shear. The sum of all random conditions plus the lack of understanding for determining this value theoretically makes it some times necessary to determine it empirically.

Shear-rate-dependent viscosity of size and shape

The size of particles as a function of shear rate has an important role in emulsion behavior. Finer emulsions can organize a better structure network than

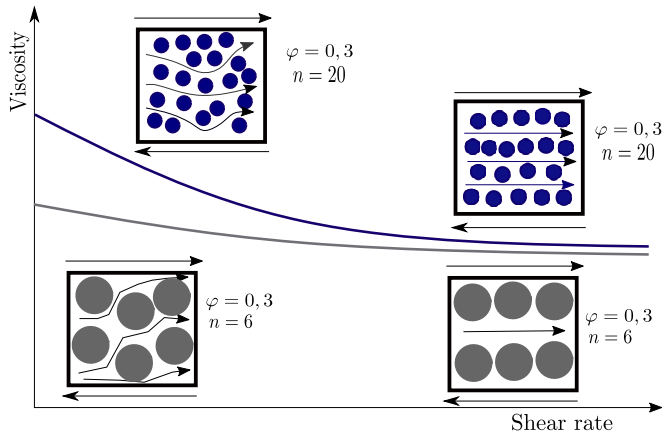

Figure 2.8: Scheme of the dependence of the sphere size with the shear rate for the same concentration of dispersed phase. The fine spheres and coarse spheres are represented by blue and gray color, respectively. Adapted from [62]

coarse emulsions. Smaller particles display a higher surface charge than larger ones, and the hydration of the droplets is potentially strong having an effect on the effective hydrodynamic particle size. This has a high effect on the Brownian forces, which help against an extrenal shear force. Also, smaller particles are less deformable, hence, less affected by the external shear [6, 49, 65]. Emulsion with smaller particles can have higher viscosity at low shear rates compared to emulsions with coarser particles, as it schematized in Figure **2.8**, and the same viscosity value at large shear rates due to the organized structure that is arranged with the flow [47, 49].

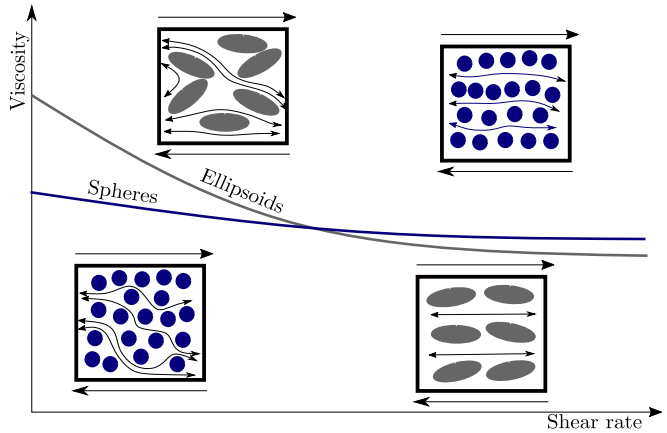

Figure 2.9: Scheme of the dependence of the sphere shape with the shear rate for the same concentration of dispersed phase. The spheres and ellipsoids particles are represented by blue and gray color, respectively. Adapted from [62]

Another factor that may affect the rheology of emulsions is the shape of particles. This characteristic gives networks a complexity in their structure due to the diversity of particle shapes, which limit their optimal geometric organization.

Therefore, this characteristic carries to increase of non-Newtonian behavior. Figure **2.9** represents a schematic design about the effect of shape in the viscosity. Particles with ellipsoid and sphere shape are drawn. In this case, the viscosity measured for the ellipsoids are higher than the one for spherical shape particles [63].

Other factors

There are other factors that affect the rheology of emulsions, for instance, the properties of the continuous phase (rheology behavior) and the interfacial film properties. For simplicity, not all of these factors were mentioned here, but some of them can be found in the references [106, 107].

2.5 Background of rheology of emulsion

The understanding of the rheology of suspensions has long been one of the classical challenges. The first record dates from 1887 when Arrhenius [4] found that the viscosities of suspensions increased logarithmically with the concentration of solid particles in the liquid [116]. One of the broadest reviews was made by Rutgers in 1962 [91]. Until this date, he reported almost 100 equations. From the Arrhenius equation to the present day, there are uncountable numbers of equations, it being impossible to mention them all in this document. Some of the most famous equations with large applicability and with important theoretical extensions will be briefly described in this section. The most relevant equations are introduced in Table **A.1** (see Appendix A). Each equation mentioned in this table will be described or referenced in the text. The behavior that relates the viscosity and concentration will be called viscosity-concentration, and the behavior that relates the viscosity with shear rate will be called viscosity-shear.

Rutgers classified the equations in five groups depending on the similarities between them [9, 91]. These groups can be reduced to three general equations as one can observe in Table **2.1**. The groups were named based on Rutgers' nomenclature. Where relative viscosity is a relation between emulsion viscosity and continuous viscosity ($\eta_r = \eta/\eta_o$).

Table 2.1: General groups of viscosity-concentration equation

Type	Name of equation group	Equation
1	Power law	$n_r = 1 + k_1\varphi + A_2\varphi^2 + k_3\varphi^3 + ... + k_n\varphi^n$
2	Logarithmical	$\ln n_r = k\varphi$
3	Crowding term	$n_r = 1 + \dfrac{k\varphi}{1 - s\varphi}$

The three equations classes are: 1) Power-law equation is a relation of one or more power series, 2) Semilogarithmic or exponential equation, and 3) the equation with the Crowding term, a term $(1 - s\varphi)$ that is added to the denominator, and which is equal to maximum packing fraction ($\varphi_m = 1/s$) when η_r becomes infinite [91].

The viscosity-concentration equations proposed along these years have had both empirical and theoretical development. All formulations followed some of the three patterns mentioned in Table **2.1**. Most of them are empirically adjusted equations for some particular application, therefore the adjustable parameters are only valid for specific systems and have some limitations. Some examples of equation with completely empirical development are: Bredée(1937) [9],Weltmann (1943) [116],Norton (1944) [58], Chong (1971) [14] and Batchelor (1977) [7]. Some authors tried to give a physical meaning for these empirical parameters by obtaining hybrid equations between theoretical and empirical developments such as the equation of Robinson (1949) [89], Mooney (1951) [55], Oldroyd (1953) [59], Krieger and Dougherty K-D (1959) [45], Wildemuth 1984 [117], Pal (1989) [74]. On the other hand, Choi (1975) [13], Yaron (1972) [120], Batchelor 1977 [7] and Quemada (2002) [84] developed theoretical equations using mechanical and geometric concepts, considering Brownian and hydrodynamic forces including particles-particles interaction and particle-medium interactions due to the attractive and repulsive forces. Other equations based on these principles formulated theories tried to predict the particle-particle formation and cluster-cluster structures including some phenomena such perturbation, collision, coalescence and flocculation. Some example are Storey (1958) [102], Rutgers (1962) [91], Cross (1965) [16], Mills (1985) [54], Quemada (1997) [81], among others.

The applicability of each equation can be limited by different characteristics of the system such as the particle shape, the supposition of hard (suspension) or smooth interface (emulsion), if it is polydisperse, and the range of concentration. In the next subsections, the equations will be classified according to their applicability and the main principle treated and incorporated in each equation.

Viscosity-concentration equation in dilute range

To start scrutinizing the viscosity equation of colloid systems it is inescapable to begin from the well-known Einstein equation. This equation can be classified as the simplest form of the power-law equation. Einstein developed a theoretical equation for dilute suspensions composed of rigid spheres in an incompressible

Newtonian fluid. It assumed that the particles are separated far enough that each of them can be treated independently and the flow around each particle can be described by the hydrodynamic equations of motion with negligible inertia (the Stokes' law) [42, 65].

The viscosity of the continuous phase is corrected by the multiplication of the effect of a single particle to the total number of particles suspended [93]. This linear relationship is valid in the limit of very low concentrations due to its restricted supposition of non-interaction between the particles [21]. Experimentaly it was confirmed that its validity is up to a maximum volume concentration of $1 - 2\%$ [15], but this limit depends on the system studied [89, 91].

The constant $[\eta]$ is denominated intrinsic viscosity. The value reported by Einstein for this constant was of 2.5, valid only for hard-spheres. It is dependent on characteristics of the particle as such: size, shape, deformability, and orientation. Also, the huge relevance of its interactions with the medium and the other particles [8, 58, 89]. The variability of this value will be analyzed in Chapter 5.

Viscosity-concentration equation to concentrated range

Weltmann (1943) [116] was one of the first authors that related non-Newtonian suspensions behavior with concentration. He modified the Arrhenius' logarithmic law. However, some limitation in its applicability was reported. It can only be used for dilute suspensions of pigments in the oil phase [58]. A similar attempt was made by Norton (1944) [58]. He developed an empirical power-law equation for a higher range of concentration. Norton worked with suspension close to the maximum packing fraction. Additionally, he attributed the responsibility for collisions and interference of the particles (or groups) with each other to a specific equation term.

Afterward, Robinson (1949) [89] introduced the concept of the "free liquid" that is defined as the liquid outside of the suspended particles, entrapped within the aggregates which will not contribute to the fluidity. This effect grows with the increase of the number of aggregates. Also, [89] pointed out that there exists a limit point of saturation in which sufficient liquid is used to fill the voids between the packed particles. In this condition, the flow of the liquid is impossible and the suspension becomes a porous solid and its viscosity tends to infinite. The term $(1 - s\varphi)$ of the equation is the free liquid and S is relative sediment volume (entrapped fluid). It depends on the shear rate, particle-size distribution, and nature and shear-story of the suspension. The "free liquid" scheme or the liquid entrapped in the porous of the aggregates used for this theory is shown in Figure

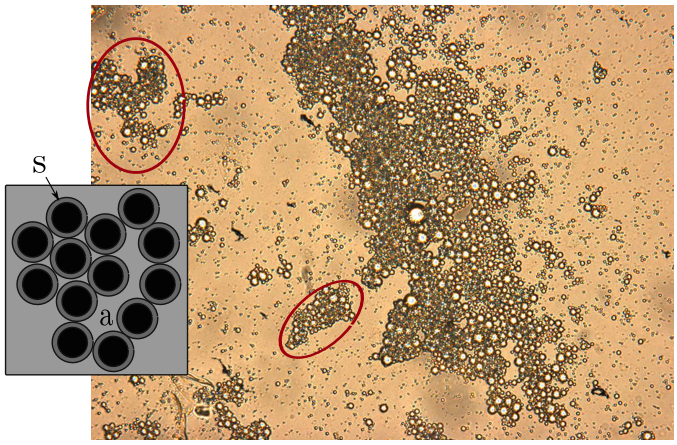

Figure 2.10: Schematic of conceptual model of a flocculated structure composed of particle enclosed by liquid solvated in the surface (s) and water trapped in the interstitial space (a). Adapted from [10]

2.10 .

Roscoe (1952) [90] generalized the Einstein formulation to dilute suspension using a new theory that incorporated the effects of the concentration increase and polydispersity of the disperse phase [69, 81]. The differential effective medium theory (D-EMT) assumes that the relative viscosity is increasing differentially with the addition of volume (see Figure **2.11**). It is presumed that the material surrounding the differential added volume is homogeneous and has well-defined properties. The properties of the surrounding homogeneous material are unaffected by the addition of this differential volume. The properties of this new dilute system are inferred by the previous dilute point [10].

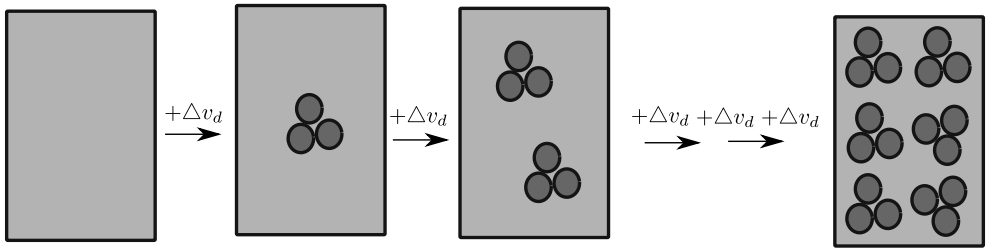

Figure 2.11: Schematic illustration of the D-EMT theory. Adapted from [74]

Many equations have been developed from D-EMT theory. Some good derivations to explain step by step the equation's deduction are in the references [10] and [41]. Mooney (1950) [55] expanded the theory of D-EMT and sharped the concept of free volume introduced by Robinson (1949) [89]. The equation is applicable for both monodisperse and polydisperse system, that involves a variable factor which measures the crowding of spheres of different radius. Pal (1990) [64, 72] applied this equation to the emulsion system with a reasonable fitting. Nonetheless, he had to modify Mooney's equation to achieve a better fit.

Krieger and Dougherty (K-D)(1959) modified Roscoe's equation and added the concept of a maximum packing fraction of φ_m. This equation is very popular in literature and amply used in different systems composed of monodispersed hard-spheres [70, 71]. They affirmed that the parameters $[\eta]$ and φ_m depend on the shear stress [45].

Frankel and Acrivos [30] based their theory on the viscous dissipation of highly concentrated suspensions that arises primarily from the flow within the gaps separating solid spheres from one another [43]. They affirmed that the rapid rise in viscosity can be solely accounted for the hydrodynamic interactions of neighboring spheres.

Farris (1968) [28] and Chong (1971) [14] developed a theoretical equation for the viscosity-concentration with the polydispersity of sizes of the suspended particles. To Farris (1968), the viscosity-concentration behavior of multimodal suspensions can be the sum of the unimodal components of each size of the suspension. Chong (1971) [14] determined the viscosities for high concentrated suspensions correlating the equation with the particle size distributions (bimodal system).

Finally, Sudduth (1993) [103] integrated a large number of the equations for the suspension viscosity giving rise to only one general equation. He showed an amply analysis of it in the reference. The general Sudduth equation is:

$$\boxed{\ln(\eta/\eta_o) = \left(\frac{-[\eta]}{s}\right)\left(\frac{1}{\sigma-1}\right)\left[(1-s\varphi)^{1-\sigma}-1\right]} \tag{2-1}$$

The new parameter in this equation is σ, which defines the particle interaction coefficient. Giving values for σ, It is possible to obtain different common equations, since a simple power-law equation to a K-D equation. In Table **2.2** there are a few examples of the principal viscosity-concentration equation with their respective parameter value.

Table 2.2: Sudduth's generalized suspension viscosity equation

Parameter	Equation	Name	Ref
0	$\ln(\eta/\eta_o) = [\eta]\varphi$	Arrhenius	[4]
0.5	$\ln(\eta/\eta_o) = \left(\frac{2[\eta]}{k}\right)(1-(1-k\varphi)^{0.5})$		
1	$\ln(\eta/\eta_o) = \left(\frac{-[\eta]}{k}\right)\ln(1-k\varphi)$	K-D	[45]
2	$\ln(\eta/\eta_o) = [\eta]\left(\frac{\varphi}{(1-k\varphi)}\right)$	Mooney	[55]

Viscosity-concentration equation including the shear rate influence

The relationship between rheology and changes in the material structure when submitted above shear stress was first explained in the reference [116]. They also noticed a change in the plastic and pseudoplastic behavior, besides the possibility of the appearance of thixotropic behavior.

Ree-Eyring showed a generalized flow theory to represent the viscosity of suspensions. The theory considers a non-Newtonian system composed of a number of flow units with different relaxation times. The three parameters depend on the shear rate at all temperatures and concentrations. However, the calculation of the parameters is very complex [79]. Maron-Pierce equation [51] applied the generalization of the Ree-Eyring theory that was later popularized by Quemada [79]. This equation conserves similarity with KD's equation with the only difference in the exponent value which is equal to $[\eta]\varphi_m = -2$ for this formulation.

Cross (1965) [16] came up with an equation for viscosity as a function of shear rate when a shear-thinning behavior is evidenced. They attribute the pseudoplastic behavior to the formation and rupture of structural linkages. The model assumed that flocculation involves groups of linked particles and that under steady shear conditions there is an average group size dependence on the magnitude of the applied shear. The system becomes completely deflocculated at very high rates $(\eta \to \eta_\infty)$ and completely flocculated at low shear rates $(\eta \to \eta_o)$. In this equation, the viscosity is only dependent on the shear rate and it is only applied to a specific concentration of the dispersed phase.

Wildemuth (1984) [117] suggested that the intrinsic viscosity and the maximum packing fraction form of the K-D equation are dependent on the shear rate due to changes in the structure. They attributed changes in the $[\eta]$ to changes in the shape of the particles or the aggregate particles when they are subjected below shear. The η_∞ represents the state of aggregation, its microstructure, and its resistance to breakup. He tried to demonstrate the dependence of this parameter with the shear rate.

A theoretical model was proposed by Mills (1985) [54]. He explained the non-Newtonian behavior of flocculated suspensions as originated from the immobilized fluid between the particles which forms flocs. It was used an approximation to estimate the mean radius of flowing flocs in a simple shear field, and consequently, the amount of immobilized fluid in flocs. He introduced the parameter, effective particle volume fraction φ_{eff}, which takes into account the volume fraction of the particles and the trapped fluid inside the flowing flocs. Also,

he gave a formula of φ_{eff} that depends on the stress or shear rate.

Pal [74] showed a theoretical/empirical equation for suspensions with empirical parameters that correlated the influence of solvent volume immobilized in the porous of the flocs with the suspension viscosity. The parameter $\varphi_{\eta_r=100}$ is dependent on the shear rate. However, Bullard [10] demonstrated the ambiguities involved in the Pal's derivation.

Quemada [81] used Cross's equation besides the D-EMT theory to develop his equation. He presented a series of articles explaining extensively the concept and the possible reasons for the non-Newtonian behavior of suspension and their relation with the changes in the structure [80–84].

Viscosity-concentration equation including deformability of interface (emulsion)

Taylor 1932 [110] extended Einstein's equation for a liquid drop inside another fluid. He took into account the viscous dissipation of energy due to the flow inside the droplets. Some works have used the Taylor formula for developing other equations to describe the viscosity of colloidal systems [68, 77]. Oldroyd [59] used the theory of Taylor and the idea of the existence of surface viscosity proposed by Boussinesq [19] and developed a formula for the viscosity of a diluted monodisperse emulsion where the droplets have viscous interfaces. Additionally, Danov [19] added in the model effects due to the presence of surfactants.

Pal [68, 77] proposed two different hybrid equations for emulsions combining the Taylor development and the theory of D-EMT. Both of them need a numerical solution. The reference [77] can be applied for a multi-component system of droplets of diverse sizes. The equation of the reference [68] is basically a combination of the Taylor and K-D equation.

Based on the formulation of the Pal equation, Dan (2006) [18] and Wei (2013) [115] formulated some modified equations to correlate empirical viscosity-concentration to the specified case of non-Newtonian W/O emulsion with good fitting.

2.6 Comments

The understanding of the logarithmic relation between the viscosity of emulsions and concentration has been amply studied. There are many equations that have been reported in literature for almost 130 years, many of them with empirical setting and other with theoretical approximations, some of them

for specific systems and a limited range of applications. There is not one general equation that summarizes the complete understanding of all phenomena involved here. The relevance of some parameters for the emulsion viscosity such as concentration, polydispersity, shear rate, deformability had been shown. The viscosity is defined by the kind of forces that are present (Brownian or hydrodynamic) and how enclosed the system is (φ). These conditions are defined by the particle-particle interaction (DLVO theory) and particle-medium, which are responsible for the phenomena of flocculation and coalescence of the droplets. It can be concluded, however, that there are many studies and equations trying to understand and predict the emulsion behavior. There is still a complex microscopic world to be discovered and modeled.

3
Experimental work

3.1
Material and methods

In this section, all issues related to the experimental procedures will be shown. It will also show preliminary experimental results which will help to explain the theoretical results and post-analysis that will be seen in the next chapters. Initially, the material and the emulsification process will be specified. Two crude oil with different API gravity were used as continuous phase, while synthetic ocean water (ASTM Standard D1141-98) was used as the dispersed phase. The two oils used will be referenced in the text as **Crude A** and **Crude B**. The temperature of the emulsification process and experimental analysis for both oils was set to 40 °C . This temperature was determined as being roughly the average temperature between the offshore platform and oil reservoir. The experimental work is based on rheology analysis (i.e. flow curve, peak hold) and the size distribution function of the W/O emulsion.

3.1.1
Material

Crude Oil

The viscosity and density of crude oils are determined by its composition [40]. One of the conventional classification of crude oil is its API[1] gravity, which is a measure of how heavy or light a petroleum liquid is compared to water . The density was measured with a DMA-4500M density meter from Anton Paar and the viscosity was measured using a DHR-3 rheometer from TA Instruments. All the oils used in this work's experiments were light crude oils with similar density values (see Tab. **3.1**). The rheology-behavior of the oils was Newtonian for a huge range of shear-analyses at the temperature of 40 °C. Crude A had approximately twice the viscosity of Crude B.

Oils are composed of thousands of individual substances which can be

[1]The definition of the API gravity is: API gravity $= \frac{141.5}{\text{SG}} - 131.5$ where SG is the specific gravity in relation to the water at 15.6 °C

classified by SARA[2] method into four groups: saturates, aromatics, resins, and asphaltenes. These groups are defined by the method of extraction [27, 40, 101]. Asphaltenes are defined as the fraction of crude oil that is insoluble in n-alkanes such as n-heptane or n-pentane but soluble in benzene or toluene. Resins are insoluble in propane but soluble in n-pentane or n-heptane. The resin and asphaltene fractions represent the highest molecular weight of crude oil. Table **3.2** contains the SARA of the crude oils used in this work before pretreatment.

Pretreatment

Light oil may have a high viscosity due to the formation of colloidal structures from waxy components [40]. These formations depend on temperature, disappearing when it is increased above the melting point (WAT), and in turn decreasing the viscosity. Due to its complexity and the constant volatility of its light components, oils are normally submitted to thermal pretreatment in order to obtain a better repeatability of the rheological results [50].

These pretreatments may be adapted to each system in attempt to for minimal changes in chemical composition of the pretreated oil in relation to the original crude. Besides, the thermal pretreatment helps to erase the thermal memory of the oil by redissolving the waxes and obtaining oil with more homogeneous paraffin crystals size [50]. Figures **3.1**a and **3.1**b are microscopic images of oil Crude A, before and after pretreatment, respectively. There were noticeable changes in the native oil's crystals size, which were smaller and more homogeneous after pretreatment.

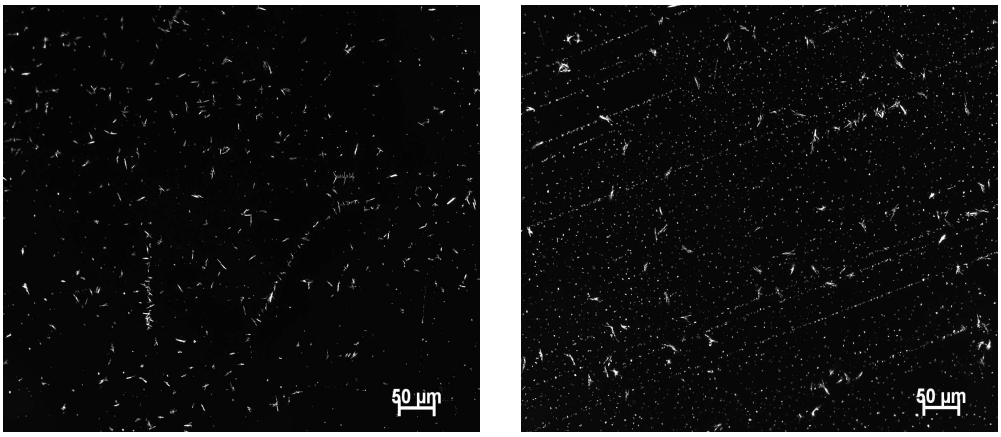

(a) Before pretreatment (b) After pretreatment

Figure 3.1: Microscopy images of paraffin crystals observed on the Crude A before and after the pretreatment.

[2]SARA is a method for characterization of heavy oils based on fractionation

Following the method proposed by [50], a specific pretreatment for these crudes was adapted. Firstly, a thermal cycle analysis of the crudes was done. The thermal cycle helps to determine the point at which the minimum amount of wax crystals starts to have a non-Newtonian effect in the behavior of the oil, achieving the non-Arrhenius behavior. This point is observed by the change in the curve slope (see Figs. **3.2**a and **3.2**b). As it depends on chemical characteristics, this point will be different for each oil. In this work, it will be called T_{ICA}.

The determination of this value establishes the temperature that will be used in the pretreatment. The temperature must be higher than T_{ICA} for the crystals to disappear completely, but not so high as to lose the chemical characteristics of the crude. In this process, it is possible for some light components to volatilize. The treatment must be optimized in search of the minimum time for redissolving the crystals but with minor loss of volatile components. Afterwards, it will be necessary to cool the oil slowly to guarantee a formation of new crystals with small size, consequently, a new oil more homogeneous.

Figures **3.2**a and **3.2**b show the thermal cycle for both oils. As expected, both oils have similar T_{ICA}, 25°C and 30°C due to the similar chemical characteristics. For this reason, similar process conditions were established for the pretreatment of both oils.

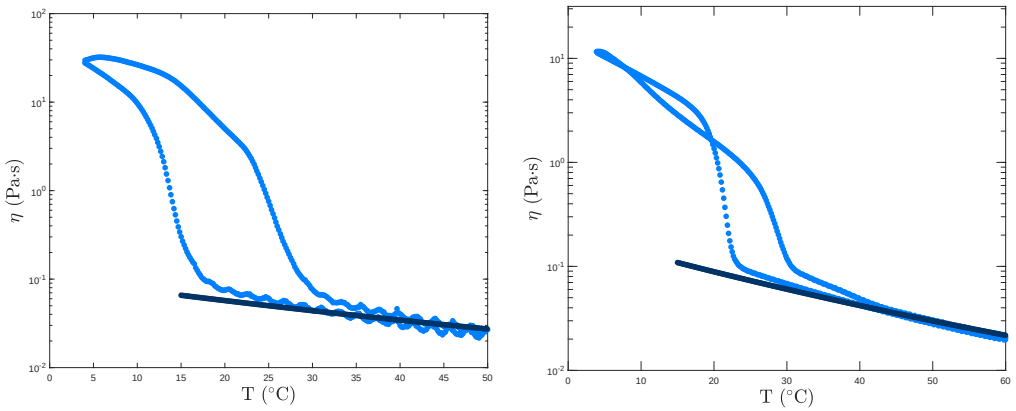

(a) Crude A (b) Crude B

Figure 3.2: Thermal cycle curve before pretreatment with heating and freezing rate of $T_c = 0.5$ (°C/s) and shear rate of $\dot{\gamma} = 1$ (1/s). Experimental curve (●) and extrapolated Arrhenius equation (—)

Figure **3.3** shows the schematic process of pretreatment. The oil is placed in water bath that is previously heated. The temperature chosen was 60 °C, and the total time was 60 min. A rotation of 250 rpm was used on the heating plate in order to homogenize the temperature in the whole bulk of water. During the entire heating time, the glass bottle was used without the cap to promote the

evaporation of the volatile fraction of oil.

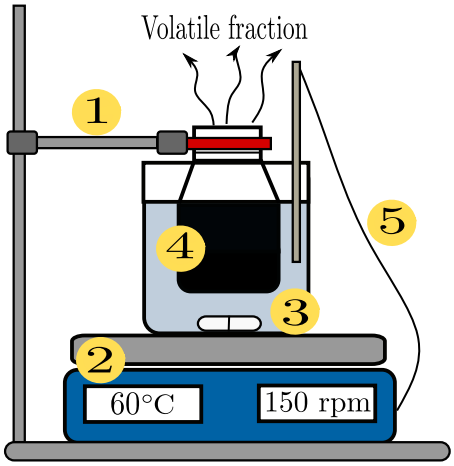

Figure 3.3: Schematic process of crude oil pretreatment 1. Metallic base and clamp; 2. Heating plate; 3. Bain-marie; 4.Glass bottle without cap with oil; 5. thermocouple.

Table **3.1** summarizes the physical and chemical properties of the oils after pretreatment.

Table 3.1: Physicochemical properties of the oils at 40 °C

	Crude A	Crude B	Units	Method
API gravity (15°C)	24.50	25.41		ISO 12185
Water	0.43	xxx	%	Karl Fischer
Viscosity	0.033	0.019	Pa.s	shear-viscosity
Density	889.04	883.63	g/l	ISO 12185

Table **3.2** contains the SARA analysis for Crude A.

Table 3.2: SARA Analysis of Crude A

	Units	Crude A
Saturate	wt%	56.20
Aromatic	wt%	22.5
Resin	wt%	20.8
Asphaltene	wt%	0.50

Synthetic Ocean Water

The preparation of synthetic water was done following the ASTM Standard D1141-98.2013, "Standard Practice for the Preparation of Substitute Ocean Water" [1]. The composition of synthetic ocean water is presented in Table **3.3**.

Table 3.3: Chemical composition of Synthetic Ocean Water

Compound	Concentration [=] g/l
NaCl	24.53
$MgCl_2$	5.20
Na_2SO_4	4.09
$CaCl_2$	1.16
KCl	0.695
$NaHCO_3$	0.201
KBr	0.101
H_3BO_3	0.027
$SrCl_2$	0.025
NaF	0.003
$Ba(NO_3)_2$	0.0000994
$Mn(NO_2)_2$	0.0000340
$Cu(NO_3)_2$	0.0000308
$Zn(NO_3)_2$	0.0000096
$Pb(NO_3)_2$	0.0000066
$AgNO_3$	0.00000049

3.1.2 Method: emulsification process

The schematic process of emulsification is shown in Figure **3.4**. First, the required amounts of water and oil are calculated and weighed in a glass bottle. These quantities will depend on the water concentration required for the emulsion. Second, the glass is put in bain-marie, previously heated at 40°C and homogenized using a magnetic stirrer at 150 rpm. The temperature of the system is maintained at 40°C for 40 min before the emulsification process begins. The temperature was controlled using a thermocouple. To emulsify, a dispersor ULTRA-TURRAX®from IKA was used; the rotations were 8000, 10000 and 12000 rpm during 10 and 5 min.

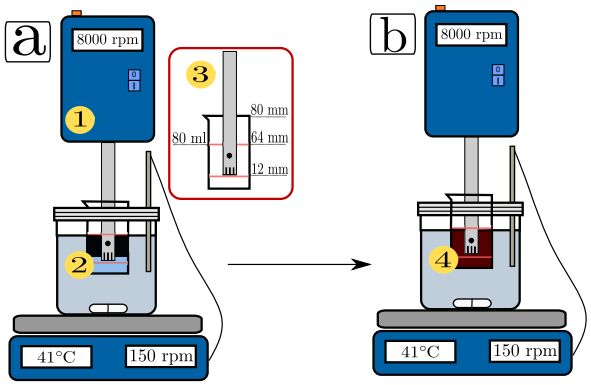

Figure 3.4: Schematic emulsification process. a)Before emulsification (1. Dispersor Ultra Turrax; 2. Oil and synthetic water phases; 3. Glass vessel). b) After emulsification (4. Emulsion)

The freshly prepared emulsion is transferred to a separation funnel (see Fig.

3.5 a.) and left for 30 min until the phases are separated. Later, the free water was collected in graduated cylinders and its amount was measured.

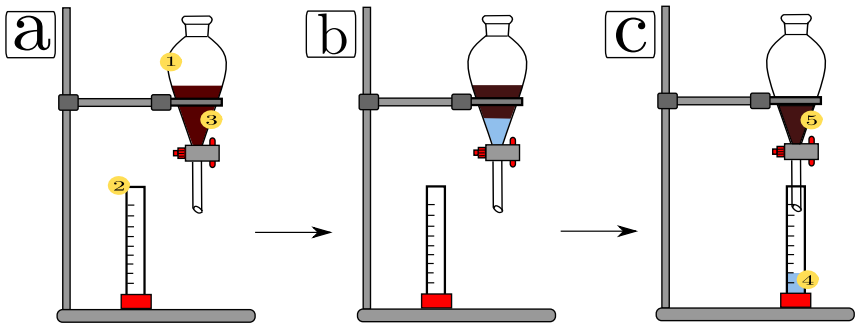

Figure 3.5: Schematic process of separation between the emulsion and the free water. Separation steps of emulsion after the process of emulsification a) $t = 0$ min (1. Separation funnel ; 2. Graduated cylinders; 3. Emulsion. b) $t = 30$ min c) t > 30 min (4. Free water; 5. Emulsion)

As was previously seen, the fraction volume on point [a] of Figure **3.5** can be different from point [c] due to the process of coalescence and separation of the dispersed phase. The quantity of free water will depend on the emulsification rotation used. Obviously, the final concentration of water on point [c] will be greater for a greater rotation. The calculation of the emulsion concentration at point [c] was done using the following equation:

$$\varphi = \frac{V_{EW}}{V_E} = \frac{V_W - V_{SW}}{V_T - V_{SW}} \tag{3-1}$$

Where V_{EW} is the final volume of emulsified water , V_E is the final emulsion volume, V_{SW} is the final volume of separated water (free water), V_W is the initial water volume, and V_T is the initial total volume.

3.2 Characterization of materials

3.2.1 Rheological characterization

The characterization of different materials was done using a Rheometer DHR-3 from TA Instruments (see Figure **3.6**). Some geometries used were: Parallel plates, Cone-plate and Couette. The oils and emulsions were characterized by flow sweeps, which are steady regime curves that relate the viscosity with the shear rate. All test points were taken with previous shearing and heating ($40°$C) for 600 s to ensure the homogeneity and temperature of the entire sample.

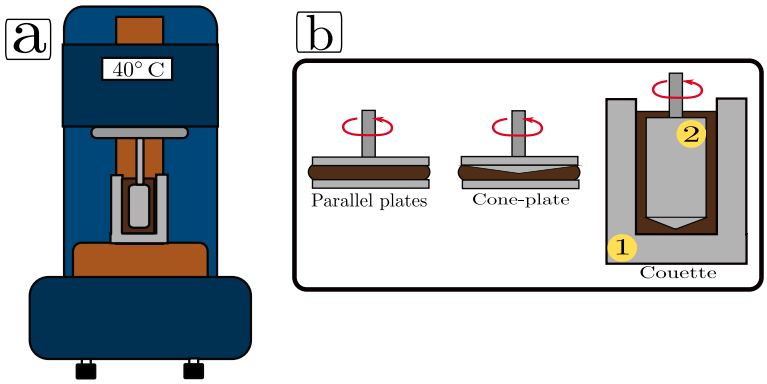

Figure 3.6: a) The DHR-3 Rheometer . b) Rheometer geometries (Couette geometry: 1. Cup and 2. Bob).

3.2.2 Droplets Distribution function

To obtain the size distribution function, a Nikon Eclipse LV100 pol light microscope (see Figure **3.7**) to take photos of the emulsion sample was used. All the images were taken employing a 50x objective lent. The samples were diluted in mineral oil with a lower viscosity than the original crude oil due to the emulsion sample's opaque brown color, which made obtaining a direct image from it difficult. This characteristic of opacity is given depending on the concentration of the dispersed phase in another liquid. The mineral oil used was EXXSOL D60 ($\eta = 1.54e^{-3}$ Pa·s). The samples were visualized in a Petri plate pretreated with a Glass Shield Autoshine. This pretreatment gives hydrophobic characteristics to the glass, hence preventing the adhesion of droplets to the surface, and reducing the possibility of deformation and breakage of the droplets. In order to guarantee good representative data, 30 photos were taken in the microscope for each sample.

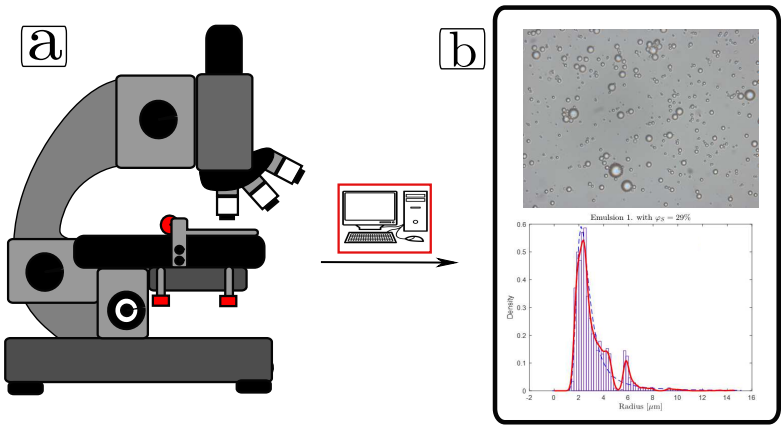

Figure 3.7: a) The Optical Microscope and b) Image processing.

The images were analyzed and processed using a MatLab®program. It was

developed an algorithm to measure the diameter of the droplets and determine the size distribution function ($f(d_p)$). The details of the algorithm and the processing are in Appendix A.

3.3 Experimental Results

Initially, the influence of some emulsification parameters (rotation, shearing time, etc.) on the emulsions properties (d_m,d_{32},η, etc.) was analyzed. Secondly, the shearing effect on the materials' structure was examined (flow curves). Solid/liquid transition depending on the concentration of dispersed phase was studied, as was well as its relation with the rheology behavior. Following, the possibility of the fluid suffering some destabilization process (e.g. flocculation or coalescence) while shearing was inquired. In order to verify flocculation and coalescence, multi-sweep curves and $f(d_p)$ were done. Thirdly, the threshold point and the conditions of non-equilibrium for concentrated emulsions were analyzed.

3.3.1 Previous experimental analysis

Influence of emulsification parameters

As previously mentioned, the emulsification process parameter will define the characteristics of the emulsion. These characteristics can be the droplet size, polydispersity or droplet size distribution function, and viscosity. Therefore, it is necessary to specify the rotation and time of shearing. Depending on these parameters of the emulsification process and the emulsion characteristics obtained, the system can have a maximum point of fraction volume incorporated. This point will be called the saturation point.

The relationship between the volume fractions at points a (φ_a) and c (φ_c), calculated by Equation 3-1, can be observed in Figure **3.8**. Two different condition processes were plotted in Figure. The saturation point for two different emulsification processes for the same oil (Crude A) was illustrated. The emulsification rotations were 12000 rpm and 8000 rpm, both with the same time of emulsification, 5 min. As expected, the point of saturation for both processes was different. The saturation point for 12000 rpm was over $\varphi_c = 70\%$, and for 8000 rpm, this point was approximately equal to $\varphi_c = 40\%$. Particularly, for 8000 rpm, there is a limit of concentration of water in which separation starts to appear ($\approx 30\%$), a little below the saturation point. Above 30%, it is possible to reach

their maximum point of saturation increasing the quantity of water added in the point a.

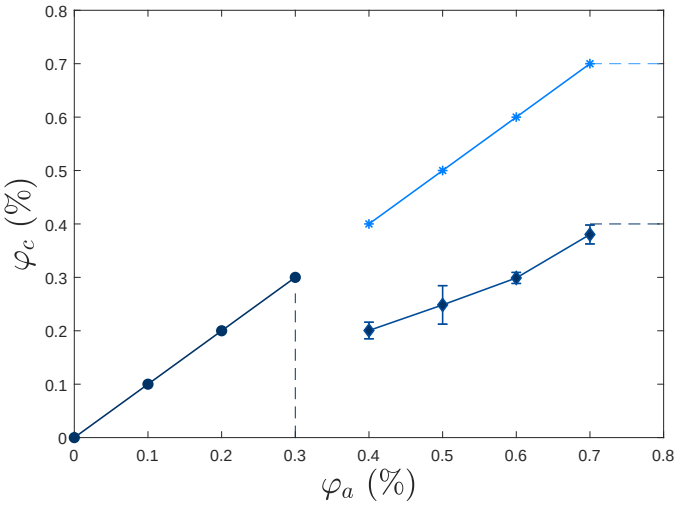

Figure 3.8: Effect of the emulsification conditions in the saturation point. 12000 rpm (—✳—), 8000 rpm (—◇—)

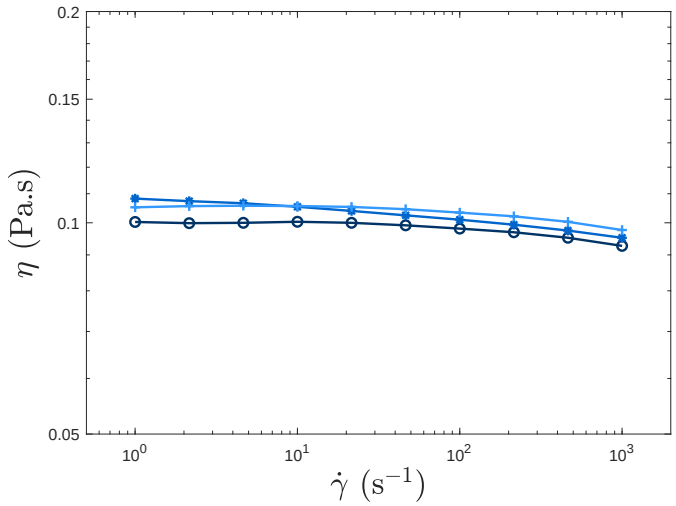

Figure 3.9: Effect of the rotation on the viscosity. Flow curve test of W/O emulsion with $\varphi = 30\%$ of concentration using Crude A. The rotations of emulsification process were: 12000 rpm (—○—), 10000 rpm (—✳—), 8000 rpm (—┼—)

Probably, if sufficient energy is applied to break up the droplets and reduce their size, the saturation point will increase. Therefore, the stability of the emulsion will increase too. This fact can be verified for the 12000 rotation where it is possible to reach a high limit of saturation (Maybe $> 70\%$, not verified experimentally) due to the high energy used. Now, it is clear that the maximum point of saturation can be increased when it is emulsified at a high rotation. How high this value can get will depend on the chemical characteristics of the system. In summary,

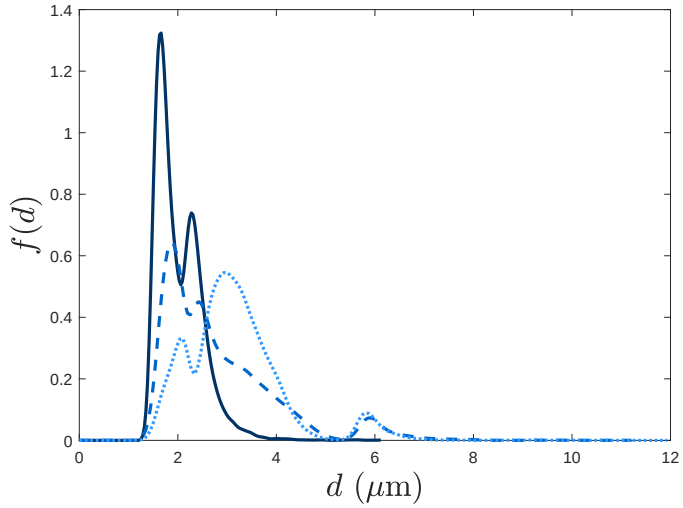

Figure 3.10: Effect of the rotation on $f(d)$. W/O emulsion with $\varphi = 30\%$ of concentration using Crude A. The rotation of emulsification process were: 12000 rpm (——), 10000 rpm (– – –), 8000 rpm (· · ·)

a specific emulsification process will provide the energy to break the droplets at one specific d_p and $f(d_p)$, and the polydispersity of the emulsion will define the maximum packing fraction of the system and its maximum saturation point.

Table 3.4: Properties of $f(d_p)$ varynig the shering rotation to the same concentration (30%)

Moment	12000 rpm	10000 rpm	8000 rpm
d_m	2.02	3.15	2.83
d_{32}	2.26	3.87	3.92

Now, the effect of droplet size and $f(d_p)$ on the viscosity was compared. Three emulsions were prepared at different shearing rotations (12000, 10000 and 8000 rpm) for the same concentration (30%). This concentration value was chosen because it is an achievable point in which no separation occurs, regardless of the rotation speed. The viscosities for the three emulsions are depicted in Figure **3.9** and the $f(d_p)$ curves are in Figure **3.10**. For 12000 rpm the number of small droplets was very high whereas for 10000 and 8000 rpm a higher polydispersity was observed. Additionally, the d_m and d_{32} were similar between the ones with lower rotation speeds (see Tab. **3.4**).

Although each system had a different maximum packing fractions due to their polydispersity, the difference between their viscosities was minimum. This result can be explained due to the fact that this concentration is not high enough for strong interactions to appear. The effect of polydispersity on the viscosity can be disregarded until this threshold, that must be carefully defined for each

system. It is interesting to point out that the viscosity had a Newtonian behavior, corroborating that the viscosity does not depend on the network structure (or polydispersity) under this threshold.

Is there coalescence droplets while the test is running?

In this subsection, the possibility of droplet coalescence during the experiment was studied. For that, the $f(d_p)$ result before and after the test was compared, in order to find any difference in droplet size or any changes in polydispersity.

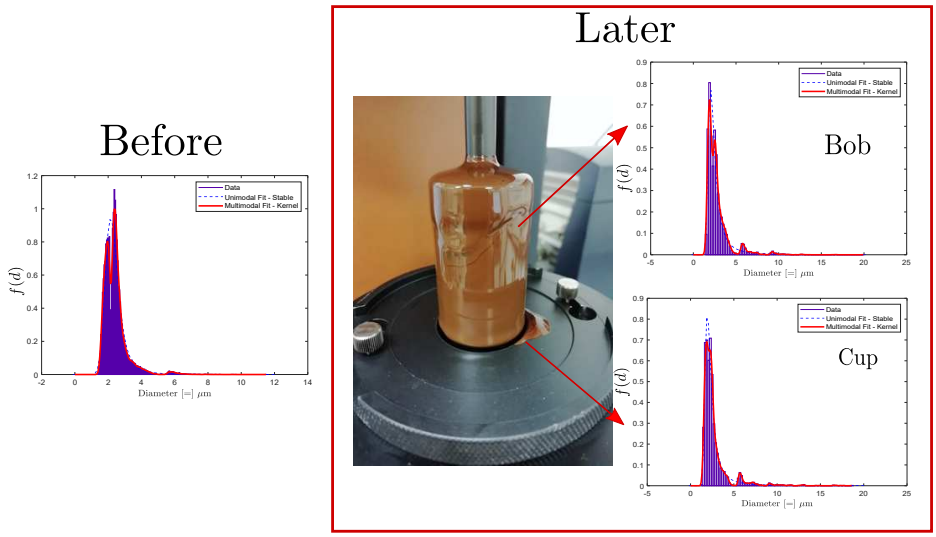

Figure 3.11: Schematic diagram of the sampling points for the verification of coalescence in the emulsion

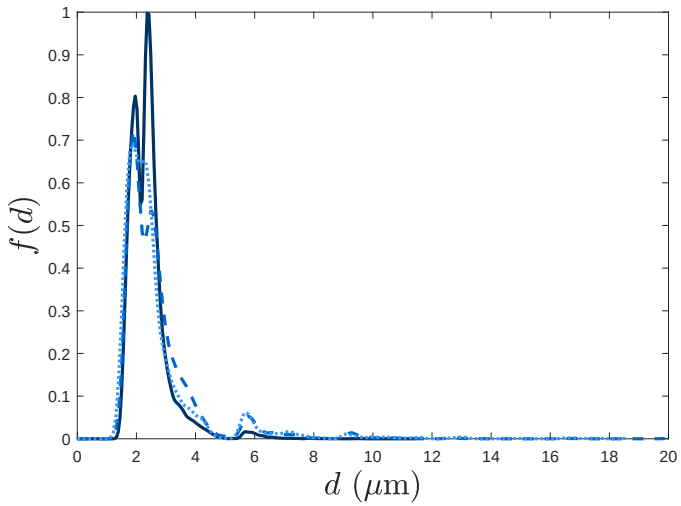

Figure 3.12: Comparative $f(d)$ of the emulsion using Crude A with 64% of concentration before and after the test had finished. Before (——), Later-Bob (- - -), Later-Cup (···)

After the test was completed, a sample of the bob and the cup were taken (see Fig. **3.11**). The result of this analysis was plotted in Figure **3.12**. It is seen

Table 3.5: Comparative properties of PDF to the verification of the existence of coalescence in the emulsion at 8000 rpm

Moment	Before	Later-Bob	Later-Cup
d_m	2.40	2.75	2.69
d_{32}	2.92	4.81	5.85

that the $f(d_p)$s were similar. The d_m and d_{32} calculated for the samples is in Table **3.5**. These results corroborated that the difference between them was minimum.

To sum up, it can be affirmed that during this shear process the coalescence phenomenon was not observed. This condition can be explained due to the rigidity of the droplet interface given by the asphaltenes and resins, preventing their coalescence.

3.3.2 Influence of the concentration

The concentration has a strong influence on the interaction of the droplets, as the distance between them are smaller when the concentration is higher. A smaller distance leads to agglomeration/flocculation. These agglomerates form complex structures with random arrangement, increasing the flow resistance. To measure the influence of the concentration of dispersed phase in the rheology behavior of these emulsions, flow curves for different values of concentration were made. All the flow curves were done at 40°C.

The range of shear rate used was chosen by a statistic analysis and the minimum torque criterion. The torque criterion is given by the limitation of the rheometer used. The minimum torque reported for the DHR-3 rheometer is of 5 μN. The viscosities were considered as confident data if the torque values measured were above this minimum torque. Since the stress depends directly on the torque [3], it is clear that the viscosity must be high enough for this condition to be fulfilled when the system is under low-stress shearing. This is the reason why the following flow curves are on a different range of shear rates depending on the concentration tested. To an statistic analysis end, the sum of squared residual values were minimized for all experimental data. A minimum of two runs were done for each concentration, and the flow curve plotted is the mean curve of these runs. Also, an error bar for each point of the curves is visualized. The equation to calculate

[3]For definition $\tau(\mathrm{M}) = \dot{\gamma}\eta$ where τ is the stress, η is the viscosity, $\dot{\gamma}$ is the shear rate and M is the torque.

the squared residuals was:

$$S = \sum_{i=1}^{n} (r_i^2) \tag{3-2}$$

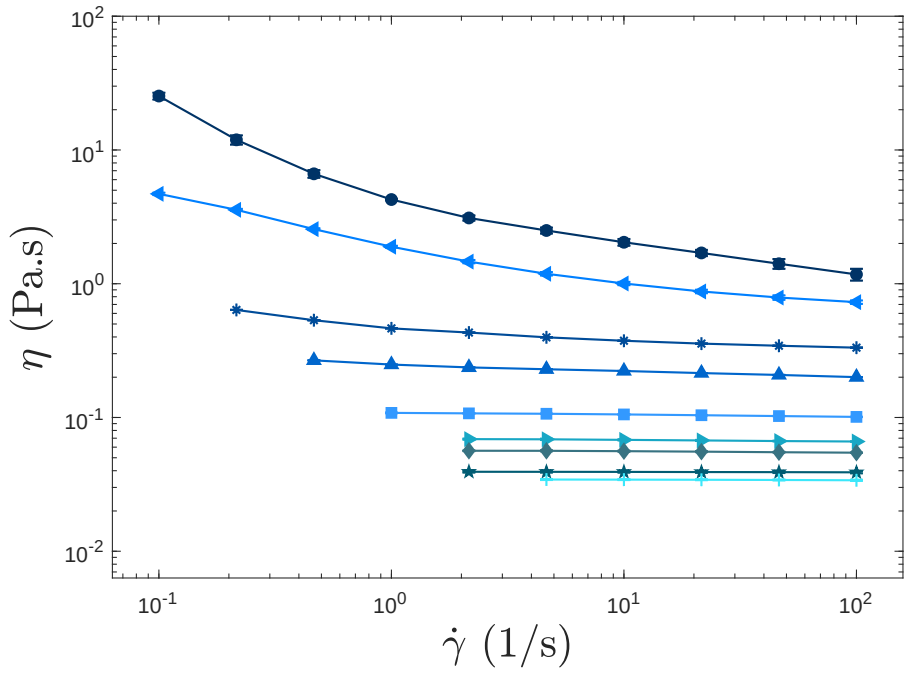

Figure 3.13: Flow curve of Crude A varying the concentration at 40°C. $\varphi = 70\%$ (●), $\varphi = 60\%$ (◀), $\varphi = 50\%$ (✱), $\varphi = 40\%$ (▲), $\varphi = 30\%$ (■), $\varphi = 20\%$ (▶), $\varphi = 15\%$ (◇), $\varphi = 5\%$ (★), $\varphi = 0\%$ (+)

Figures **3.13** and **3.14** show the experimental results for Crude A (0.1 - 100 s^{-1}) and Crude B (0.01 - 1000 s^{-1}), respectively. For both, the crude oil viscosity had a Newtonian behavior (continuous phase) as previously seen. It is noted that over the semi-diluted concentration ($> 30\%$), the behavior for all emulsions was non-Newtonian in shear values below 1 s^{-1}. Also, it was observed a rising tendency of the curve with the increase of concentration.

On the other hand, at higher shear rates, the behavior became Newtonian due to the imposition of hydrodynamic forces on the system. This phenomenon is due to the formation of flocs or clusters that are continually created and destroyed in a shear field [66,81]. These flocs translate and rotate as the emulsion is sheared. With an increase in shear rate, the average floc size decreases. Consequently, the viscosity decreases. At a given shear rate, the average size and concentration of flocs are expected to increase with the disperse phase concentration, therefore also increasing the viscosity. All the curves for concentrated emulsions show non-Newtonian behavior with pseudoplastic characteristic, with the exception of concentration above 60%, which are initially pseudoplastic and later become plastic

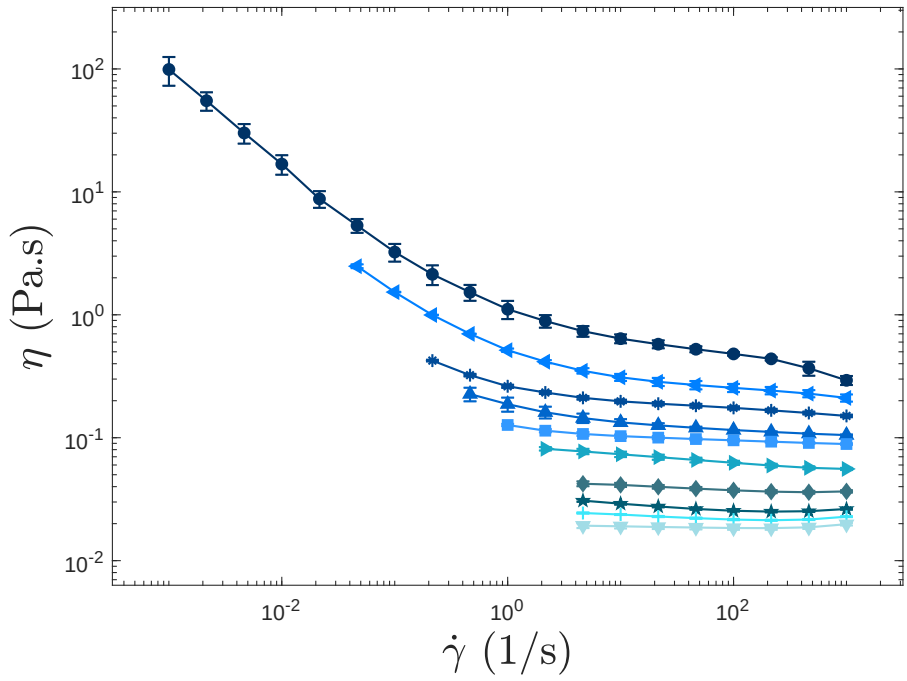

Figure 3.14: Flow curve of Crude B varying the concentration at 40°C. $\varphi_s = 64\%$ (●), $\varphi = 60\%$ (◀), $\varphi = 50\%$ (✱), $\varphi = 45\%$ (▲), $\varphi = 40\%$ (■), $\varphi = 30\%$ (▶), $\varphi = 20\%$ (◇), $\varphi = 10\%$ (★), $\varphi = 5\%$ (+),$\varphi = 0\%$ (△)

and exhibit yield stress. This same characteristic has been reported in literature for suspensions and emulsions [6, 21, 61, 72, 107].

3.3.3 Threshold point for concentrated emulsions

Multisweep Test (is there flocculation?)

Flocculation is largely responsible for a non-Newtonian behavior in emulsions. Tadros inferred that some emulsions may show time dependency and reversibility during flow, called thixotropy [105]. In order to study this effect, he suggests a sequence of shear rate regimes within controlled periods. Hence, multi-sweep tests were conducted to evaluate the process of network breaking under stress. This analysis was only done for higher ranges of disperse phase concentration (50%, 60% and 70%) as they definitely showed non-Newtonian behavior. Figures **3.15**a and **3.15**b plot the viscosity vs. shear rate and the stress vs. shear rate, respectively. The emulsion was initially sheared with increasing shear rates ($0.1 - 100\ s^{-1}$ - "low-to-high" stage), after which immediately followed a backward sweep, with decreasing shear rates ($100 - 0.1\ s^{-1}$ - "high-to-low"). Different rheological responses were observed between the two tests. The low-to-high shearing shows a

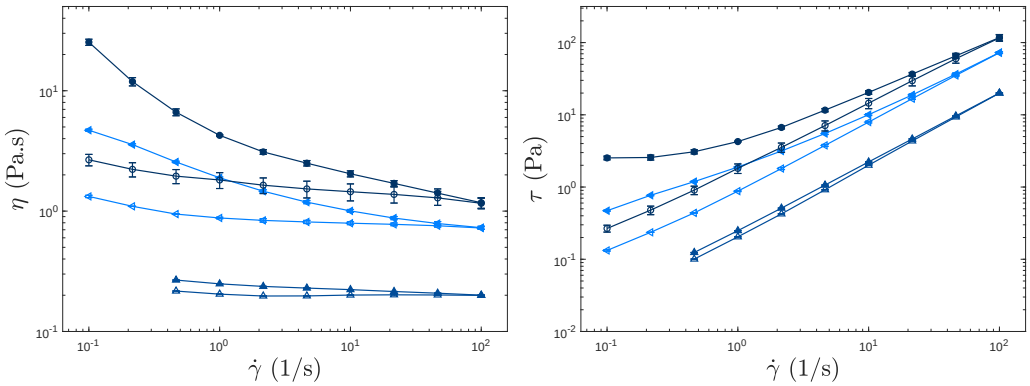

(a) Viscosity vs shear rate (b) Stress vs shear rate

Figure 3.15: Sequence shear flow of W/O emulsion using Crude A for 64% water at 40°C for different concentration. Shear rate goes of low-to-high. 70% (low-to-high) (—●—) and 70% (high-to-low) (—○—), 60% - (low-to-high)(—◀—) and 60% (high-to-low) (—◁—), 50% (low-to-high) (—▲—)and Up (—△—)

decrease in viscosity to a constant level. The initial cluster structures are broken in higher shear values and clusters assume a uniform unitary size. The consecutive high-to-low stage shows an increase in viscosity due to the formation of a new aggregate network. With each backward step, the previous unitary clusters broken down during high shearing in the low-to-high stage begin to build up new links between themselves, creating a more organized structure than before, and thus has a lower viscosity value.

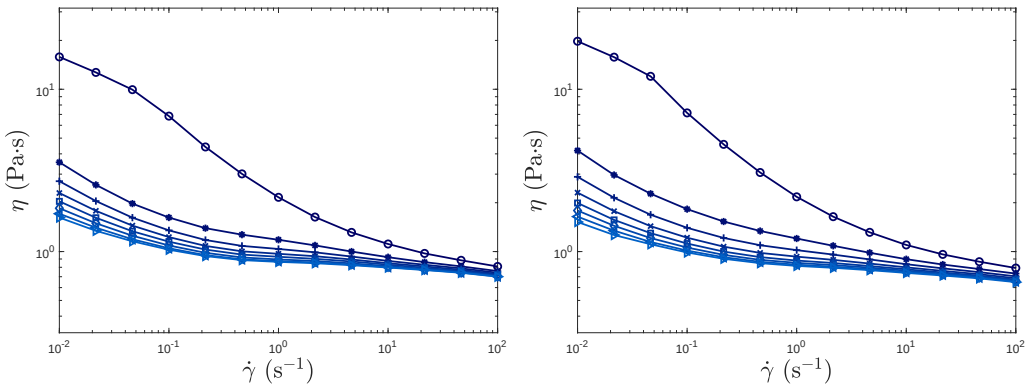

(a) Waiting time of 15 min (b) Waiting time of 30 min

Figure 3.16: Consecutive flow curves for W/O emulsion using Crude A with 64% water at 40°C for different measurements sequences: only increasing with 15 min of waiting time. FC indicates Flow curve (low-to-high) and 1,2, 3,...n are test number. FC1 (—○—), FC2 (—✳—), FC3 (—+—), FC4 (—×—),FC5 (—□—),FC6 (—◇—),FC7 (—◁—),FC8 (—▷—)

To complement this understanding, consecutive flow curves were performed. Eight different sweeps were run with resting time intervals between them. In

order to measure the resting time influence on the emulsion viscosity and cluster formation, two distinct time intervals were chosen: 15 minutes (Fig. **3.16**a) and 30 minutes (Fig. **3.16**b).

As it was previously explained, the network of clusters changes with shearing. At rest, or at lower shear rates, a new structure state is built, but one that does not have the same level of aggregation as before. The initial network probably is a very heterogeneous structure, with many different floc sizes. Shearing breaks this complex arrangement into unitary clusters (aggregates with a small number of individual droplets) and it rebuilds itself in a much more homogeneous structure. All the sweep experiment results presented a similar behaviour: the breakage of the aggregates into unitary clusters. The final point for each flow curve in Figure **3.16**a demonstrates this fact. It is also noted that different resting time intervals have little effect on the overall structure, as figures **3.16**a and **3.16**b show little distinction between them.

In conclusion, the structure constantly changes with the applied shear rate, and as it becomes more homogeneous and less complex, the emulsion viscosity gradually lowers. Moreover, the rheological behavior depends on the flow history, showing irreversible changes due to hysteresis as observed in the figures above [15]. These phenomena make the complete understanding of emulsions from a rheological point a view a great challenge.

Non-equilibrium condition

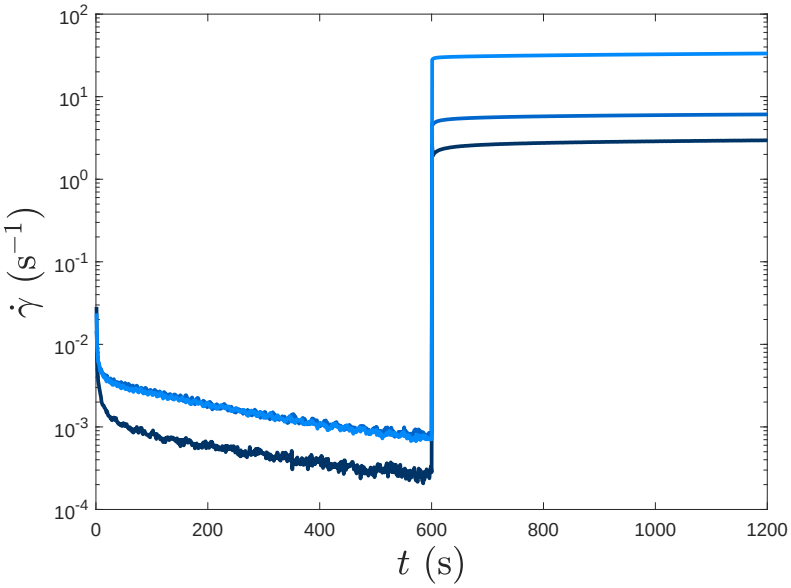

Figure 3.17: Destruction test of W/O Emulsion with 64% water using Crude B for low tension. 3 Pa (—), 5 Pa (—), 20 Pa (—)

At low shear rates, the emulsions with high concentration have a condition of non-equilibrium due to the constant dispute between the breaking and aggregating process of the droplets caused by free particle motion (Brownian motion and interparticle forces) and hydrodynamic regime [54]. This condition of non-equilibrium is noticed for systems with a concentration above φ_g (threshold point or glass point) [54]. The inverse happens for systems with low concentration, as it achieves a stable state quickly. This condition has a relative relevance when setting the rheological test. A maximum equilibration time must be defined in order to make rheometrical measurements. For the sake of praticality, the maximum equilibration time was defined as 1000s for all samples.

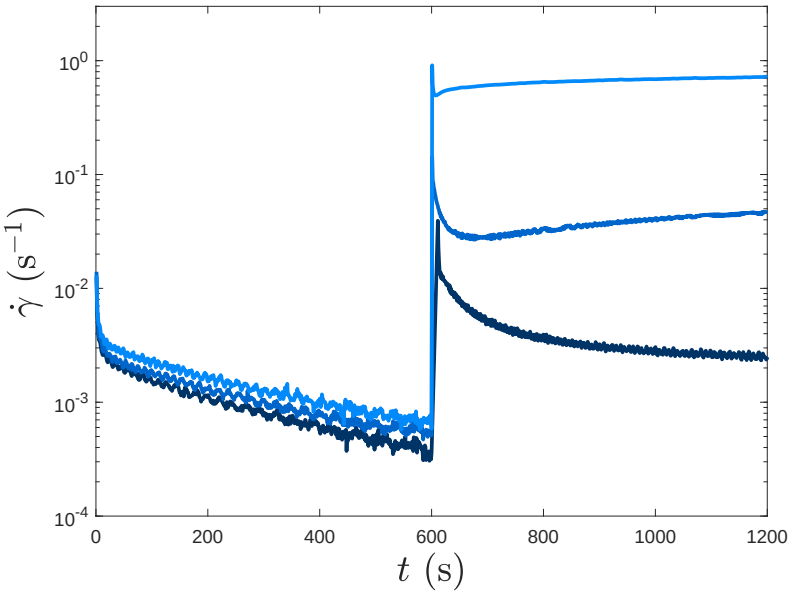

Figure 3.18: Destruction test of W/O Emulsion with 64% water using Crude B for high tension. 0.15 Pa (—), 0.3 Pa (—), 1 Pa (—)

The same can be observed with destruction creep testing. Figures **3.17** and **3.18** represent the behavior of an emulsion with concentration of 64% for two different ranges of stress. In Figure **3.17** the response to the emulsion when it was sheared at lower stress was plotted. When the stress is low, the Brownian forces are dominant, and the system experiments a constant dispute between these forces, being impossible to achieve a constant value of shear rate.

Otherwise, when the stress is high, the structure is immediately broken, rapidly achieving a stable state in the first minutes. This indicates that Brownian forces did not dominate in this range of stress.

3.4 Comments

After all, it is possible to conclude: 1. The emulsification process determine the emulsion properties such as size droplet, polydispersity, maximum concentration packing, and the maximum point of saturation. 2. The emulsion behavior will be defined by the concentration (drop-drop interaction level) and by the kind of forces that dominate, Brownian regime (low level of shear rate) or hydrodynamic (high level of shear rate). As such, it can said that $\eta = f(\dot{\gamma}, \varphi)$. Also, a transition of behavior with the increase of the concentration was observed. The concentrated emulsion presented high viscosity and non-Newtonian behavior, which can be characterized as solid-like. On the other hand, Newtonian emulsion, with low concentration and minimum interaction, can be considered as fluid. 3. The existence of a flocculation phenomenon, irreversible and shear history dependent, was observed. The existence of the coalescence phenomenon was disregarded for this emulsion, due to the rigidity of the interface and the small size of the droplets. 4. The concentrated emulsion showed a non-stable or non-equilibrium condition for the low shear rate. This may be explained be explained due to constant changes in the structure given by the struggle between Brownian and hydrodynamic forces at this level of stress.

4
Thermo-rheological analysis of droplet aggregation

A colloid is a mixture of two substances in which one of them is microscopically dispersed in the other. An emulsion is classified within the colloid group. For thermodynamic science, colloidal systems are regarded as exhibiting analogies with atomic systems, i.e., the particles or droplets standing for atoms or molecules [3, 96]. Depending on the droplet aggregation, by analogy, the colloidal system could be seen as a gas, liquid or solid aggregation phase.

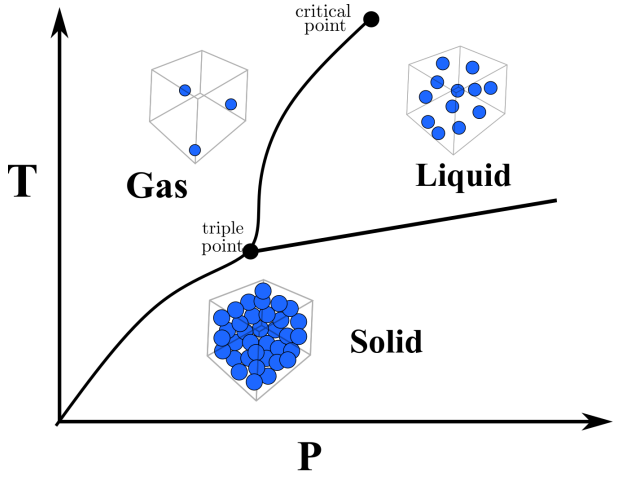

Figure 4.1: Schematic diagram of thermodynamic equilibrium of a pure water

The Gibbs phase rule describes the possible number of degrees of freedom in a closed system at equilibrium [1]. They are the numbers of independent intensive variables that the system needs to establish its state. For instance, a system with only one component and one phase has two degrees of freedom ($F = 2$), therefore needing two independent variables to be defined. A phase transition diagram for a pure substance is schematized in **4.1**. For this diagram, pressure and temperature were chosen as independent variables. In a gas, molecules are so far from each other that their interactions are considered imperceptible. In a liquid, molecules are closer and held together by intermolecular bonds. Like gas, liquid is able to flow, but its density is much higher, being usually closer to the one of a solid. The molecules at solid phase are closely packed together, and may be arranged in

[1] The definition of the Gibbs' phase rule is: $\mathrm{F} = \mathrm{C} - \pi + 2$ where F is the degrees of freedom, π is the number of phase and C is the number of components.

an orderly or irregular pattern. A solid is characterized by structural rigidity and resistance against any external force applied. Liquids and solids are both termed condensed matter.

If a colloidal system is regarded as a pure substance and its droplets considered molecules, Gibbs' phase rule can be applied. Similar to the previous example, two independent variables are required. However, instead of pressure, osmotic pressure will be used.

In this chapter, thermodynamic approach is applied to build up the phase diagram for a W/O crude emulsion varying some parameters such as droplet mean diameter (d_p) and surfactant layer's thickness (t_c). Rheological data is compared with its corresponding state on the phase diagram. A correlation between transition phase theory and emulsion rhelogical behavior was studied.

4.1 Thermodynamical model

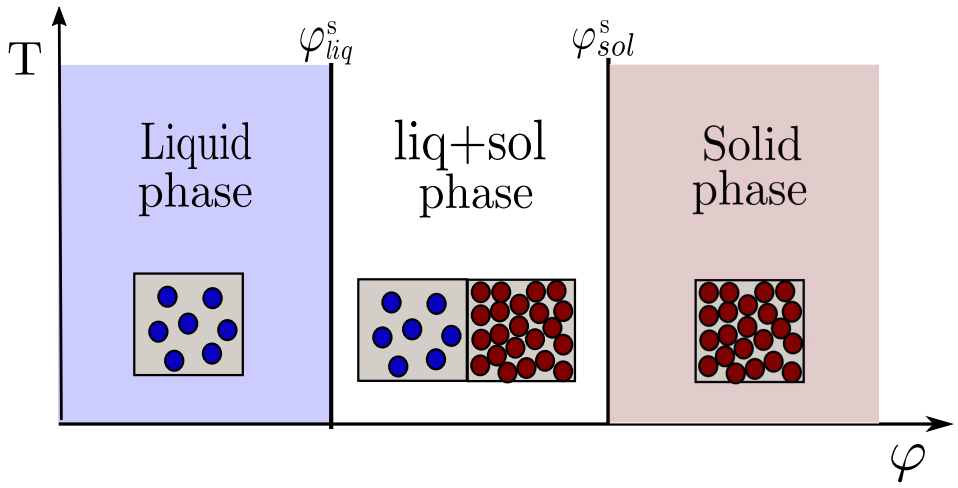

Figure 4.2: Schematic diagram of thermodynamic equilibrium of pure water

Thermodynamic models for colloidal systems are based on the McMillan-Mayer framework [53], which estimates thermodynamic properties of systems from averaged interactions between its solute particles [17]. Depending on the interaction range between particles, (hard sphere, long-ranged or short-ranged) a different kind of phase diagram can be built [3, 33, 78, 113]. For example, the simplest phase diagram applying hard sphere model is shown in Figure **4.2**. In it, three regions are defined: 1) The liquid phase region, divided by the saturated line φ^{s}_{liq}. Droplets (represented in blue) are apart from each other and interactions between them are disregarded. 2) The liquid/solid region, in which both phases coexist. Aggregates or cluster units (represented by red) are present at the same

time as individual droplets. 3) The solid phase region, with emulsion concentration over the saturated solid line (φ^s_{sol}). Complex structures are formed.

On the other hand, the formulation of short-ranged repulsive and long-ranged attractive interactions gives a better approach to equilibrium properties. Barker-Henderson perturbation theory is an example [100]. Thermodynamic equilibrium models based on the previous formulations have been applied in different colloidal systems [86, 87, 97, 109]. The present work uses a model based on that proposed by [96], which considers W/O crude emulsions under the influence of an external electric field. Some modifications to this model were made: the effective interaction potential was calculated disregarding the electric field potential; the radial distribution function of the solid phase was calculated by [44]; compressibility factor of the reference fluid (hard sphere) was based on [35]. The complete details of the thermodynamics model and algorithm are presented in B.

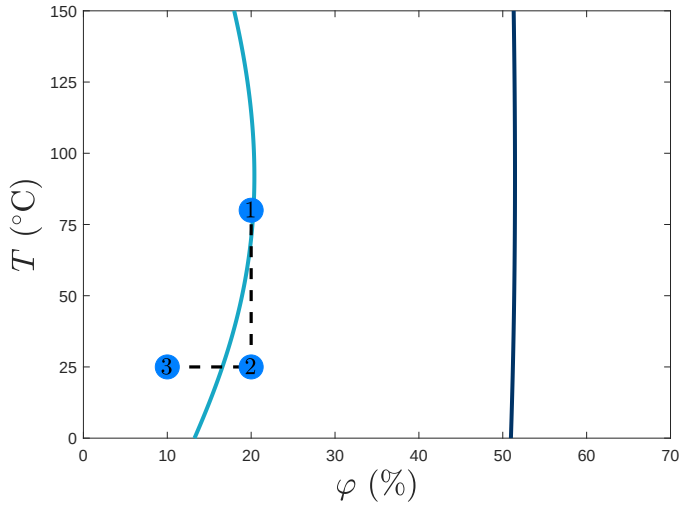

Figure 4.3: Phase diagram for W/O emulsion for $t_c = 13.5$ nm and $d_p = 6$ μm. The saturated liquid line (—) and the saturated solid line (—).

As a case study, a W/O crude emulsion composed of droplets with layer thickness of $tc = 13.5$ nm and mean diameter of $d_p = 6$ μm was used. The phase diagram, divided into three aggregation phases (liquid, liquid/solid, and solid) by the binodal curve, is plotted in Figure **4.3**. As was previously seen, if two independent variables are given, the matter's state can be specified. The transition between aggregation phases while varying its independent variables is illustrated in Figure **4.3**. The first state is ate $T = 75$°C and $\varphi = 20\%$, in which the droplets are far enough from each other that its interactions are considered minimal. Posteriorly, the point is dislocated towards the second state by decreasing its temperature to 25°C, consequently moving the system from the liquid saturation

line to the liquid/solid region. Some clusters are probably formed owing to the increased interactions. Finally, the point is relocated to $\varphi = 10\%$ at $25°C$, going from the liquid/solid phase to the liquid phase, where its interactions can be disregarded.

Diameter effect

Droplet diameter effect in the thermodynamic equilibrium is analyzed in this subsection. A binodal curve (d_p vs φ) with $t_c = 13.5$ nm and $T = 40°C$ was made (see Fig. **4.4**).

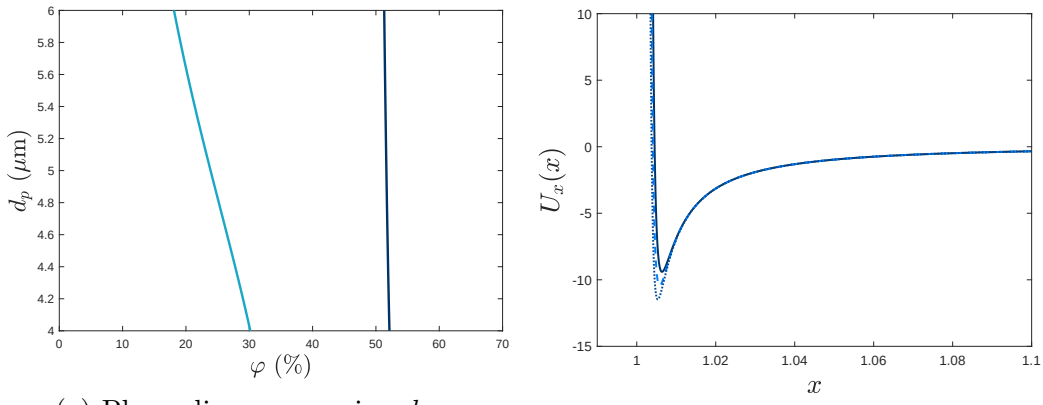

(a) Phase diagram varying d_P.

(b) $U_x(x)$ to different d_p's.

Figure 4.4: Droplet diameter effect in the equilibrium thermodynamic for a W/O emulsion with $t_c = 13.5$ nm and $T = 40°C$. a) Saturation liquid line (——) and saturation solid line (——). b) $d_p = 5$ μm (——); $d_p = 5.5$ μm; (- - -); $d_p = 6$ μm (···)

The liquid saturation line (φ^s_{liq}) varies inversely with d_p, i.e. the saturated liquid line for a small droplet is higher than for a bigger one. (e.g. $d_p = 4.4$, $\varphi^s_{liq} \approx 20\%$ and $d_p = 5.6$, $\varphi^s_{liq} \approx 30\%$). Analyzing the effective interaction potential (See Appendix B, Eq. C-19), a similar conclusion was drawn. To illustrate, $U(x)$'s for three different droplet diameters were plotted in Figure **4.4**b. The deepest minimum energy point was found for the biggest droplet ($d_p = 6$ μm)), showing that in the aggregation process of emulsions composed of coarser droplets, lower values of φ^s_{liq} are more likely. Meanwhile, the solid saturation line (φ^s_{sol}) was constant for the entire analyzed range, being independent of d_p. In other words, for the aggregation solid phase, the droplets are so close that their size stops mattering, and geometric parameters are needed to define its arrangement as random or crystal packing.

Thickness effect

A similar investigation was made varying the surfactant monolayer thickness. Dispersed droplets are considered spherical particles surrounded by an interfacial film. Asphaltenes are adsorbed at the W/O interface, giving the droplets a rigid surface that prevents their coalescence [104]. The asphaltenic film thickness may vary widely: values between 7nm and 40 nm are reported [104, 111, 118]. This variation may be a consequence of the complex structures formed by asphaltene molecules on the droplet interface. Figure **4.5** shows the thermodynamic equilibrium for a W/O emulsion with $d_p = 6$ μm and $T = 40$°C. Both saturation lines change for the entire t_c range. The liquid/solid region thins out at higher thickness values. An increase in droplet interactions was observed at lower thickness values, i.e. φ^s_{lig} is considerably reduced.

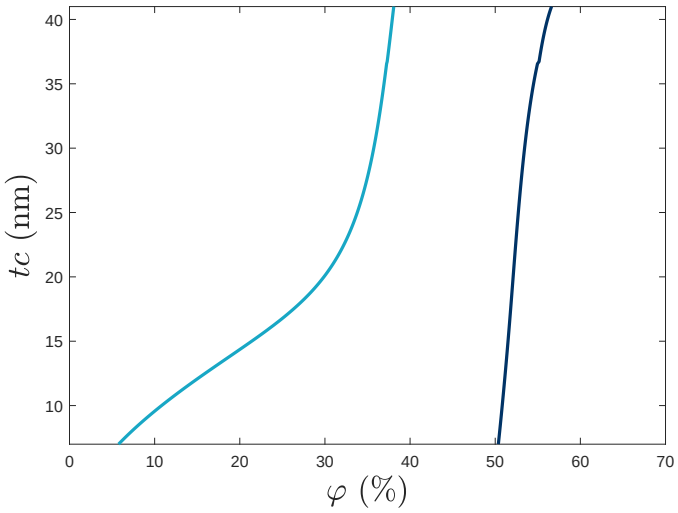

Figure 4.5: Effect of the thickness in the equilibrium thermodynamic for W/O emulsion for $d_p = 6$ μm and $T = 40$°C. Phase diagram correlating the t_c with the φ. Binodal curve of liquid phase (—) and binodal curve of solid phase (—).

Interactions between water droplets in an continuous oil medium are considered as being mainly attractive (Hamaker) and repulsive (steric forces) [118]. The layer effect was confirmed when $U_x(x)$ was analyzed (see Fig. **4.6**). While observing them separately, it is possible to see that the attractive energy remains the same, regardless of the thickness, and the repulsive energy changes. The deepest value for the minimum energy point was found at the lowest layer thickness, i.e. repulsive forces are stronger in thicker layers, which inhibits flocculation from happening. Therefore, the aggregation process is more relevant for droplets with a thinner surfactant film.

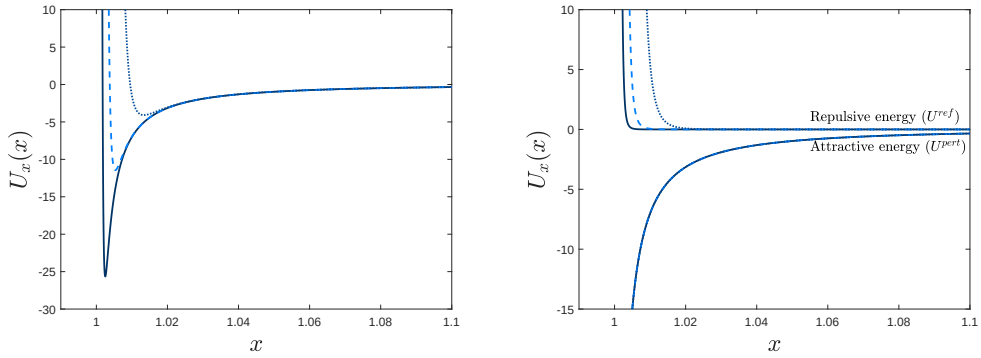

(a) Total $U_x(x)$ (b) Attractive and repulsive energies.

Figure 4.6: Total effective interaction potential varying t_c. (t_c = 7.5 nm (——); t_c = 16 nn; (- - -); t_c = 40 nm (···)

4.2 Linking with rheological behavior

Two different forces play an important role in an emulsion's rheological behavior: free particle motion (Brownian motion and interparticle forces) and hydrodynamic regimes. The governing force depends on the intensity of shearing applied to a system. Figure **4.7** schematizes a typical rheological curve for W/O emulsions, but correlating dimensionless parameters such as Pe and η_r instead of the usual $\dot{\gamma}$ and η. Pe is the dimensionless shear rate, defined as the ratio of time scales for Brownian motion and convective motion [8].

$$Pe = \frac{\dot{\gamma}}{D_r} = \frac{V_p \eta \dot{\gamma}}{k_B T} \tag{4-1}$$

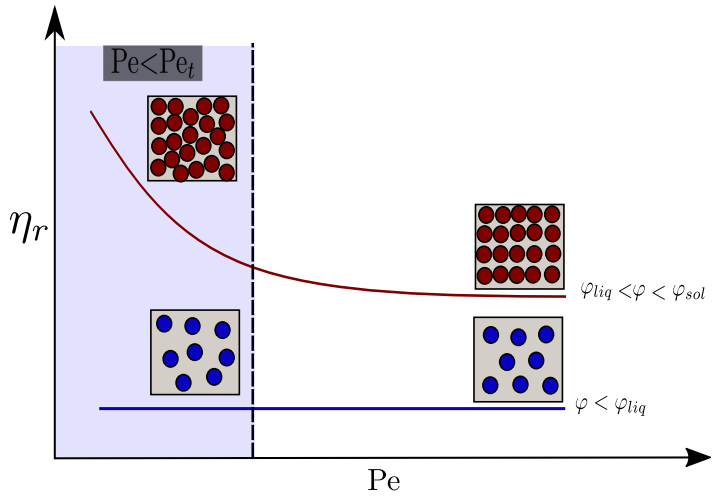

Figure 4.7: Schematic diagram of rheology behavior of W/O emulsion correlating Peclet number (Pe) with the relative viscosity (η_r)

Where D_r is the rotational diffusion coefficient (or the Stokes-Einstein diffusivity), k_B is Boltzmann's constant, T is the absolute temperature and V is the particle volume. Experimental and numerical data have demonstrated that viscosity becomes independent of the Peclet number for $Pe > 10^3$ [57,72]. Above this value, the Brownian interactions are less significant in relation to the hydrodynamic forces. The Brownian area of influence is highlighted in blue in Figure **4.7**.

According to Section 2.4. the viscosity of an emulsion has a Newtonian behavior when its droplets do not interact between themselves. This behavior is typically observed for dilute emulsions. Whereas non-Newtonian behavior is present in concentrated emulsions. The critical concentration (φ_{crit}) in which the droplet-droplet interactions begin having an effect on rheological behavior (i.e. the transition point from Newtonian to non-Newtonian) will depend on the chemical characteristics of each emulsion. The inclination of a concentrated emulsion's rheology curve also depends on the aggregation state, increasing due to the exponential rise in cluster formation in higher droplet concentrations. Hence, the understanding of the interaction forces between droplets will help obtaining a better apprehension of rheological behavior and emulsion stability [118].

This chapter proposes a qualitative correlation between the thermodynamic model and the rheological behavior when the system is free particle motion regime ($P_e < 10^3$). For each case study, T, φ, d_p and t_c were set, and the resulting rheology curves were compared to the corresponding points on the thermodynamic phase diagram.

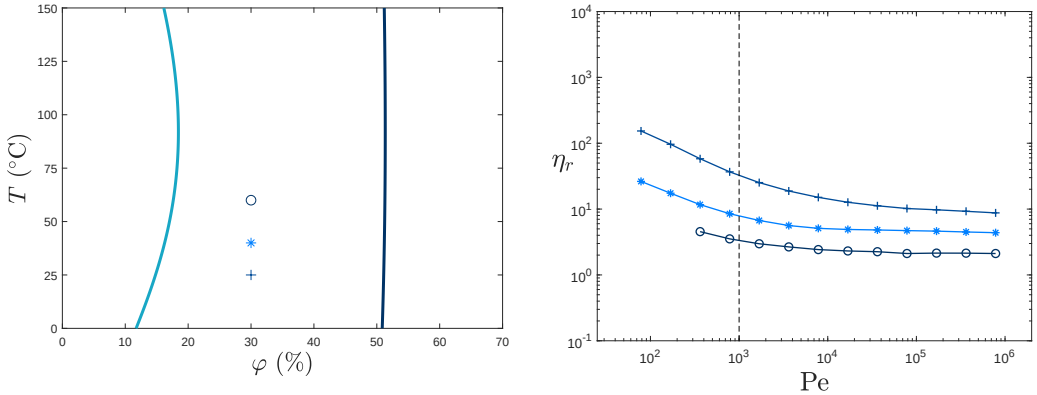

(a) Phase diagram

(b) Rheological results

Figure 4.8: Behavior aggregation analysis of a W/O emulsion with $t_c = 13.5$ nm, $\varphi = 30\%$ and $dp = 6.4$ μm. Varying the temperatures. T= 25°C (+); T= 40°C (∗); T= 60°C (o)

Following the experimental procedures presented in Chapter 3, a W/O emulsion with a droplet concentration of $\varphi = 30\%$ was prepared. The mean

diameter, obtained through the image analysis treatment showed in Section 3.2, was $dp = 6.4\ \mu$m. An average value for all the case studies between asphaltene monolayer thickness was $t_c = 13.5$ nm. The phase diagram and rheological curves are plotted in Figure **4.8** for three different temperatures: T= 25°C, T= 40°C and T= 60°C. In the phase diagram, all cases are located within the liq/sol aggregation phase, indicating a cluster formation. All samples showed a non-Newtonian behavior, as expected.

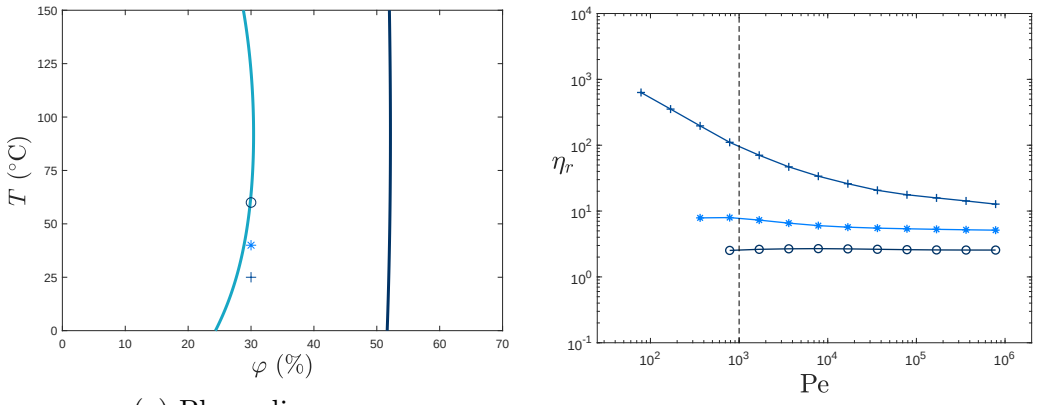

(a) Phase diagram

(b) Rheological results

Figure 4.9: Behavior aggregation analysis of a W/O emulsion with $\varphi = 30\%$, $t_c = 13.5$ nm and $dp = 4.22\ \mu$m varying the temperatures. T= 25°C (+); T= 40°C (∗); T= 60°C (o)

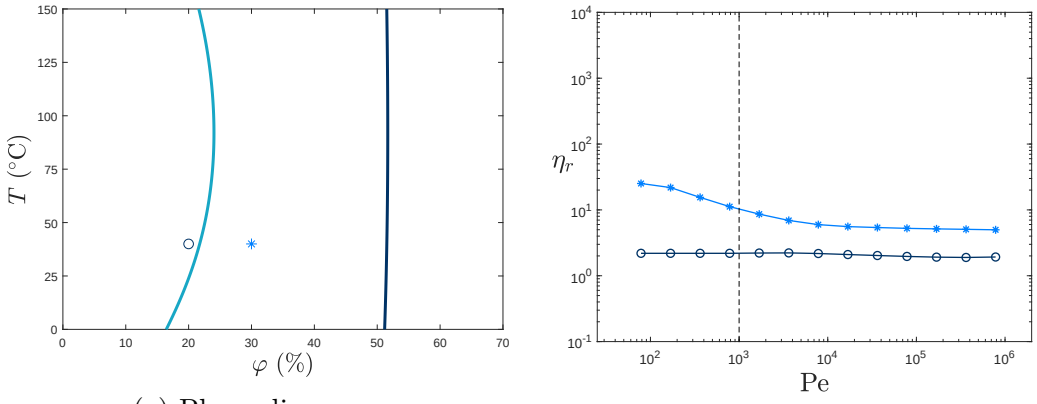

(a) Phase diagram

(b) Rheological results

Figure 4.10: Behavior aggregation analysis of a W/O emulsion with $t_c = 13.5$ nm, $dp = 5.34\ \mu$m, T= 40°C varying its concentration. $\varphi = 20\%$ (+); $\varphi = 30\%$ (∗)

Another W/O emulsion, prepared with the same droplet concentration, was evaluated. The emulsification process' rotation was increased to 12000 rpm, resulting in a mean droplet diameter of $d_p = 4.22\ \mu$m. Figure **4.9**a shows

the diagram phase and Figure **4.9**b, the rheological curve. The surfactant layer thickness was the same as the previous case, as were the chosen temperatures. Two points fell near the saturation liquid line (T= $40°$C and $T = 60°$C) and one was within the liquid/solid region ($T = 25°$C). Consequently, the two former samples should have Newtonian behavior, while the latter should be non-Newtonian. The rheology curves confirmed this assessment.

A third case study kept the temperature constant at $25°$C and varied φ. The resulting points were located in distinct regions (see Figure **4.10**). This may lead us to predict that each one of them will have a different rheological behavior, which proves to be true: $\varphi = 20\%$ is Newtonian while $\varphi = 30\%$ is non-Newtonian.

4.3 Comments

The thermodynamic analysis of W/O emulsions allows the prediction of its rheological behavior when the system is under Brownian regime (Pe $< 10^3$). If an emulsion is located, on the diagram phase, inside the liquid phase region, it will behave as a Newtonian fluid. Whereas, if the system is within the liquid/solid or solid phases, its behavior will be non-Newtonian. The difference between the two latter phases will be determined by the rheological curve inclination, it being higher at the solid aggregation phase. This tendency is a consequence of clustering formation between the droplets, which increases exponentially with the rise of concentration. Some relevant parameters that determine the thermodynamic and rheology answers are droplet mean diameter (d_p), monolayer thickness of surfactant (t_c), temperature (T) and concentration (φ). The level of emulsion flocculation is dependent on the oil and surfactant chemical characteristics. When the surfactant's film thickness is smaller, the repulsive forces will be weak, and consequently attractive forces will dominate droplet-droplet interactions. This increases the droplet aggregate formation, i.e. flocculation phenomenon will be stronger in this case. In sum, the thermodynamic analysis provides us an idea of the emulsion's rheological response, giving the concentration critical point in which its type of behavior will change. The φ_{crit} is also dependent on the chosen emulsion's parameters and chemical characteristics.

5
Rheological model

As shown in Chapter 2, in literature there are many empirical and theoretical equations to predict suspension and emulsion rheological behavior. Mostly, viscosity-concentration equations given a specific shear rate ($\eta_{r,\dot{\gamma}} = \eta_r(\varphi)$), which, therefore, consider the viscosity only dependent on concentration. Besides, these equations have some limitations to their application, as they are valid for a restricted concentration range and a particular system. In this chapter, the application of three classical equations to fit the experimental data of W/O crude oil emulsions for a wide range of concentrations (0-64$\%$) is presented. The application of Pal formulation to solve $\eta_{r,\dot{\gamma}} = \eta_r(\varphi)$ is compared with the methodology proposed. K-D and Sudduth classic equations were used as an example of application of this method. A generalized algorithm renders these equations shear rate dependent. The parameters dependency with the shear rate is justified from a microscale analysis of the organization of droplets as sub-systems (or flocks). There is wide applicability of this methodology for any kind of system.

5.1
Pal equation

One viscosity-concentration equation which also includes the shear rate was proposed by Pal (1989) [73, 74]. This equation is a hybrid formulation between empirical and theoretical relationships. Pal (1989) affirmed that this viscosity-concentration equation is valid for both oil-in-water and water-in-oil emulsions and both Newtonian and non-Newtonian rheological behaviors. The authors suggested an empirical equation to correlate the viscosity experimental data as following:

$$\eta_r = \eta_r \left(\frac{\varphi}{\varphi_{\eta_r=100}} \right) \tag{5-1}$$

Where $\varphi_{\eta_{r=100}}$ is the dispersed-phase concentration at which the relative viscosity becomes equal to 100. Posteriorly, in Pal's next publication, a theoretical model to justify the use of this empirical equation was presented. The theoretical model was based on the D-EMT theory hypothesis proposed by Roscoe [90].

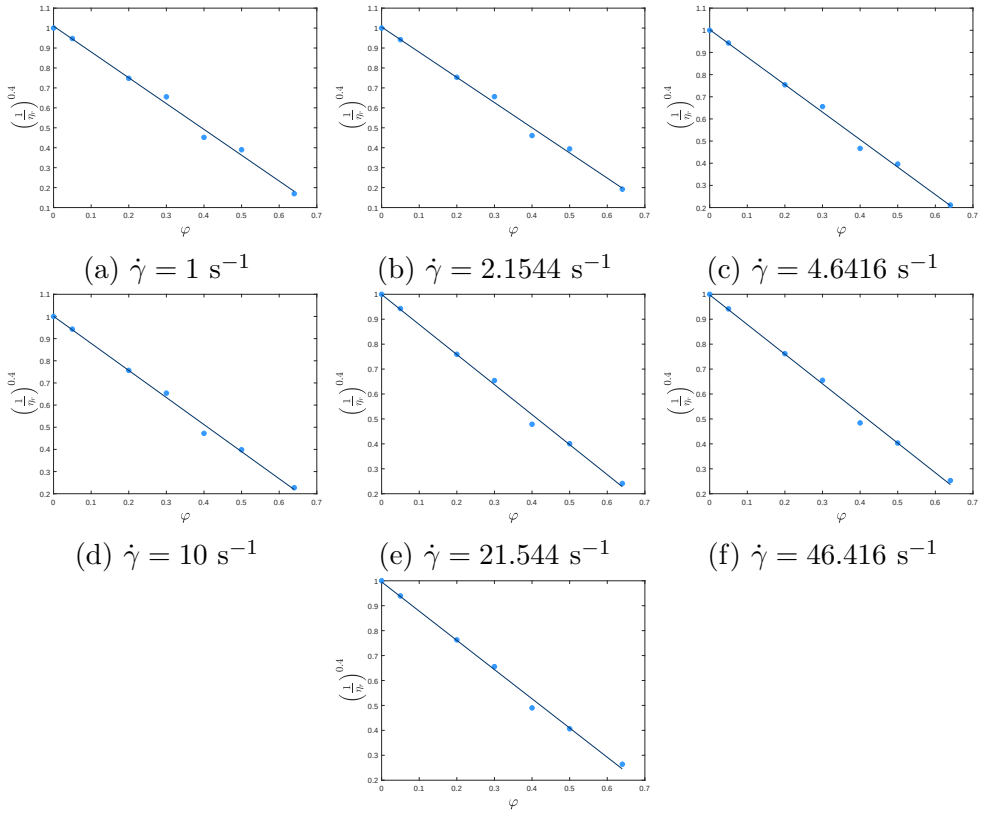

(a) $\dot{\gamma} = 1\ \mathrm{s}^{-1}$ (b) $\dot{\gamma} = 2.1544\ \mathrm{s}^{-1}$ (c) $\dot{\gamma} = 4.6416\ \mathrm{s}^{-1}$

(d) $\dot{\gamma} = 10\ \mathrm{s}^{-1}$ (e) $\dot{\gamma} = 21.544\ \mathrm{s}^{-1}$ (f) $\dot{\gamma} = 46.416\ \mathrm{s}^{-1}$

(g) $\dot{\gamma} = 100\ \mathrm{s}^{-1}$

Figure 5.1: Viscosity-concentration fit for each shear rate. The symbols are the experimental dates (●) and the line is the curve fitted (——).

The model tried to associate non-Newtonian behavior as a consequence of the aggregates formation due to the London-van der Waal's attractive forces between the droplets. In this aggregation process, fluid is immobilized between the aggregates. Consequently, the effective dispersed-phase concentration will be higher than its true concentration. Moreover, the shear rate was referred to as responsible for the hydration effect, i.e, the fluid surrounding droplets. The viscosity equation is rewritten as:

$$\eta_r = [1 - K_0 K_F(\dot{\gamma})\varphi]^{-2.5} \tag{5-2}$$

Where K_0 is the hydrating factor and K_F is the flocculation factor. Substituting $\eta_{r=100}$ in 5-2, the following relation is found

$$K_0 K_F(\dot{\gamma}) = 0.8415/\eta_{r=100} \tag{5-3}$$

Therefore, the Pal (1989) equation shown in Table **A.1** can be obtained. For the determination of its parameters, at any shear rate, the data of $(1/\eta_r)^{0.4}$ versus φ must be plotted. From these plots, linear relationships are obtained, being its

slope equal to $-K_0K_F$ and intercept equal to unit.

As an example of this fitting procedure, Figure **5.1** shows the experimental data of emulsion A. The linear fittings for all shear rates were plotted. The magnitude of the slopes (K_0K_F) decreases with the increase in the shear rate. Due to the flocculation phenomenon, K_F factor should decrease with the increase of shear rate. According to [74], the hydration factor varies from one emulsion system to another depending upon the chemical natures of emulsifier, quantity of dispersed phase, and rheological characteristics of continuous phase. Besides, the hydration can be also be dependent on the emulsifier concentration [74].

Small deviations of the experimental data in relation to the fitting in Figure **5.2** was noticed. This equation may not be valid at very high dispersed-phase concentrations, where emulsion rheology becomes non-Newtonian "exhibiting yield stresses" and where droplets can suffer deformations, factors not consider in Pal's derivation.

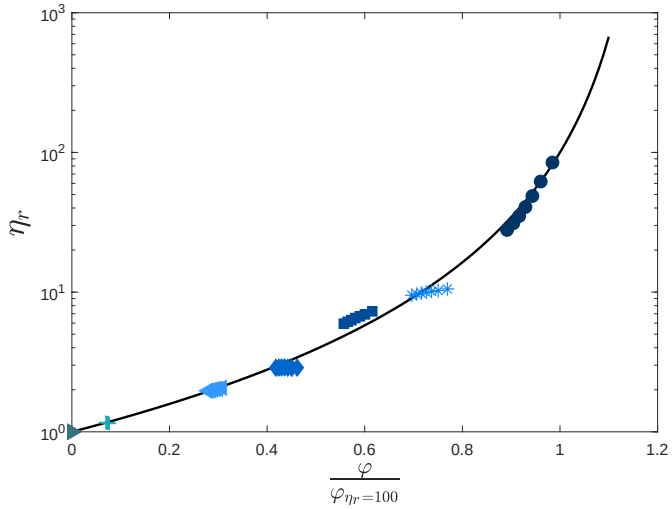

Figure 5.2: Experimental data of Crude A fitted with the Pal's equation. The symbols are the experimental data and the continuous line is fitted curve. $\varphi = 64\%$ (●), $\varphi = 50\%$ (∗), $\varphi = 40\%$ (■), $\varphi = 30\%$ (♦), $\varphi = 20\%$ (◀), $\varphi = 5\%$ (+),$\varphi = 0\%$ (▶)

The hybrid viscosity-concentration equation presented a good fit for all emulsions of both crude oil used. Nevertheless, the relation between viscosity and shear rate could not be expanded because it is not an explicit formulation. Besides, [10] demonstrated that the Pal equation presented ambiguities in its formulation. They indicated that the equation violates one of the main D-EMT assumptions, which affirms that the viscosity of the surrounding medium must not change when the differential volume of new particles is added. An effect that can pile up notice when it works in higher concentrations. [10] insisted on the importance of applying the D-EMT theory carefully when it includes clusters

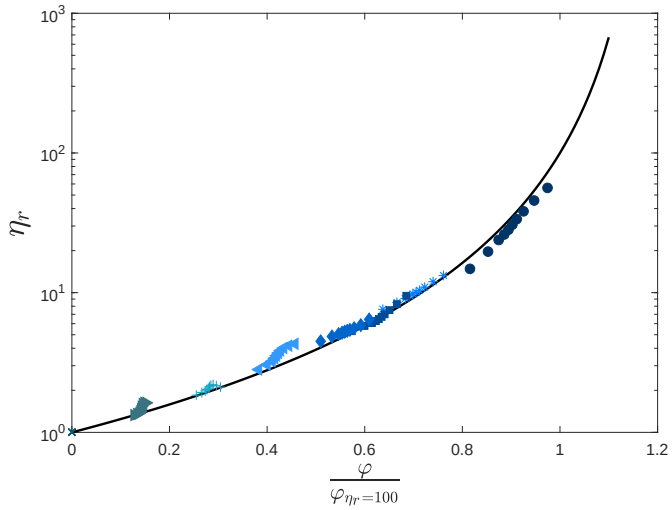

Figure 5.3: Experimental data of Crude B fitted with the Pal's equation. The symbols are the experimental data and the continuous line is fitted curve. $\varphi = 64\%$ (●), $\varphi = 50\%$ (∗), $\varphi = 45\%$ (■), $\varphi = 40\%$ (♦), $\varphi = 30\%$ (◀), $\varphi = 20\%$ (+),$\varphi = 10\%$ (▶),$\varphi = 0\%$ (×)

formation, considering solvation or occlusion in order to prevent any infringement of the principle of mass conservation.

5.2 Generalization of KD's equation for shear dependence

KD equation can be applied to the simplest case where the system is a suspension of small rigid monodisperse spheres in a Newtonian fluid. The relative viscosity is an expression that only depends on φ:

$$\eta_r = \eta_r(\varphi) \tag{5-4}$$

Quemada (1997) published a series of papers where he widely discussed some important concepts in modeling rheologically complex fluids [80–83]. Quemada's equation published in [81] will be presented in this section as a case study. He analyzed the KD parameters dependency with $\dot{\gamma}$ and φ and introduced the concept "effective volume fraction" (φ_{eff}), explaining its dependence on flow conditions such as particle interactions, hydrodynamic forces, flock units. All of these concepts were based on the Roscoe theory (D-EMT).

From KD's equation, φ must be redefined due to the continuum liquid phase that is trapped by the aggregates or clusters. Quemada proposed the following modification for the KD equation:

$$\eta_r = \left(1 - \frac{\varphi_{eff}}{\varphi_m}\right)^{-[\eta]\varphi_m} \tag{5-5}$$

Where φ_m and φ_{eff} are setting parameters. Assuming that emulsions have the same behavior as a suspension with hard spheres, $[\eta]$ is assumed as a constant $(= 2.5)$. Re-defined $\varphi_{eff} = \varphi\alpha$, one getting

$$\eta_r = \left(1 - \frac{\varphi\alpha}{\varphi_m}\right)^{-[\eta]\varphi_m} \tag{5-6}$$

Or

$$\eta_r = \left(1 - \frac{\varphi}{\varphi_{PK}}\right)^{-[\eta]\varphi_m} \tag{5-7}$$

Where $\varphi_{PK} = \frac{\varphi_m}{\alpha}$ is defined as "effective maximum packing". This equation has been used at a specific shear rate because there is not a direct relation between the relative viscosity and the shear rate. For this reason, in this work, a methodology to solve the viscosity dependence with the shear rate using the Quemada concentration-equation (Eq. 5-6) is proposed ($\eta_r = \eta_r(\varphi, \dot{\gamma})$). φ_{PK} and φ_m are the parameters that relate to $\dot{\gamma}$. Finally, after its optimizing, they are used to solve the KD equation and then built the flow curve for all concentrations of the same oil system.

Specifically, the presented methodology consists in taking, at constant shear rate, the relative viscosity experimental data for various concentrations and fitting them into a concentration equation (eq. 5-6). The best φ_m and φ_{PK} values that fit the concentration group at each shear rate are found. Therefore, two curves that relate these parameters with the shear rate are obtained.

This methodology optimizes the fitting parameters minimizing the mean squared error (MSE). In statistics, the MSE measures the average of the squares of the errors, i.e., the average squared difference between the estimated values and the actual value $(e = (Y_i^{exp} - Y_i^{calc}))$. The MSE formula is written as

$$f_{min} = MSE = \frac{1}{n}\sum_{i=1}^{n}(Y_i^{exp} - Y_i^{calc})^2 \tag{5-8}$$

In this work, the first optimization function (f_{min}^1) was calculated by the following equation:

$$f_{min}^1(\varphi_{PK}^{f^1}) = \frac{1}{N_\varphi}\sum_{i=1}^{N_\varphi}(\eta_{r,i}^{cal} - \eta_{r,i}^{exp})^2 \quad \text{for} \quad \dot{\gamma} = constant \tag{5-9}$$

Where η_i^{cal} is calculated by Equation 5-6 and N_φ is the total number of η_i^{exp}

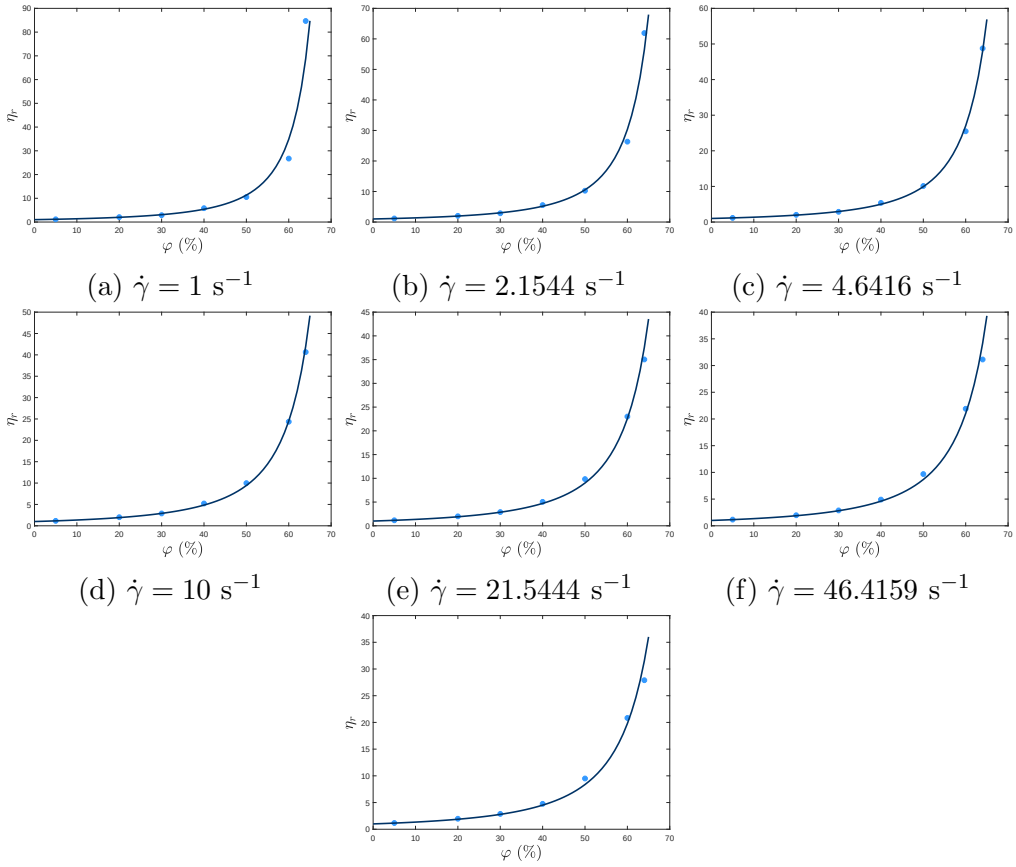

(a) $\dot{\gamma} = 1\ s^{-1}$ (b) $\dot{\gamma} = 2.1544\ s^{-1}$ (c) $\dot{\gamma} = 4.6416\ s^{-1}$

(d) $\dot{\gamma} = 10\ s^{-1}$ (e) $\dot{\gamma} = 21.5444\ s^{-1}$ (f) $\dot{\gamma} = 46.4159\ s^{-1}$

(g) $\dot{\gamma} = 100\ s^{-1}$

Figure 5.4: Viscosity-concentration fit for each shear rate for emulsions from Crude A. The symbols are the experimental dates (●) and the line is the curve fitted (—).

associated to each φ. Then, the best φ_{PK}^{f1} for each $\dot{\gamma}$ is obtained. Therefore, a curve of $\varphi_{PK} f^1 = f(\dot{\gamma})$ is built. The second optimization equation is chosen by observation, i.e., initially, a first-run is done and depending on the generated curve (e.g. exponential, polynomial, etc), a mathematical equation that best represents it is proposed. A function of data's tendency of the curve for this system was proposed as being:

$$\varphi_{PK}^{calc} = \varphi_m(1 + a\dot{\gamma}^{-b}) \tag{5-10}$$

The second optimization function ($f_{min}^2(\varphi_m, a, b)$) was

$$f_{min}^2(\varphi_m, a, b) = \frac{1}{N_{\dot{\gamma}}} \sum_{i=1}^{N_{\dot{\gamma}}} (\varphi_{PK,i}^{f_1} - \varphi_{PK,i}^{calc})^2 \tag{5-11}$$

The calculation algorithm is in Appendix D (See Fig. **E.2**). A Matlab program and its functions *Optimset* and *fmsearch* as optimization functions were

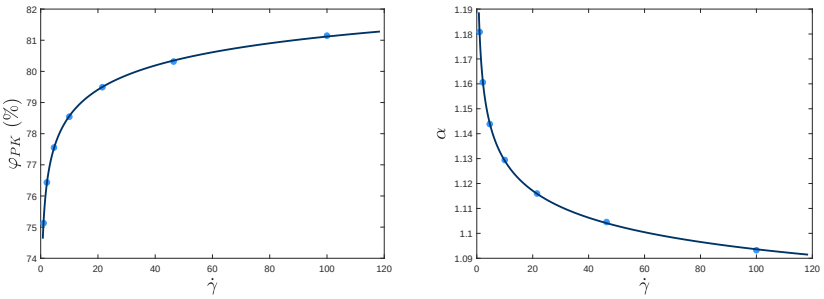

(a) φ_{PK} vs $\dot{\gamma}$ (b) α vs $\dot{\gamma}$

Figure 5.5: Fitting parameters from KD's equation for emulsions from Crude A. The symbols are the experimental dates (●) and the line is the curve fitted (——).

used.

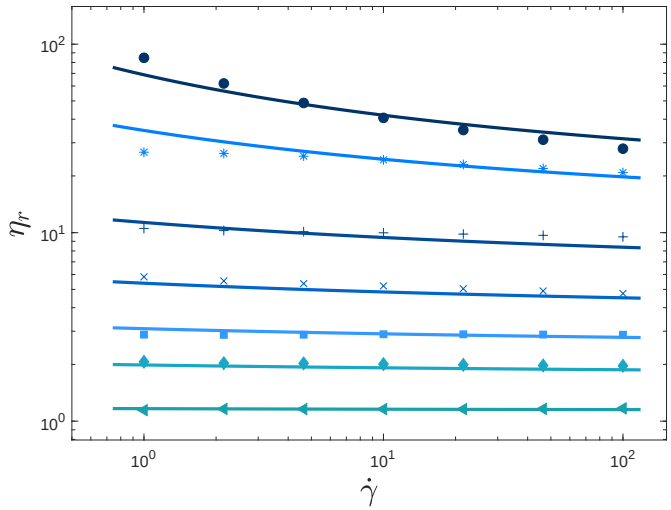

Figure 5.6: Experimental data of emulsions from Crude A fitted with the KD's equation. The symbols are the experimental data and the continuous lines are fitted curves. $\varphi = 64\%$ (—●—), $\varphi = 50\%$ (—✳—), $\varphi = 40\%$ (—+—), $\varphi = 30\%$ (—×—),$\varphi = 20\%$ (—■—),$\varphi = 5\%$ (—◆—)

As an example of the setting, the viscosity-concentration figures for each value of $\dot{\gamma}$ for emulsions from crude A are presented in Figure **5.4**. The φ_{PK} and φ_m curves were plotted in Figures **5.5**a and **5.5**b, respectively. φ_m increased with $\dot{\gamma}$, starting at a value near 65% and finishing near the unit for higher values of $\dot{\gamma}$. This result is certainly coherent since as the droplets can suffer deformation and the structure under shearing may be rearranged, φ_m can be higher than the geometrically allowed value. For φ_{PK}, the change was less than φ_m, achieving a constant value near 80%. These adjusted parameters are used to solve KD equation and built the Figure **5.6** for emulsion from crude A. The curve showed a good fitting for all concentration. The Newtonian emulsions had a better fitting than the non-Newtonian emulsions.

In general, KD's is a good empirical equation to model simple suspension cases. Quemada's equation help to understand the most relevant parameters and their limitations. Nevertheless, its supposition that $[\eta]$ is constant is not totally true, as explained below.

5.3 Dealing with clusters as sub-systems

Flocculation promotes local variations in the droplet concentration, i.e., a concentration gradient of droplets throughout the emulsion. Therefore, the flocs can be regarded as sub-systems of a droplets aggregates group, which will form a structure.

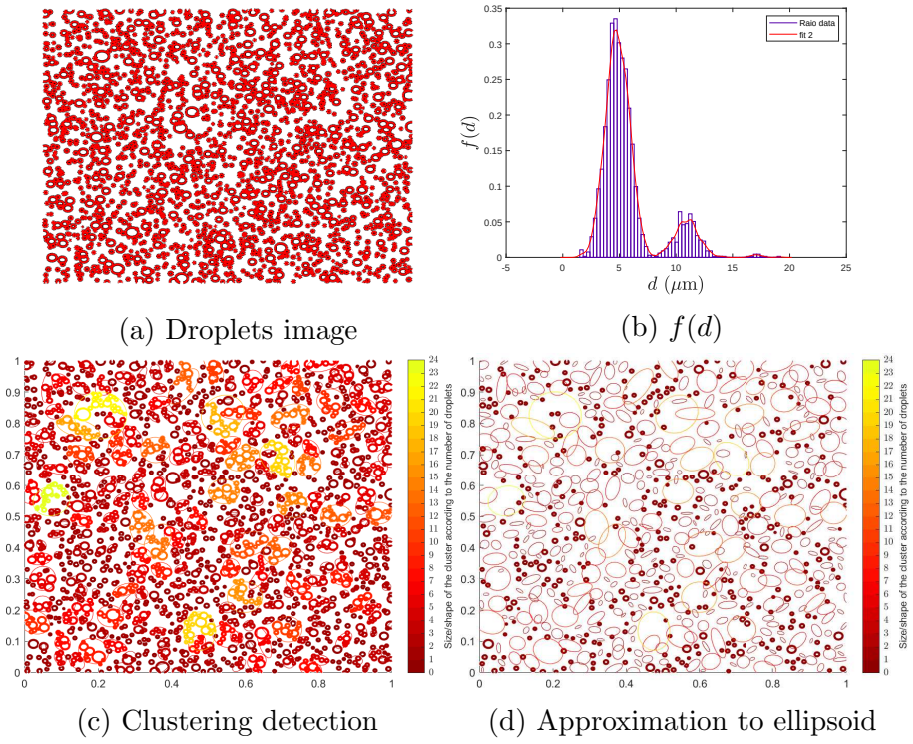

(a) Droplets image (b) $f(d)$

(c) Clustering detection (d) Approximation to ellipsoid

Figure 5.7: Schematic size distribution of droplets aggregated when is regarded as sub-systems

Two systems, both composed of different sized droplet aggregate sub-systems, are schematized in figures **5.7** and **5.8**. Both examples have the same number of droplets (1000 droplets) with the same $f(d)$ (polydisperse). The spatial distribution and $f(d)$ were generated by `rand` function in Matlab®. A software to measure the size of a cluster and its number of droplets was programmed in MatLab . All the details of the program are in Appendix C.

Figures **5.7**a and **5.8**a show the droplets spatially distributed, being one different than the other. Figures **5.7**b and **5.8**b are the $f(d_p)$'s for each example,

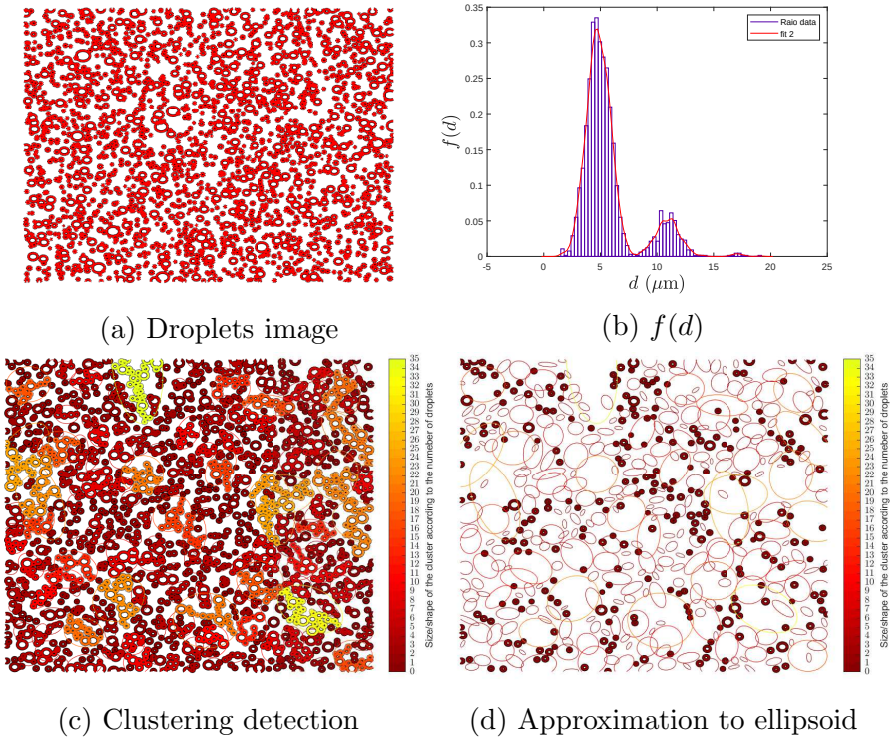

(a) Droplets image (b) $f(d)$

(c) Clustering detection (d) Approximation to ellipsoid

Figure 5.8: Schematic size distribution of droplets aggregated when is regarded as sub-systems

both equal because the droplets have the same sizes and same quantities. Owing to droplets spatial distribution, some different clusters or sub-systems were created. The bar color illustrates the number of droplets that each sub-system has, being: red, the individual droplets and yellow, the highest number of droplets (see Fig. **5.7**c and **5.8**c). For each example, two different sizes and shapes with the same quantity of droplets can be observed. Consequently, it is possible demonstrate that for an emulsion with the same $f(d_p)$ and droplets number, different random shapes and size distributions of sub-systems can be obtained (Fig. **5.7**d and **5.8**d).

The emulsion viscosity will depend on this aggregation state given by the flocculation process, as was demonstrated in the previous chapters. During the emulsion preparation small flocs (or sub-systems of aggregates) may be formed, generated due to strong potential energy in the first minimum point. The value of this minimum point will determine how aggregated the system will be. If the first minimum is not strong and the second minimum has a strong value, the structure will be more porous, resulting in a higher viscosity owing to the formed structure. A schematic representation of this is shown in Figure **5.9**. The flocculation depends on the emulsion's storage time and shear history, as was corroborated in Chapter 2. Different samples of the same emulsion may have different aggregation states even before the start of a rheological test. This will depend on its shearing history, i.e.

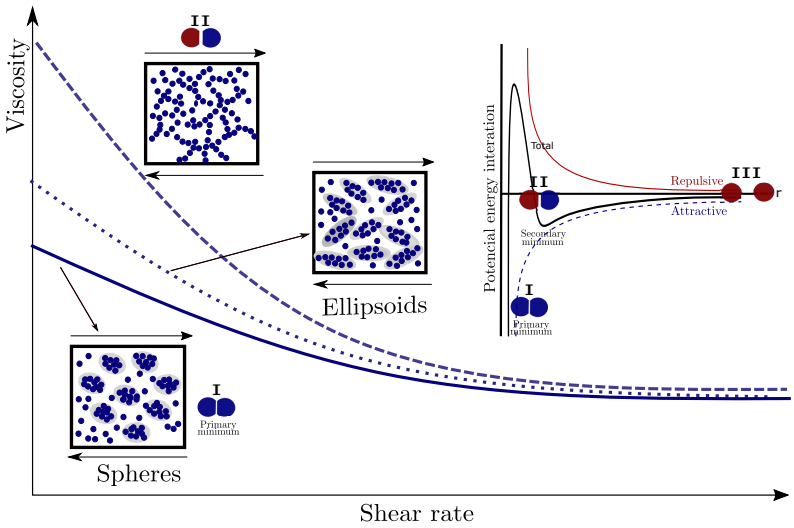

Figure 5.9: Schematic illustration of the relation between the emulsion structure and its viscosity answer under shearing

polydispersity and shape of sub-systems. Nevertheless, these samples may achieve the same viscosity at higher shearing rates since the emulsion's sub-systems achieve the same size at this condition. This is due to the breakage of the flocculated system, orginally composed of heterogeneous sub-systems.

This can explain because the emulsion's sub-systems achieve the same size when is under high values of shearing due to breakage of the flocculated system originally composed for heterogeneous sub-system, as it is represented schematically in Figure **5.9**.

In sum, an emulsion must be seen/faced as a system composed of sub-sytems with different distribution sizes and shapes and not as droplets units. Therefore, some equation parameters for modeling its rheology behavior must be reanalyzed. For instance, the parameter φ_m and $[\eta]$ that is associated with particle shape, must be treated as fitting parameters due to the shape and polydispersity of these sub-systems, instead of unitary particles and droplets. Since these are shear-rate dependant, so must be the aforementioned parameters.

5.3.1 Shear-rate dependence of intrinsic viscosity ($[\eta]$)

The intrinsic viscosity is generally defined as

$$[\eta] = \lim_{\varphi \to \infty} = \frac{\eta - \eta_0}{\varphi \eta_0} \tag{5-12}$$

Einstein estimated it as being equal to 2.5 for a dilute hard sphere suspension [25]. This value was corrected later by experimental observations

[8]. This value can suffer a deviation often ascribed to small particle asphericity or particle clustering. As an example, nearly spherical particles in low-concentration suspensions ($< 1\%$) are commonly given a value of 2.7, corroborated experimentally [23]. Despite the fundamental importance in determining $[\eta]$, there are few analytical developments to nonspherical objects due to the number of necessary approximations [8, 41]. Besides, the formalism required to treat these more general shapes is complicated because there is limited progress in the solution of the steady-state Navier-Stokes equation. For that reason, developing experimental relations between electrical properties and geometric parameters of particle shape has been highly used to approximate the $[\eta]$ variation. [8] define the "aspect ratio" $A_f = (c/a)$ as a measure of particle asymmetry. Being $A_f > 1$ for prolate ellipsoids (approximating fibers), $A_f = 1$ for spheres, and $A_f < 1$ for oblate ellipsoids (approximating plate-lets). This parameter was associated with $[\eta]$ by an equation and experimental curve [8, 23].

On the other hand, in these specific emulsions, surface tension or internal pressure tends to make the droplet resistant to any deformation due to the small size of its droplets. Therefore, the droplets can be considered as an undeformable system. This conclusion is corroborated by the experimental results presented in Chapter 3. Now, knowing that the droplets do not change their size, but there is flocculation, one can conclude that the flocculation, and consequently, the emulsion viscosity is associated with the organization (ou arrangement) of these sub-systems and theirs changes of sizes.

5.4 Generalization of Sudduth's equation for shear dependence

Sudduth (1993) proposed a general concentration-equation ($\eta_r = f(\varphi)$) [103]. He observed the similarities between the derivation of various concentration-equations and analyzed the best way to associate the most relevant parameters into the same general equation. The general Sudduth equation is:

$$\ln(\eta_r) = (-[\eta]\varphi_m)\left(\frac{1}{\sigma - 1}\right)\left[\left(1 - \frac{\varphi}{\varphi_m}\right)^{1-\sigma} - 1\right] \tag{5-13}$$

If σ is changed, different famous equations for suspended systems can be obtained. For instance, the KD equation can be deduced if σ is equal to 1 and $[\eta]$ equal to $5/2$. Other equations and their corresponding σ value are in Table **2.2**. Due to its simples generalization and its few fitting parameters, this equation was chosen as the best equation to be used to fit the experimental data. Similar

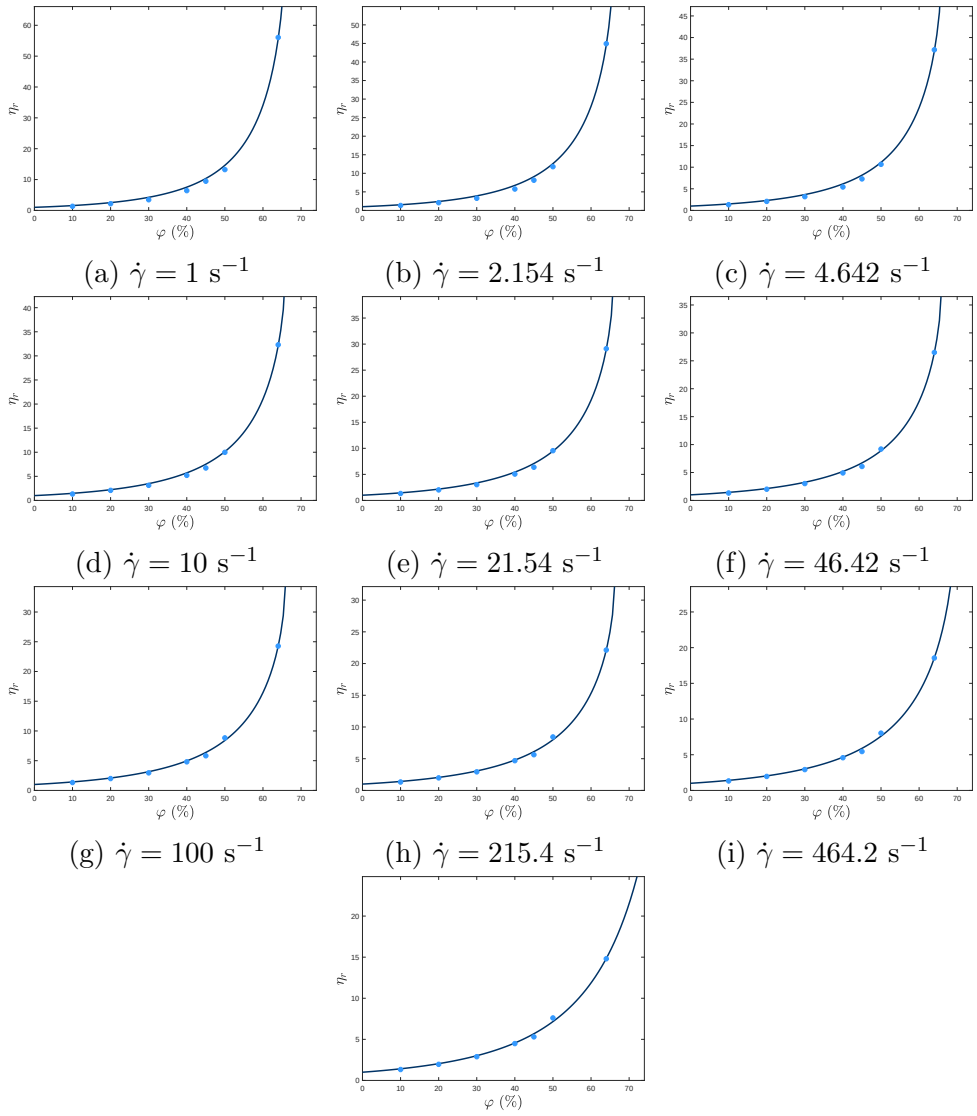

(a) $\dot{\gamma} = 1\ \mathrm{s}^{-1}$ (b) $\dot{\gamma} = 2.154\ \mathrm{s}^{-1}$ (c) $\dot{\gamma} = 4.642\ \mathrm{s}^{-1}$

(d) $\dot{\gamma} = 10\ \mathrm{s}^{-1}$ (e) $\dot{\gamma} = 21.54\ \mathrm{s}^{-1}$ (f) $\dot{\gamma} = 46.42\ \mathrm{s}^{-1}$

(g) $\dot{\gamma} = 100\ \mathrm{s}^{-1}$ (h) $\dot{\gamma} = 215.4\ \mathrm{s}^{-1}$ (i) $\dot{\gamma} = 464.2\ \mathrm{s}^{-1}$

(j) $\dot{\gamma} = 1000\ \mathrm{s}^{-1}$

Figure 5.10: Viscosity-concentration fit for each shear rate. The symbols are the experimental dates (●) and the line is the curve fitted (——).

to the previous methodology, one algorithm for solving this equation in the form $\eta_r = f(\varphi, \dot{\gamma})$ was implemented.

Its fitting parameter are: σ,φ_m,$(\dot{\gamma})$ and $[\eta](\dot{\gamma})$. The first function to optimize was

$$f^1_{min}(\varphi_m, [\eta]) = \frac{1}{N_\varphi} \sum_{i=1}^{N_\varphi} (\eta^{cal}_{r,i} - \eta^{exp}_{r,i})^2 \quad \text{for} \quad \dot{\gamma} = constant \tag{5-14}$$

η^{cal}_r was calculated by Equation5-13. The second optimization system were 5-15 and 5-16. $f^2_{min,1}$ and $f^2_{min,2}$ were chosen by observation of curve behaviors. A second order polynomial equation was fitted to $\varphi^{f^1}_{m,i}$ and $[\eta]^{f^1}_i$ curves. The

parameter of two polynomial equations is in Appendix D, Table **E.1**.

$$f^2_{min,1}(x) = \frac{1}{N_{\dot{\gamma}}} \sum_{i=1}^{N_{\dot{\gamma}}} ([\eta]_i^{f^1} - [\eta]_i^{calc})^2 \tag{5-15}$$

$$f^2_{min,2}(x) = \frac{1}{N_{\dot{\gamma}}} \sum_{i=1}^{N_{\dot{\gamma}}} (\varphi_{m,i}^{f^1} - \varphi_{m,i}^{calc})^2 \tag{5-16}$$

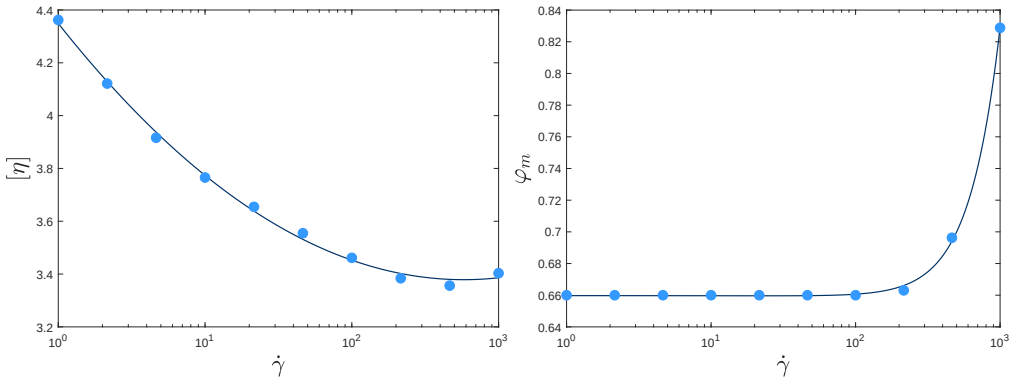

(a) $[\eta]$ vs $\dot{\gamma}$ (b) φ_m vs $\dot{\gamma}$

Figure 5.11: Variation of fit parameters with the shear rate using the Sudduth's equation. Symbols are the values fitted (●) with the equation and the line is the quadratic polynomial fit of results (—).

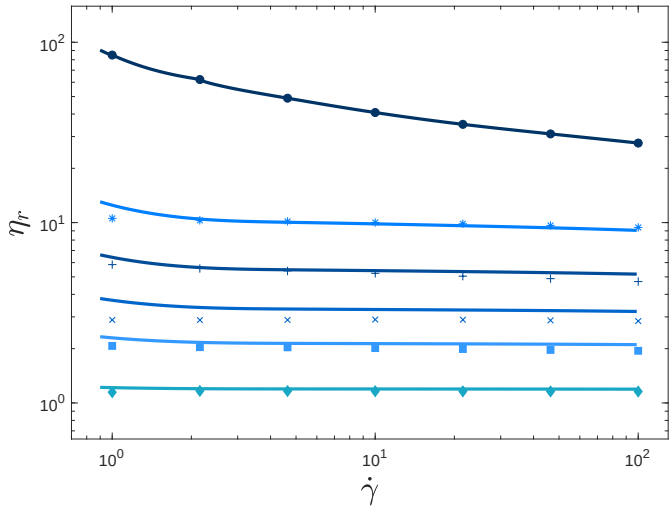

Figure 5.12: Experimental data of Crude A fitted with the Sudduth's equation. The symbols are the experimental data and the continuous lines are fitted curves. $\varphi = 64\%$ (—●—), $\varphi = 50\%$ (—✳—), $\varphi = 40\%$ (—+—), $\varphi = 30\%$ (—×—),$\varphi = 20\%$ (—■—),$\varphi = 5\%$ (—◆—)

The viscosity-concentration figures for each $\dot{\gamma}$ are presented in Figure **5.10**. Emulsion B was used as a calculation example. For each $\dot{\gamma}$, equation 5-13 was applied setting $[\eta]$ and φ_m. Their relations with shear rate were plotted in Figure

5.11. $[\eta] = f(\dot{\gamma})$ varied between 3.9 for lower shear rate and 3.3 for the highest shear rate. Therefore, A_f varied from a prolate ellipsoid ($A_f \sim 4$) tendency almost spherical shape ($A_f \sim 2$) with the increase of shearing. The maximum packing fraction (φ_m) exhibited a similar behavior in both the KD and Sudduth fittings: it increases with the increase of shear rate due to a better arrangement of the system when these sub-systems are broken. σ was equal to 0.45 for emulsion A and 0.36 for emulsion B.

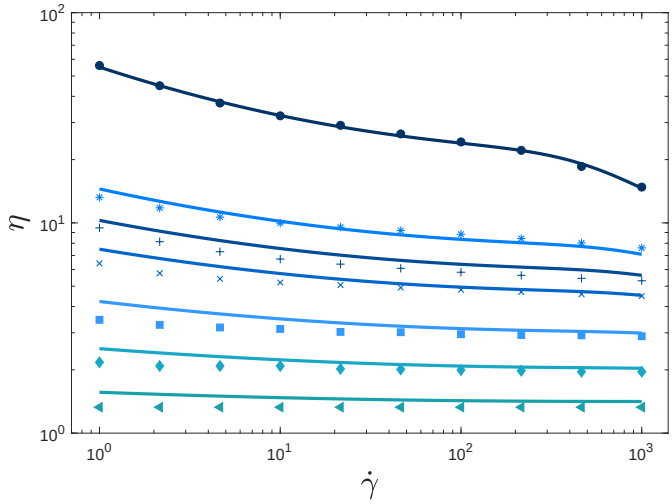

Figure 5.13: Experimental data of Crude A fitted with the Sudduth's equation. The symbols are the experimental data and the continuous lines are fitted curves. $\varphi = 64\%$ (●), $\varphi = 50\%$ (✳), $\varphi = 45\%$ (+), $\varphi = 40\%$ (×),$\varphi = 30\%$ (■),$\varphi = 20\%$ (◆),$\varphi = 10\%$ (◀)

It is likely that the values are similar because both oils have similarities in their chemical composition (both are light oils). Also, the structure of the asphaltenes molecules in these oils are likely to be similar. For all emulsions of both crude, a good correlation between the data and fitting was observed. Observing Figure **5.12** for emulsion A and Figure **5.13** for emulsion B, one can note that Sudduth equation had a better fit for non-Newtonian emulsions than the fitting obtained using KD equation.

5.5 Comments

The methodology presented in this chapter permits to solve a formulation $\eta_r = f(\varphi, \dot{\gamma})$ using a typical concentration-viscosity equation ($\eta_r = f(\varphi)$). The Pal method is an example of a solution to this kind of formulation. However, ambiguities in its derivation were demonstrated, rendering it unemployable. The generalization of KD's is a good empirical equation to model a simple suspension

case. A good fitting of experimental data was achieved by applying this methodology. Nevertheless, its supposition that $[\eta]$ is constant is not a good assumption, as was demonstrated and analyzed in the previous chapters. An emulsion system should not be assumed to be a group of individual droplets. Otherwise, it should be treated as a system composed of sub-systems of droplet aggregates (flocks) with different shapes and widely polydisperse. Therefore, this methodology was applied to the general Sudduth equation. The parameters $[\eta]$ and φ_m were related to the shear rate and σ was associated with characteristics of the systems, i.e, it depends on the kind of interactions involved, being constant for each system. Finally, the methodology showed a good fitting of experimental data, validating its application.

6
Conclusions

There are many studies and equations that aim the understand and prediction of the emulsion behavior. However, there is still a complex microscopic world to be discovered and modeled. This work was a small effort towards that, and some conclusion were drawn:

1. At the experimental side: the emulsification process determines emulsion properties such as d_p, $f(x)$, φ_m, and φ^{st}. Moreover, the emulsion behavior will be defined by $\eta = f(\dot{\gamma}, \varphi)$. The existence of a flocculation phenomenon, irreversible and shear history dependent, was observed. The concentrated emulsion showed a non-stable or non-equilibrium condition for low shear rates. This may be explained due to constant changes in the structure given by the struggle between Brownian and hydrodynamic forces at this level of stress.

2. The thermodynamic analysis provides us an idea of the emulsion's rheological answer, giving the concentration critical point in which its type of behavior will change. The φ_{crit} is also dependent on the chosen emulsion's parameters and chemical characteristics.

3. The presented methodology permits to solve a formulation $\eta_r = f(\varphi, \dot{\gamma})$ using a typical concentration-viscosity equation ($\eta_r = f(\varphi)$). The methodology was applied to the general Sudduth equation. The parameters $[\eta]$ and φ_m were related to the shear rate and σ was associated with characteristics of the systems, i.e, depends on the kind of interactions involved, being constant for each system. An emulsion system should not be assumed to be a group of individual droplets. Otherwise, it should be treated as a system composed of sub-systems of droplet aggregates (flocks) with different shapes and widely polydisperse. Finally, the methodology showed a good fitting of experimental data, validating its application.

Future works

Additionally, according to everything previously mentioned, some futures works are proposed:

1. To do rheological experiments with a deeper analysis of the flocculation/aggregation process and the non-equilibrium point when emulsion concentration is above the concentration glass point.

2. To do the same thermodynamic analysis for other emulsion systems with different chemical characteristics and compare them with the rheological answer. To modify the model to include the polydispersity of droplets.

3. To develop a microscale model based on statistics in order to predict the formation and breakage of complex random structures of aggregates under shear.

References

[1] Astm standard d1141-98, 2013, "standard practice for the preparation of substitute ocean water", 2013.

[2] Ancheyta, J., Trejo, F., and Rana, M. S. *Asphaltenes: Chemical Transformation during Hydroprocessing of Heavy Oils (Chemical Industries Book 126)*. CRC Press, 2010.

[3] Anderson, V. J., and Lekkerkerker, H. N. W. Insights into phase transition kinetics from colloid science. *Nature 416*, 6883 (apr 2002), 811–815.

[4] Arrhenius, S. Über die innere reibung verdünnter wässeriger lösungen. *Zeitschrift für Physikalische Chemie 1U*, 1 (jan 1887).

[5] Balsamo, M., Erto, A., and Lancia, A. Chemical demulsification of model water-in-oil emulsions with low water content by means of ionic liquids. *Brazilian Journal of Chemical Engineering 34*, 1 (jan 2017), 273–282.

[6] Barnes, H. A. Rheology of emulsions — a review. *Colloids and Surfaces A: Physicochemical and Engineering Aspects 91* (nov 1994), 89–95.

[7] Batchelor, G. K. The effect of brownian motion on the bulk stress in a suspension of spherical particles. *Journal of Fluid Mechanics 83*, 1 (nov 1977), 97–117.

[8] Bicerano, J., Douglas, J. F., and Brune, D. A. Model for the viscosity of particle dispersions. *Journal of Macromolecular Science, Part C: Polymer Reviews 39*, 4 (sep 1999), 561–642.

[9] Bredée, H. L., and Booys, J. Kritische auswertung der viskositäts-konzentrationsformeln kolloider lösungen. i. *Kolloid-Zeitschrift 79*, 1 (apr 1937), 31–43.

[10] Bullard, J. W., Pauli, A. T., Garboczi, E. J., and Martys, N. S. A comparison of viscosity–concentration relationships for emulsions. *Journal of Colloid and Interface Science 330*, 1 (feb 2009), 186–193.

[11] Butt, H.-J., Butt, H.-J. B., Graf, K., and Kappl, M. *Physics and chemistry of interfaces*. John Wiley & Sons, 2003.

[12] Chang, J., and Sandler, S. I. A real function representation for the structure of the hard-sphere fluid. *Molecular Physics 81*, 3 (feb 1994), 735–744.

[13] Choi, S. J., and Schowalter, W. R. Rheological properties of nondilute suspensions of deformable particles. *Physics of Fluids 18*, 4 (1975), 420.

[14] Chong, J. S., Christiansen, E. B., and Baer, A. D. Rheology of concentrated suspensions. *Journal of Applied Polymer Science 15*, 8 (aug 1971), 2007–2021.

[15] Coussot, P. Introduction to the rheology of complex fluids. In *Understanding the Rheology of Concrete*. Elsevier, 2012, pp. 3–22.

[16] Cross, M. M. Rheology of non-newtonian fluids: A new flow equation for pseudoplastic systems. *Journal of Colloid Science 20*, 5 (jun 1965), 417–437.

[17] Curtis, R., Newman, J., Blanch, H., and Prausnitz, J. Mcmillan-mayer solution thermodynamics for a protein in a mixed solvent. *Fluid Phase Equilibria 192*, 1-2 (dec 2001), 131–153.

[18] Dan, D., and Jing, G. Apparent viscosity prediction of non-newtonian water-in-crude oil emulsions. *Journal of Petroleum Science and Engineering 53*, 1-2 (aug 2006), 113–122.

[19] Danov, K. D. On the viscosity of dilute emulsions. *Journal of Colloid and Interface Science 235*, 1 (mar 2001), 144–149.

[20] de Gennes, P. Conjectures on the transition from poiseuille to plug flow in suspensions. *Journal de Physique 40*, 8 (1979), 783–787.

[21] Derkach, S. R. Rheology of emulsions. *Advances in Colloid and Interface Science 151*, 1-2 (oct 2009), 1–23.

[22] Dicharry, C., Arla, D., Sinquin, A., Graciaa, A., and Bouriat, P. Stability of water/crude oil emulsions based on interfacial dilatational rheology. *Journal of Colloid and Interface Science 297*, 2 (may 2006), 785–791.

[23] Douglas, J. F., and Garboczi, E. J. *Intrinsic viscosity and the polarizability of particles having a wide range of shapes*, vol. 91. Advances in chemical physics, 1995.

[24] Eilers, H. Die viskosität von emulsionen hochviskoser stoffe als funktion der konzentration. *Kolloid-Zeitschrift 97*, 3 (dec 1941), 313–321.

[25] Einstein, A. Eine neue bestimmung der moleküldimensionen. *Annalen der Physik 324*, 2 (1906), 289–306.

[26] Ese, M.-H., and Kilpatrick, P. K. Stabilization of water-in-oil emulsions by naphthenic acids and their salts: Model compounds, role of pH, and soap:acid ratio. *Journal of Dispersion Science and Technology 25*, 3 (dec 2004), 253–261.

[27] Fan, Y., Simon, S., and Sjöblom, J. Interfacial shear rheology of asphaltenes at oil–water interface and its relation to emulsion stability: Influence of concentration, solvent aromaticity and nonionic surfactant. *Colloids and Surfaces A: Physicochemical and Engineering Aspects 366*, 1-3 (aug 2010), 120–128.

[28] Farris, R. J. Prediction of the viscosity of multimodal suspensions from unimodal viscosity data. *Transactions of the Society of Rheology 12*, 2 (jul 1968), 281–301.

[29] Fortuny, M., Oliveira, C. B. Z., Melo, R. L. F. V., Nele, M., Coutinho, R. C. C., and Santos, A. F. Effect of salinity, temperature, water content, and pH on the microwave demulsification of crude oil emulsions†. *Energy & Fuels 21*, 3 (may 2007), 1358–1364.

[30] Frankel, N., and Acrivos, A. On the viscosity of a concentrated suspension of solid spheres. *Chemical Engineering Science 22*, 6 (jun 1967), 847–853.

[31] Gal-Or, B., and Waslo, S. Hydrodynamics of an ensemble of drops (or bubbles) in the presence or absence of surfactants. *Chemical Engineering Science 23*, 12 (dec 1968), 1431–1446.

[32] Gallier, S., Lemaire, E., Peters, F., and Lobry, L. Percolation in suspensions and de gennes conjectures. *Physical Review E 92*, 2 (aug 2015).

[33] Gasser, U. Real-space imaging of nucleation and growth in colloidal crystallization. *Science 292*, 5515 (apr 2001), 258–262.

[34] Goual, L., and Firoozabadi, A. Measuring asphaltenes and resins, and dipole moment in petroleum fluids. *AIChE Journal 48*, 11 (nov 2002), 2646–2663.

[35] Hall, K. R. Another hard-sphere equation of state. *The Journal of Chemical Physics 57*, 6 (sep 1972), 2252–2254.

[36] Hamaker, H. The london - van der waals attraction between spherical particles. *Physica 4*, 10 (oct 1937), 1058–1072.

[37] Hess, W., Vilgis, T. A., and Winter, H. H. Dynamical critical behavior during chemical gelation and vulcanization. *Macromolecules 21*, 8 (aug 1988), 2536–2542.

[38] Ho, W., and Hall, W. F. Measurements of the dielectric properties of seawater and NaCl solutions at 2.65 GHz. *Journal of Geophysical Research 78*, 27 (sep 1973), 6301–6315.

[39] Hu, Y.-T., Ting, Y., Hu, J.-Y., and Hsieh, S.-C. Techniques and methods to study functional characteristics of emulsion systems. *Journal of Food and Drug Analysis 25*, 1 (jan 2017), 16–26.

[40] Ilyin, S., Arinina, M., Polyakova, M., Bondarenko, G., Konstantinov, I., Kulichikhin, V., and Malkin, A. Asphaltenes in heavy crude oil: Designation, precipitation, solutions, and effects on viscosity. *Journal of Petroleum Science and Engineering 147* (nov 2016), 211–217.

[41] Jan Mewis, N. J. W. *Colloidal suspension rheology*. Cambridge University Press, 2016.

[42] Jeffrey, D. J., and Acrivos, A. The rheological properties of suspensions of rigid particles. *AIChE Journal 22*, 3 (may 1976), 417–432.

[43] Kamal, M., and Mutel, A. Rheological properties of suspensions in newtonian and non-newtonian fluids. *Journal of Polymer Engineering 5*, 4 (oct 1985).

[44] Kincaid, J., and Weis, J. Radial distribution function of a hard-sphere solid. *Molecular Physics 34*, 4 (oct 1977), 931–938.

[45] Krieger, I. M., and Dougherty, T. J. A mechanism for non-newtonian flow in suspensions of rigid spheres. *Transactions of the Society of Rheology 3*, 1 (mar 1959), 137–152.

[46] Leiva, J., and Geffroy, E. Evolution of the size distribution of an emulsion under a simple shear flow. *Fluids 3*, 3 (jun 2018), 46.

[47] Liu, C., Li, M., Han, R., Li, J., and Liu, C. Rheology of water-in-oil emulsions with different drop sizes. *Journal of Dispersion Science and Technology 37*, 3 (sep 2015), 333–344.

[48] Macosko, C. W. *Rheology: Principle, measurements, and Applications*. Wiley-Blackwell, 1994.

[49] Malkin, A. Y., Masalova, I., Slatter, P., and Wilson, K. Effect of droplet size on the rheological properties of highly-concentrated w/o emulsions. *Rheologica Acta 43*, 6 (apr 2004), 584–591.

[50] Marchesini, F. H., Alicke, A. A., de Souza Mendes, P. R., and Ziglio, C. M. Rheological characterization of waxy crude oils: Sample preparation. *Energy & Fuels 26*, 5 (mar 2012), 2566–2577.

[51] Maron, S. H., and Pierce, P. E. Application of ree-eyring generalized flow theory to suspensions of spherical particles. *Journal of Colloid Science 11*, 1 (feb 1956), 80–95.

[52] Mason, T. G. New fundamental concepts in emulsion rheology. *Current Opinion in Colloid & Interface Science 4*, 3 (jun 1999), 231–238.

[53] McMillan, W. G., and Mayer, J. E. The statistical thermodynamics of multicomponent systems. *The Journal of Chemical Physics 13*, 7 (jul 1945), 276–305.

[54] Mills, P. Non-newtonian behaviour of flocculated suspensions. *Journal de Physique Lettres 46*, 7 (1985), 301–309.

[55] Mooney, M. The viscosity of a concentrated suspension of spherical particles. *Journal of Colloid Science 6*, 2 (apr 1951), 162–170.

[56] Moreno, R., and Bannier, E. Feedstock suspensions and solutions. In *Future Development of Thermal Spray Coatings*. Elsevier, 2015, pp. 51–80.

[57] Mueller, S., Llewellin, E. W., and Mader, H. M. The rheology of suspensions of solid particles. *Proceedings of the Royal Society A: Mathematical, Physical and Engineering Sciences 466*, 2116 (dec 2009), 1201–1228.

[58] Norton, F. H., Johnson, A. L., and Lawrence, W. G. Fundamental study of clay: Vi, flow properties of keolinite-water suspension. *Journal of the American Ceramic Society 27*, 5 (may 1944), 149–164.

[59] Oldroyd, J. G. The elastic and viscous properties of emulsions and suspensions. *Proceedings of the Royal Society of London. Series A. Mathematical and Physical Sciences 218*, 1132 (jun 1953), 122–132.

[60] Otsubo, Y., and homme, R. K. P. Effect of drop size distribution on the flow behavior of oil-in-water emulsions. *Rheologica Acta 33*, 4 (1994), 303–306.

[61] Otsubo, Y., and Prudhomme, R. K. Rheology of oil-in-water emulsions. *Rheologica Acta 33*, 1 (1994), 29–37.

[62] Paar, A. The influence of particles on suspension rheology. https://wiki.anton-paar.com/en/the-influence-of-particles-on-suspension-rheology/.

[63] Pabst, W., Gregorová, E., and Berthold, C. Particle shape and suspension rheology of short-fiber systems. *Journal of the European Ceramic Society 26*, 1-2 (jan 2006), 149–160.

[64] Pal, R. Evaluation of the mooney viscosity/concentration equation for liquid-liquid emulsions. *Chemical Engineering Communications 89*, 1 (mar 1990), 209–214.

[65] Pal, R. Effect of droplet size on the rheology of emulsions. *AIChE Journal 42*, 11 (nov 1996), 3181–3190.

[66] Pal, R. Scaling of relative viscosity of emulsions. *Journal of Rheology 41*, 1 (jan 1997), 141–150.

[67] Pal, R. A novel method to correlate emulsion viscosity data. *Colloids and Surfaces A: Physicochemical and Engineering Aspects 137*, 1-3 (jun 1998), 275–286.

[68] Pal, R. Novel viscosity equations for emulsions of two immiscible liquids. *Journal of Rheology 45*, 2 (mar 2001), 509–520.

[69] Pal, R. Modeling the viscosity of concentrated nanoemulsions and nanosuspensions. *Fluids 1*, 2 (apr 2016), 11.

[70] Pal, R. Modeling and scaling of the viscosity of suspensions of asphaltene nanoaggregates. *Energies 10*, 6 (jun 2017), 767.

[71] Pal, R. A simple model for the viscosity of pickering emulsions. *Fluids 3*, 1 (dec 2017), 2.

[72] Pal, R. Viscosity-concentration relationships for nanodispersions based on glass transition point. *The Canadian Journal of Chemical Engineering 95*, 8 (mar 2017), 1605–1614.

[73] Pal, R., and Rhodes, E. A novel viscosity correlation for non-newtonian concentrated emulsions. *Journal of Colloid and Interface Science 107*, 2 (oct 1985), 301–307.

[74] Pal, R., and Rhodes, E. Viscosity/concentration relationships for emulsions. *Journal of Rheology 33*, 7 (oct 1989), 1021–1045.

[75] Pauchard, V., Rane, J. P., Zarkar, S., Couzis, A., and Banerjee, S. Long-term adsorption kinetics of asphaltenes at the oil–water interface: A random sequential adsorption perspective. *Langmuir 30*, 28 (jul 2014), 8381–8390.

[76] Petsev, D. N. Theory of emulsion flocculation. In *Interface Science and Technology*. Elsevier, 2004, pp. 313–350.

[77] Phan-Thien, N., and Pham, D. Differential multiphase models for polydispersed suspensions and particulate solids. *Journal of Non-Newtonian Fluid Mechanics 72*, 2-3 (oct 1997), 305–318.

[78] Pusey, P. N., and van Megen, W. Phase behaviour of concentrated suspensions of nearly hard colloidal spheres. *Nature 320*, 6060 (mar 1986), 340–342.

[79] Quemada, D. Rheology of concentrated disperse systems and minimum energy dissipation principle. *Rheologica Acta 16*, 1 (jan 1977), 82–94.

[80] Quemada, D. Rheological modeling of complex fluids: III. dilatant behavior of stabilized suspensions. *The European Physical Journal Applied Physics 3*, 3 (sep 1998), 309–320.

[81] Quemada, D. Rheological modelling of complex fluids. i. the concept of effective volume fraction revisited. *The European Physical Journal Applied Physics 1*, 1 (jan 1998), 119–127.

[82] Quemada, D. Rheological modelling of complex fluids: II. shear thickening behavior due to shear induced flocculation. *The European Physical Journal Applied Physics 2*, 2 (may 1998), 175–181.

[83] Quemada, D. Rheological modelling of complex fluids: IV: Thixotropic and "thixoelastic? behaviour. start-up and stress relaxation, creep tests and hysteresis cycles. *The European Physical Journal Applied Physics 5*, 2 (feb 1999), 191–207.

[84] Quemada, D., and Berli, C. Energy of interaction in colloids and its implications in rheological modeling. *Advances in Colloid and Interface Science 98*, 1 (apr 2002), 51–85.

[85] Rane, J. P., Zarkar, S., Pauchard, V., Mullins, O. C., Christie, D., Andrews, A. B., Pomerantz, A. E., and Banerjee, S. Applicability of the langmuir equation of state for asphaltene adsorption at the oil–water interface: Coal-derived, petroleum, and synthetic asphaltenes. *Energy & Fuels 29*, 6 (may 2015), 3584–3590.

[86] Rayat, K., and Feyzi, F. Influence of external electric field on the polarity of water droplets in water-in-oil emulsion phase transition. *Colloids and Surfaces A: Physicochemical and Engineering Aspects 375*, 1-3 (feb 2011), 61–67.

[87] Rayat, K., and Feyzi, F. Estimation of the electric field strength required for breaking the water-in-oil emulsion: a thermodynamic approach considering droplets deformation and the effect of interfacial tension. *Fluid Phase Equilibria 316* (feb 2012), 156–163.

[88] Ree, T., and Eyring, H. Theory of non-newtonian flow. i. solid plastic system. *Journal of Applied Physics 26*, 7 (jul 1955), 793–800.

[89] Robinson, J. V. The viscosity of suspensions of spheres. *The Journal of Physical and Colloid Chemistry 53*, 7 (jul 1949), 1042–1056.

[90] Roscoe, R. The viscosity of suspensions of rigid spheres. *British Journal of Applied Physics 3*, 8 (aug 1952), 267–269.

[91] Rutgers, I. R. Relative viscosity and concentration. *Rheologica Acta 2*, 4 (dec 1962), 305–348.

[92] Samaniuk, J. R., Hermans, E., Verwijlen, T., Pauchard, V., and Vermant, J. Soft-glassy rheology of asphaltenes at liquid interfaces. *Journal of Dispersion Science and Technology 36*, 10 (apr 2015), 1444–1451.

[93] Schowalter, W. R., Chaffey, C. E., and Brenner, H. Rheological behavior of a dilute emulsion. *Journal of Colloid and Interface Science 26*, 2 (feb 1968), 152–160.

[94] Schramm, L. L. *Emulsions, Foams, Suspensions, and Aerosols*. Wiley VCH Verlag GmbH, 2014.

[95] Seifert, W. K., and Howells, W. G. Interfacially active acids in a california crude oil. isolation of carboxylic acids and phenols. *Analytical Chemistry 41*, 4 (apr 1969), 554–562.

[96] Silva, F., Tavares, F., and Cardoso, M. Phase transition of water–in–oil emulsions over influence of an external electric field. *Colloids and Surfaces A: Physicochemical and Engineering Aspects 326*, 1-2 (aug 2008), 10–17.

[97] Silva, F. L. M. C., Tavares, F. W., and Cardoso, M. J. E. M. Thermodynamic stability of water-in-oil emulsions. *Brazilian Journal of Petroleum and Gas 7*, 1 (apr 2013), 1–13.

[98] Skodvin, T. *Dielectric properties of flocculated water-in-oil emulsions*. University of Bergen, Department of Chemistry, 1995.

[99] Skodvin, T. *Dielectric Properties of Flocculated Water-in-Oil Emulsions*. PhD thesis, Bergen Univ. (Norway), 1995.

[100] Solana, J. R. *Perturbation theories for the thermodynamic properties of fluids and solids*. CRC Press, 2013.

[101] Spiecker, P. M., and Kilpatrick, P. K. Interfacial rheology of petroleum asphaltenes at the oil-water interface. *Langmuir 20*, 10 (may 2004), 4022–4032.

[102] Storey, B. T., and Merrill, E. W. The rheology of aqueous solutions of amylose and amylopectin with reference to molecular configuration and

intermolecular association. *Journal of Polymer Science 33*, 126 (dec 1958), 361–375.

[103] Sudduth, R. D. A generalized model to predict the viscosity of solutions with suspended particles. i. *Journal of Applied Polymer Science 48*, 1 (apr 1993), 25–36.

[104] Sztukowski, D. M., Jafari, M., Alboudwarej, H., and Yarranton, H. W. Asphaltene self-association and water-in-hydrocarbon emulsions. *Journal of Colloid and Interface Science 265*, 1 (sep 2003), 179–186.

[105] Tadros, T. Application of rheology for assessment and prediction of the long-term physical stability of emulsions. *Advances in Colloid and Interface Science 108-109* (may 2004), 227–258.

[106] Tadros, T. F. Fundamental principles of emulsion rheology and their applications. *Colloids and Surfaces A: Physicochemical and Engineering Aspects 91* (nov 1994), 39–55.

[107] Tadros, T. F. Emulsion formation, stability, and rheology. In *Emulsion Formation and Stability*. Wiley-VCH Verlag GmbH & Co. KGaA, jan 2013, pp. 1–75.

[108] Tambe, D. E., and Sharma, M. M. The effect of colloidal particles on fluid-fluid interfacial properties and emulsion stability. *Advances in Colloid and Interface Science 52* (sep 1994), 1–63.

[109] Tavares, F. W., and Prausnitz, J. M. Analytic calculation of phase diagrams for solutions containing colloids or globular proteins. *Colloid & Polymer Science 282*, 6 (apr 2004), 620–632.

[110] Taylor, G. I. The viscosity of a fluid containing small drops of another fluid. *Proceedings of the Royal Society A: Mathematical, Physical and Engineering Sciences 138*, 834 (oct 1932), 41–48.

[111] Tchoukov, P., Yang, F., Xu, Z., Dabros, T., Czarnecki, J., and Sjöblom, J. Role of asphaltenes in stabilizing thin liquid emulsion films. *Langmuir 30*, 11 (mar 2014), 3024–3033.

[112] Varadaraj, R., and Brons, C. Molecular origins of heavy oil interfacial activity part 1: fundamental interfacial properties of asphaltenes derived

from heavy crude oils and their correlation to chemical composition. *Energy & Fuels 21*, 1 (jan 2007), 195–198.

[113] Velasco, E., Mederos, L., and Navascués, G. Phase diagram of colloidal systems. *Langmuir 14*, 19 (sep 1998), 5652–5655.

[114] Visser, J. On hamaker constants: A comparison between hamaker constants and lifshitz-van der waals constants. *Advances in Colloid and Interface Science 3*, 4 (dec 1972), 331–363.

[115] Wang, W., Wang, P., Li, K., Duan, J., Wu, K., and Gong, J. Prediction of the apparent viscosity of non-newtonian water-in-crude oil emulsions. *Petroleum Exploration and Development 40*, 1 (feb 2013), 130–133.

[116] Weltmann, R. N., and Green, H. Rheological properties of colloidal solutions, pigment suspensions, and oil mixtures. *Journal of Applied Physics 14*, 11 (nov 1943), 569–576.

[117] Wildemuth, C. R., and Williams, M. C. Viscosity of suspensions modeled with a shear-dependent maximum packing fraction. *Rheologica Acta 23*, 6 (nov 1984), 627–635.

[118] Wu, X., van de Ven, T., and Czarnecki, J. Colloidal forces between emulsified water droplets in toluene-diluted bitumen. *Colloids and Surfaces A: Physicochemical and Engineering Aspects 149*, 1-3 (apr 1999), 577–583.

[119] Yang, X., Verruto, V. J., and Kilpatrick, P. K. Dynamic asphaltene-resin exchange at the oil/water interface: time-dependent w/o emulsion stability for asphaltene/resin model oils†. *Energy & Fuels 21*, 3 (may 2007), 1343–1349.

[120] Yaron, I., and Gal-Or, B. On viscous flow and effective viscosity of concentrated suspensions and emulsions. *Rheologica Acta 11*, 3-4 (sep 1972), 241–252.

[121] Zarkar, S., Pauchard, V., Farooq, U., Couzis, A., and Banerjee, S. Interfacial properties of asphaltenes at toluene–water interfaces. *Langmuir 31*, 17 (apr 2015), 4878–4886.

[122] Zhang, Z., and McClements, D. J. Overview of nanoemulsion properties: stability, rheology, and appearance. In *Nanoemulsions*. Elsevier, 2018, pp. 21–49.

A
Summary of rheological equations for colloidal systems.

Table A.1: Background of rheological equations of suspension

Name	Equation	Type*	Setting parameters	Application	Background	Ref
			Viscosity-concentration equation in dilute range			
Arrhenius (1887)	$\eta_r(\varphi) = \exp(k\varphi)$	T	k	Newtonian behavior and dilute suspension.		[4]
Einstein (1906/1911)	$\eta_r(\varphi) = 1 + [\eta]\varphi$	T	$[\eta] = 2.5$	Dilute suspension and Monodidispere distribution	Stoke low (creeping flow)	[25]
Bredée (1937)	$\eta_r(\varphi) = \left(1 + \frac{2.5\varphi}{6}\right)^6$	E		Synthetic high polymers. Specific applicability	Parameter without physical meaning	[9]
Eilers (1941)	$\eta_r(\varphi) = \left[1 + \frac{k_1\varphi}{2(1-\varphi/\varphi_p)}\right]^2$	E	k_1,φ_p	Emulsões de hidrocarbonetos altamente viscosos	Parameter without physical meaning	[24]
			Viscosity-concentration equation in concentrated range			

* T=Theoretical, E= Empirical

Continued on next page

Table A.1 – *Continued from previous page*

Name	Equation	Type*	Setting parameters	Application	Background	Ref
Welmann (1943)	$\eta(\varphi) = (\eta_0 - k_1)\exp(k_2\varphi)$	E	k_1, k_2	Pigment suspension. Concentrate suspensions.	Based into the Arrhenius equation. First to associate the non-Newtonian behavior to the particle shape, particle size, force of flocculation and the shear rate used.	[116]
Norton (1944)	$\eta(\varphi) = \eta_0(1-\varphi) + k_1\varphi + k_2\varphi^n$	E	k_1 , k_2	Semi-dilute suspension.	Without direct physical significance [89]	[58]
Robinson (1949)	$\eta_r(\varphi) = \dfrac{k\varphi}{(1-S\varphi)}$	E/T	k, S	Concentrated suspension	Introduced the concept free liquid in the suspension.	[89]
Roscoe (1952)	$\eta_r(\varphi) = (1-\varphi_{eff})^{(-5/2)}$	T	$\varphi_{eff} = s\varphi$, s	Semi-dilute suspension and polydispersion system. Does not account the packing of particles for high concentrations [69].	Generalization of Einstein formula utilizing the D-EMT theory [69] and effects of polydispersity [**?**].	[90]
Mooney (1950)	$\eta_r(\varphi) = \exp\left(\dfrac{2.5\varphi}{1-\varphi/\varphi_m}\right)$	E/T	φ_m	Concentrated suspension and polydispersity system	Contemplated the crowding effect of particles [69]	[55]
K-D (1959)	$\eta_r(\varphi) = \left(1-\dfrac{\varphi}{\varphi_m}\right)^{-2.5\varphi_m}$	T/E	φ_m	Spherical and concentrate suspension.	Introduced the concept of a maximum packing. Used D-EMT method	[45]

* T=Theoretical, E= Empirical

Continued on next page

Table A.1 – *Continued from previous page*

Name	Equation	Type*	Setting parameters	Application	Background	Ref
Frankel 1967	$\eta_r(\varphi) = \frac{9}{8}\left[\frac{(\varphi/\varphi_\infty)^{1/3}}{1-(\varphi/\varphi_\infty)^{1/3}}\right]$	T	φ_∞	Concentrated uniform solid spheres	Based on the viscous dissipation in highly concentrated suspensions	[30]
Farris (1968)	$\ln(\eta_r(\varphi)) = \prod_{i=1}^{N}\ln(H(\varphi_i))$	T	$H(\varphi_i) = \frac{\eta_i}{\eta_{i-1}}$	Multimodal suspensions of rigid particles.	Related the $\eta(\varphi)$ of multimodal suspensions to the behavior of the unimodal. Based into Brinkman-Roscoe equation	[28]
Chong (1971)	$\eta_r(\varphi) = 1 + 0.75\left(\frac{\varphi/\varphi_\infty}{1-\varphi/\varphi_\infty}\right)$	E	φ_∞	Concentrated spherical suspension	Investigated the dependence on particle size distributions	[14]
Batchelor (1977)	$\eta_r(\varphi) = 1 + k_1\varphi + K_2\varphi^2$	E	k_1, k_2	Semi-dilute suspension [69])	Based on two-particle hydrodynamic interactions.	[7]
Bicerano (1999)	$\eta_r = \left(1+\frac{\varphi}{\varphi_*}\right)^{-2}\left[1 + C_1\left(\frac{\varphi}{\varphi^*}\right) + C_2\left(\frac{\varphi}{\varphi^*}\right)^2\right]$	T	C_1, C_2 , φ^*	General concentrated dispersion (emulsion)	Based on scaling of critical phenomena [10]. Crossover between Douglas equation and virial expansion equation	[8]
		Viscosity-concentration equation including the shear rate				
Ree-Eyring (1955)	$\eta = \sum_{n=1}^{n}\frac{x_n\beta_n}{\alpha_n}\frac{sinh^-1\beta_n\dot{\gamma}}{\beta_n\dot{\gamma}}x_i$	T	β_n, α_n	General applicability		[88]
Maron-Piere (1956)	$\eta_r(\varphi) = \left(1+\frac{\varphi}{\varphi_m}\right)^{-2}$	T	$\varphi_m = 2/[\eta]$	Newtonian behavior of suspensions. Popularized by Quemada [79]	The concept of effective concentration	[51]

* T=Theoretical, E= Empirical

Continued on next page

Table A.1 – *Continued from previous page*

Name	Equation	Type*	Setting parameters	Application	Background	Ref
Cross (1965)	$\frac{\eta(\dot{\gamma})-\eta_\infty}{\eta_o-\eta_\infty}=\frac{1}{1+\alpha\dot{\gamma}^{2/3}}$	T	α, η_o, η_∞	A wide range of pseudoplastic suspension	A simple statistical random chain formation	[16]
Wildemuth (1984)	$\eta_r(\varphi,\dot{\gamma})=\left(1-\frac{\varphi}{\varphi_m(\dot{\gamma})}\right)^{-[\eta(\tau)]\varphi_m(\dot{\gamma})}$	E/T	$\eta(\tau)$, $\varphi_m(\dot{\gamma})$	Suspensions of rigid spherical particles	Generalization of Krieger-Dougherty. $[\eta]$ and φ_m characterized almost all physical and chemical features of a suspension	[117]
Mills (1985)	$\eta_r(\varphi,\dot{\gamma})=\frac{(1-\varphi_{eff})}{(1-\varphi_{eff}/\varphi^*)^2}$	T	$\varphi_{eff}=f(\dot{\gamma})$ and φ^*	Concentrated suspension of hard spheres.	Based in the Casson's equation and Fractal theory	[54]
Pal (1989)	$\eta_r(\varphi,\dot{\gamma})=\left[1-\frac{0.8415}{\varphi_{\eta_r=100}}\right]^{-2.5}$	E/T	$\varphi_{\eta_{r=100}}$	Non-Newtonian emulsions. Concentrate emulsion	Differential effective medium theory	[74]
Quemada (1997)	$\eta(\varphi,\gamma)=\eta_\infty\left(\frac{1+\gamma/\gamma_C}{\left(\frac{1-\varphi/\varphi_0}{1-\varphi/\varphi_\infty}\right)+\gamma/\gamma_C}\right)$	T	φ_0, γ_C,φ_∞,φ_∞	concentrated dispersions with approximately spherical shape and uniform size	Used the Cross's equation plus effective volume fraction concept introduced by [90]	[81, 82]

Viscosity-concentration equation including deformability of interface (emulsion)

* T=Theoretical, E= Empirical

Continued on next page

Table A.1 – *Continued from previous page*

Name	Equation	Type*	Setting parameters	Application	Background	Ref
Taylor (1932)	$\eta_r(\varphi) = 1 + [\eta]\varphi\frac{\eta_\infty + 3/2\eta}{\eta_\infty + \eta}$	T	$[\eta]$,η_∞	Dilute emulsion and Monodidispere distribution	Deformation of interface	[110]
Oldroyd (1953)	$\eta_r(\varphi) = \left[\frac{10(K+1) + 3\varphi(2+5K)}{10(K+1) - 2\varphi(2+5K)}\right]$	E/T	K	Semi-dilute system. Applicability for both emulsion and suspension.	Used the D-EMT [69]	[59]
Phan-Thien (1997)	$\eta_r^{2/5}\left[\frac{2\eta_r + 5K}{2+5K}\right]^{3/5} = (1-\varphi)^{-1}$	T	$K = \eta_d/\eta_c$	Suspensions of spheres of diverse sizes and multi-component systems	Based on Taylor and addition of infinity volume of the dispersed phase.	[77]
Pal-b (2001)	$\eta_r\left[\frac{2\eta_r + 5K}{2+5K}\right]^{3/2} = \left(1 - \frac{\varphi}{\varphi_m}\right)^{-2,5\varphi_m}$	T	$K = \eta_d/\eta_c$, φ_m	Emulsion with a large range of K and high volume concentration (until φ_m)	Based on crowding effect and D-EMT theory	[68]
	Viscosity-concentration equation for W/O emulsion					
Dan 2006	$\eta_r = (1 - K_e(\gamma,\varphi)\varphi)^{-2.5}$	E/T	$K_e(\gamma,\varphi) = a\varphi^b$	Non-Newtonian water-in-crude oil emulsions	Modification of the Pal (1989) equation.	[18]
Wei (2013)	$\eta_r^{2/5}\left(\frac{\eta_r + 2,5k}{1+2,5k}\right)^{3/5} = \left(1 - K(\varphi)K(N_{Re,p})\varphi\right)^{-1}$	E/T		Non-Newtonian water-in-crude oil emulsions	Modification of the Pal-b (2001) equation.	[115]

* T=Theoretical, E= Empirical

B
Image analyses code

In this appendix, the program to generate the $f(d_p)$ from a microscopic image is detailed. This program was written in MatLab®. A step by step description follows:

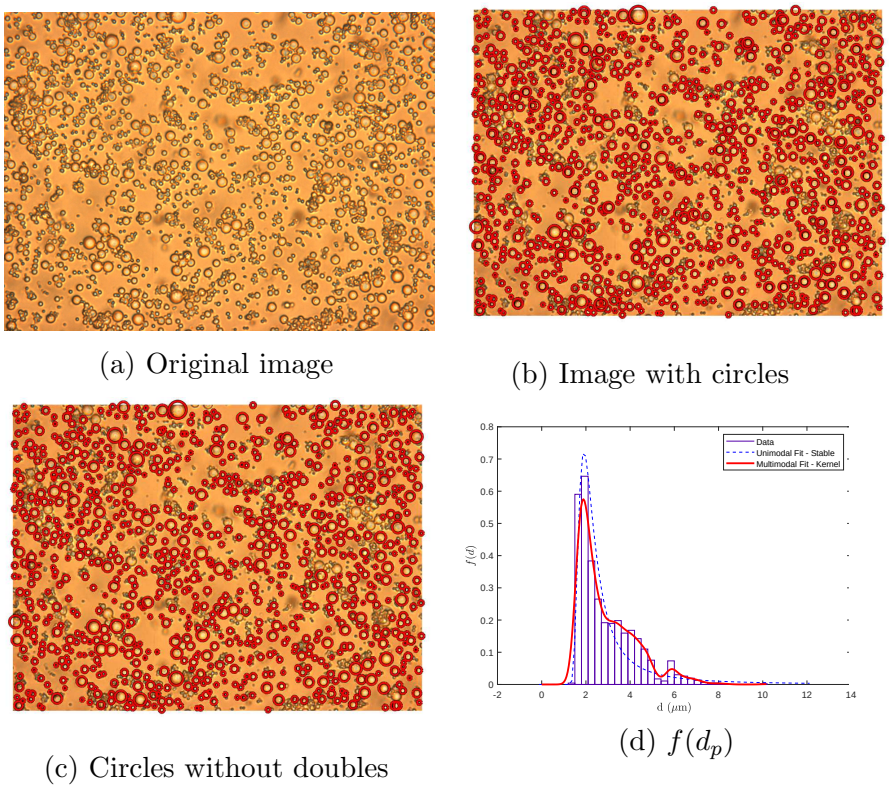

(a) Original image

(b) Image with circles

(c) Circles without doubles

(d) $f(d_p)$

Figure B.1: Step to step of treatment of images

1. The microscopical image of the emulsion is read using the function `imread`. This function reads an image from a graphics file and convert it to an RGB vector (Figure **B.1**a)

2. The `RGB` vector is an input in the function `imfindcircles` . This function finds circles using name-value pairs to control aspects of the Circular Hough Transform. The Sensitivity parameter is specified controlling the detection of the object that has similarity to a circular shape. The `Centers` and `Radii` vectors are output variables (Figure **B.1**b) of this function.

3. Depending on this sensitivity parameter, some problems can appear as a lack of detection of some droplets or the overlap of one droplet with other

droplets. To eliminate the overlap droplets, a searching algorithm to eliminate the duplicate droplets was programmed. The distances between a value from a `Centers` vector and the rest of the Centers values are calculated, later, the radii with a distance smaller than a tolerance criterion are eliminated. As to the lack of detection of higher and smaller droplets, the scale of the image is increased or reduced depending on the problem. If in this step some new radii are detected, these radii are added in the `radii` and its position in the `Centers`.

4. Finally, the histogram of diameters is built using the function `bar` (Figure **B.1**c). The radii are input in the function `fitdist`, and a probability distribution function is fitted to data using the parametric distribution "Kernel" (Figure **B.1**d).

C
Thermodynamic Model

Equilibrium thermodynamic

For the fluid phase and solid phase in equilibrium, the chemical potential and osmotic pressure for both phases should be equal:

$$\mu^{liq} = \mu^{sol} \tag{C-1}$$

$$p^{liq} = p^{sol} \tag{C-2}$$

The pressure equilibrium condition according to the compressibility factor (Z) definition can be redefined as:

$$Z^{liq}\varphi^{liq} = Z^{sol}\varphi^{sol} \tag{C-3}$$

Perturbation theory was used for the calculation of thermodynamic properties [100]. The equation is a formal power series expression in which the degree of solution exactitude will depend on the higher-order terms. A Barker–Henderson perturbation theory of first-order approximation was used [100]. The method consists in breaking the problem into two parts: the reference part and the perturbation part.

$$\frac{A}{Nk_BT} = \frac{A^{Ref}}{Nk_BT} + \frac{A^{Pert}}{Nk_BT} \tag{C-4}$$

Where A is the Helmholtz energy, k_B is the Boltzmann constant value, N is the particle number and T is the temperature. According to their thermodynamic definitions, the compressibility factor (Z) and the chemical potential (μ) are given by:

$$Z = \rho\left(\frac{\partial\left(A/Nk_BT\right)}{\partial\rho}\right)_{T,N} = Z^{ref} + Z^{Pert} \tag{C-5}$$

$$\frac{\mu}{k_BT} = \left(\frac{\partial\left(A/Nk_BT\right)}{\partial N}\right)_{V,T} = \frac{A}{Nk_BT} + Z = \frac{\mu^{Ref}}{k_BT} + \frac{\mu^{Pert}}{k_BT} \tag{C-6}$$

To calculate the reference term from equation C-4, the hard-sphere model approximation was used. A^{ref} is:

$$\frac{A^{ref}}{Nk_BT} = \frac{A^{id}}{Nk_BT} + \int_0^{\varphi^*} (Z^{ref} - 1)\frac{d\varphi^*}{\varphi^*} \tag{C-7}$$

Z^{ref} is defined as:

$$Z^{ref} = \frac{1 + \varphi^* + \varphi^{*2} - \varphi^{*3}}{(1 - \varphi^*)^3} \tag{C-8}$$

Where the effective fraction volume (φ^*) is the corrected fraction volume. This correction consists in using the soft sphere diameter (d_{sp}) instead of hard sphere diameter (d_p) [86]. A dimensionless effective hard-sphere diameter can be calculated by $d^* = d_{sp}/d_p$. The d^* and φ^* are given by the following expressions:

$$d^* = 1 + \int_{Rs}^{\infty} \left(1 + \exp\left[-\frac{U^{ref}}{k_BT}\right]\right) dv \tag{C-9}$$

$$\varphi^* = \frac{\pi\rho d^{*3}}{6} \tag{C-10}$$

Where U_x^{ref} is the reference term of potential interaction. In order to calculate the ideal contribution, the ideal gas approximation was applied. Its thermodynamic properties were calculated by the Carnaham-Starling equation of state [100].

$$\frac{A^{id}}{Nk_BT} = 3\ln\Lambda + \ln\rho - 1 \tag{C-11}$$

If A^{id} is expressed as function of φ^*, the equation remains:

$$\frac{A^{id}}{Nk_BT} = 3\ln\left(\frac{6\Lambda^3\varphi^*}{\pi d^{*3}}\right) - 1 \tag{C-12}$$

Where Λ is the Broglie wavelength that it is defined:

$$\Lambda = \left(\frac{2\pi m k_BT}{h^2}\right)^{-1/2} \tag{C-13}$$

Where $m = (Ma/Na) * 1000$ is the mass of water particle, Na is the Avogadro number and h is the Plank constant. Also, the integral term can be written as:

$$I = \frac{4\varphi^* - 3\varphi^{*2}}{(1-\varphi^*)^2} \tag{C-14}$$

Hence, equation C-7 can be rewritten as:

$$\frac{A^{ref}}{Nk_BT} = \ln\left(\frac{6\Lambda^3\varphi^*}{\pi {d_p}^3}\right) - t\frac{4\varphi^* - 3\varphi^{*2}}{(1-\varphi^*)^2} \tag{C-15}$$

On the other hand, the perturbation term (A^{Pert}) is defined as:

$$\frac{A^{Pert}}{Nk_BT} = \frac{12\varphi}{k_BT}\int_0^\infty U_x^{pert}(x)g_x(x)x^2dx \tag{C-16}$$

Where $g_x(x)$ is the radial distribution function, its calculation theory will depend on the phase that it should be applied (e.g. Solid or liquid). From equation C-5, the perturbation term (Z^{pert}) can be calculated according to:

$$Z^{pert} = \varphi\frac{\partial}{\partial\varphi}\left(\frac{A^{pert}}{Nk_BT}\right)\frac{1}{T^*} \tag{C-17}$$

Therefore, substituting C-16 into the previous equation, one can obtain:

$$Z^{pert} = \frac{12\varphi}{k_BT}\left(I + \varphi\frac{\partial I}{\partial\varphi}\right) \tag{C-18}$$

Total interation potential energy ($U_x(x)$)

Experimentally, it has been proven that the forces present in W/O emulsions are due to attractive dispersion (Hamaker) and repulsive steric interactions [118]. Therefore, the main interaction is random Brownian motion. Using these considerations, the total interaction potential between water droplets can be determined by

$$U(x) = U_S(x) + U_H(x) = U^{ref} + U^{Pert} \tag{C-19}$$

Where $U_S(x)$ is the steric repulsive potential and $U_H(x)$ is the attractive potential or also called Hamaker potential. All of these energies depend on the reduced center-to-center distance, defined as the relation between the center-to-center droplet distance (h) and the droplet diameter (d_p).

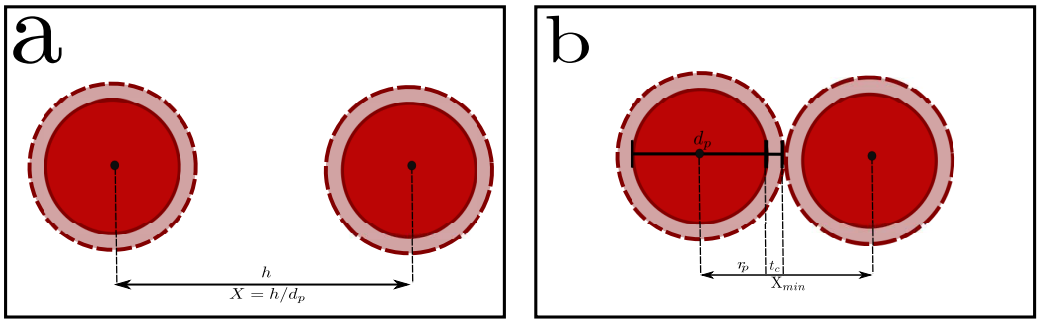

Figure C.1: a. The reduced center-to-center distance and b. Minimum droplet distance

[118] showed that water droplets dispersed in toluene are stable as a consequence of the steric repulsion between the adsorbed layers on the droplet surfaces. The steric interactions between hydrophobic parts were observed. A W/O emulsion resembles polymer-polymer iterations. The empirical equation proposed by [118] to determine $U_S(x)$ was:

$$U_S(x) = \frac{c}{6(x-1)^6} \tag{C-20}$$

The parameter c can be determined through minimization of the total potential $(U_H + U_S)$ when two undeformed drops have minimum separation distance $(x_{min} = 1 + 2t_c/d_p)$ (For more details see [87]).

$$c = \frac{(x_{min}-1)^7 A_H}{6}\left(\frac{x_{min}}{(x_{min}^2-1)^2} + \frac{1}{x_{min}^3} - \frac{2}{x_{min}(x_{min}^2-1)}\right) \tag{C-21}$$

The Lefshitz theory is a good approximation to calculate the Hamaker constant. The Litshitz-van der Waals theory is based on the bulk properties, i.e., macroscopic properties, for instance, optical data. [114]

$$A_H = \frac{3}{4}k_B T\left(\frac{\varepsilon_w - \varepsilon_o}{\varepsilon_w + \varepsilon_o}\right)^2 + \frac{3h\nu_c}{16\sqrt{2}}\frac{(n_w^2 - n_o^2)^2}{(n_w^2 - n_o^2)^{3/2}} \tag{C-22}$$

The Hamaker potential is found using the follow equation.

$$U_H(x) = -\frac{A_H}{12}\left(\frac{1}{(x^2-1)} + \frac{1}{x^2} + 2\ln\left(\frac{x^2-1}{x^2}\right)\right) \tag{C-23}$$

Sea water phase properties

[38] demonstrated that the dielectric properties of seawater can be determined by its chlorinity only. The values are substantially different from those of the $3,35wt\%$ NaCl solution, which has been taken frequently as a model for seawater. All the parameters necessary for the calculation of this property were calculated by linear fitting the experimental data presented in this article.

$$A_1 = 6.017e^{-3} + 5.027e^{-6}\left((T - 273.15) - 5.5)\right) \tag{C-24}$$

For any temperature, dielectric properties for distillate water were found as being

$$e_{wd} = 80.52 - 0.1894\left((T - 273.15) - 5.5)\right) \tag{C-25}$$

The sea salinity for the system was $s = 38.89\%$. Consequently, the chlorinity was equal to $x_{Cl} = 21.07$.

$$x_{Cl} = (s - 0.03)/1.805 \tag{C-26}$$

The sea permittivity was calculated by:

$$e_w = \frac{1 + (e_{wd} - 1)}{1 + A_1 x_{Cl}} \tag{C-27}$$

And the reflective index (A_1) of sea water [97].

$$n_w = 1.33455 - 4.50249e^{-5}\left(T - 273.15)\right) - 1.16002e^{-6}\left(T - 273.15\right)^2 \tag{C-28}$$

Oil phase properties

[34] measured the properties for different °API values. All the necessary properties were taken from this reference. For an oil with 33 ° API, the n_o was equal to 6 and e_o to 1.487. All of these properties were assumed at constant temperature $(20°\text{C})$.

Radial distribution function $g_x(x)$

For the liquid phase, $g(x)^{liq}$ was determined by the equation proposed by [12]. This is a analytic approximation for hard-sphere. A radial distribution function of liquid phase $(g(x)^{liq})$ was shown in Figure **C.2**.

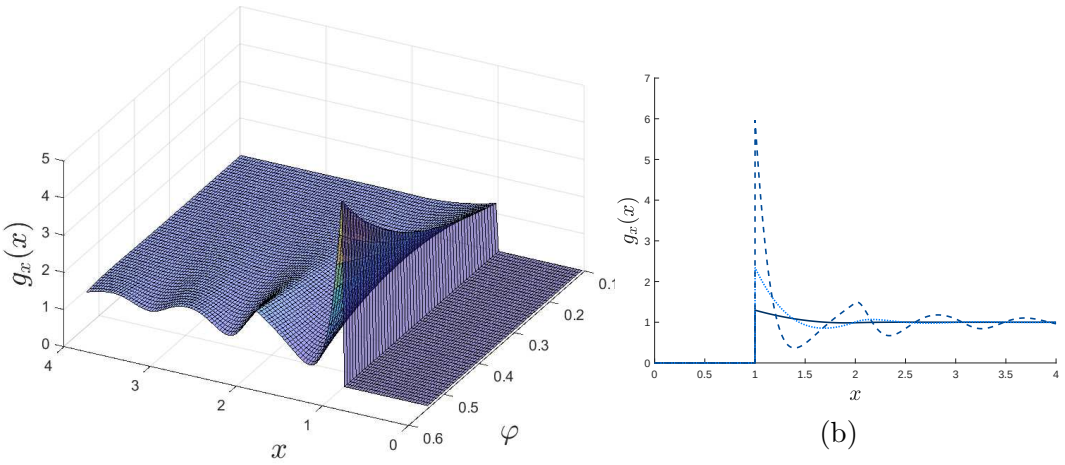

(a) (b)

Figure C.2: A radial distribution function of liquid phase $(g(x)^{liq})$. (b)$\varphi = 10\%$ ——, $\varphi = 30\%$ ···, $\varphi = 54\%$ - - -)

The difference between the reference model [96] and this model was the $g(x)^{sol}$ calculation. The solid phase is calculated with the equation published in [44]. A radial distribution function for the solid phase $(g(x)^{sol})$ is shown in Figure **C.3**

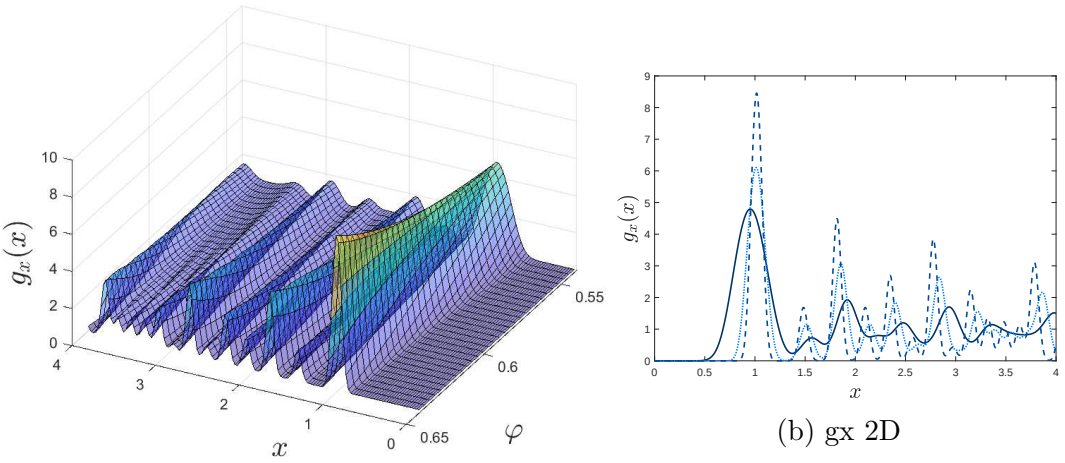

(a) gx 3D (b) gx 2D

Figure C.3: A radial distribution function of solid phase $(g(x)^{sol})$. (b)$\varphi = 54\%$ ——, $\varphi = 60\%$ ···, $\varphi = 64\%$ - - -)

Finally, the algorithm to determine φ for each phase in equilibrium is presented in Figure **C.4**

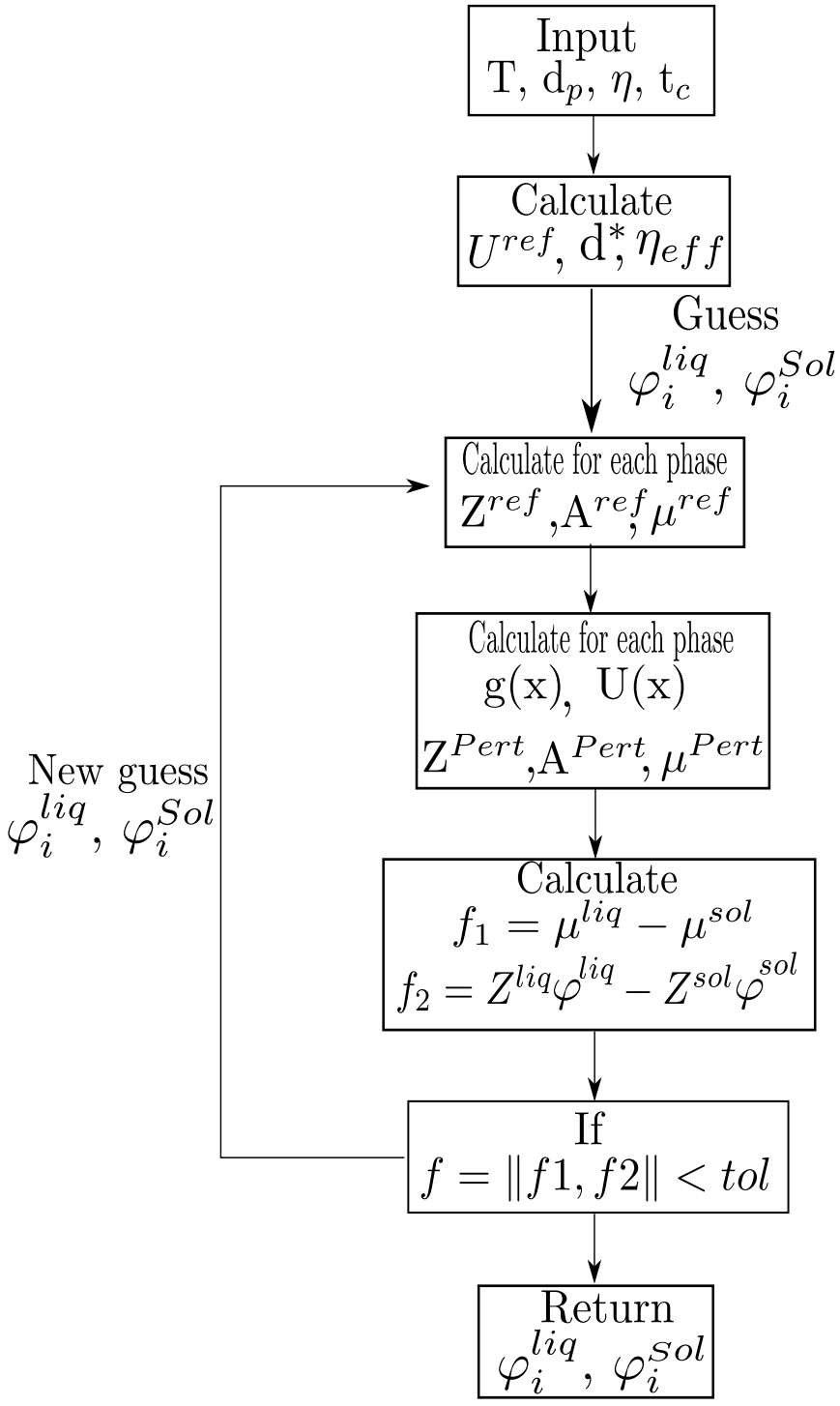

Figure C.4: Algorithm for the calculation of thermodynamic equilibrium for W/O emulsion system.

D
Clustering aggregation program

In this appendix, the pseudo-code for the calculation approximate of a cluster's size and shape and the number of droplets that belong to each cluster is detailed. In general terms, the program analyzes the centers and radii vectors generated by the Images analyses code shown in Appendix B or by the `rand` function of MatLab. *rand* function creates random positions of circles of mono-disperse sizes. For the example shown in Chapter 5, the polydisperse system was built with the sum of two monodisperse distributions of a specific droplet number. These radii and centers vectors are the input in the `aggregation` function. The program evaluates the droplet-droplet distance to determine which of them belong to the same cluster. It initially locales the cluster nucleus and afterwards finds all its droplet branches. For the search, the distance between one droplet and the other droplets is calculated by the equation

$$distance = \sqrt{(x(i) - x(:))^2 + (y(i) - y(:))^2} \tag{D-1}$$

The distance vector is compared with a specified minimum criterion . This criterion is calculated by

$$criterion = radii(i) + radii + dist\_lim \tag{D-2}$$

The distance limit is an arbitrary value given as a minimum distance between two droplets in addition to each of their radii can be considered as belonging to the same cluster. The pseudo-code was presented below.

```
input center, radii, limt_dist
% radii = [r1, r2, ..., rn]
% center = {(x1,y1),(x2,y2),...(xn,yn)}
cont = 1
flag = 0
for ri in radii do:
  if ri is r1
     calculate distances between ri and rj with i =! j
     go to 16
  else
```

```
11      if ri not in cluster{cont-1}
12         calculate distances between ri and rj with i =! j
13         go to 16
14      else
15         go to 6
16   find distances <= criterion
17   if distances is empty
18     cluster{cont} = position i % cluster of size one
19   else
20     cluster{cont} = [position i, positions_in_distances]
21     new_positions = positions_in_distances
22     cont_aux = 1
23     while cont_aux <= len(new_positions)
24       position = new_positions(cont_aux)
25       calculate distances between ri(position) and rj
26                                      with position =! j
27       find distances <= criterion
28       if position in distances not in cluster{cont}
29          add position in cont_aux
30       cont_aux = cont_aux + 1
31       go to 23
32   cont = cont +1
33   go to 6
34 return cluster
35 % number of droplet per cluster
36 for cluster in clusters
37    number = len(cluster)
38    save number
```

E
Rheology modeling algorithms

Algorithm for KD's equation

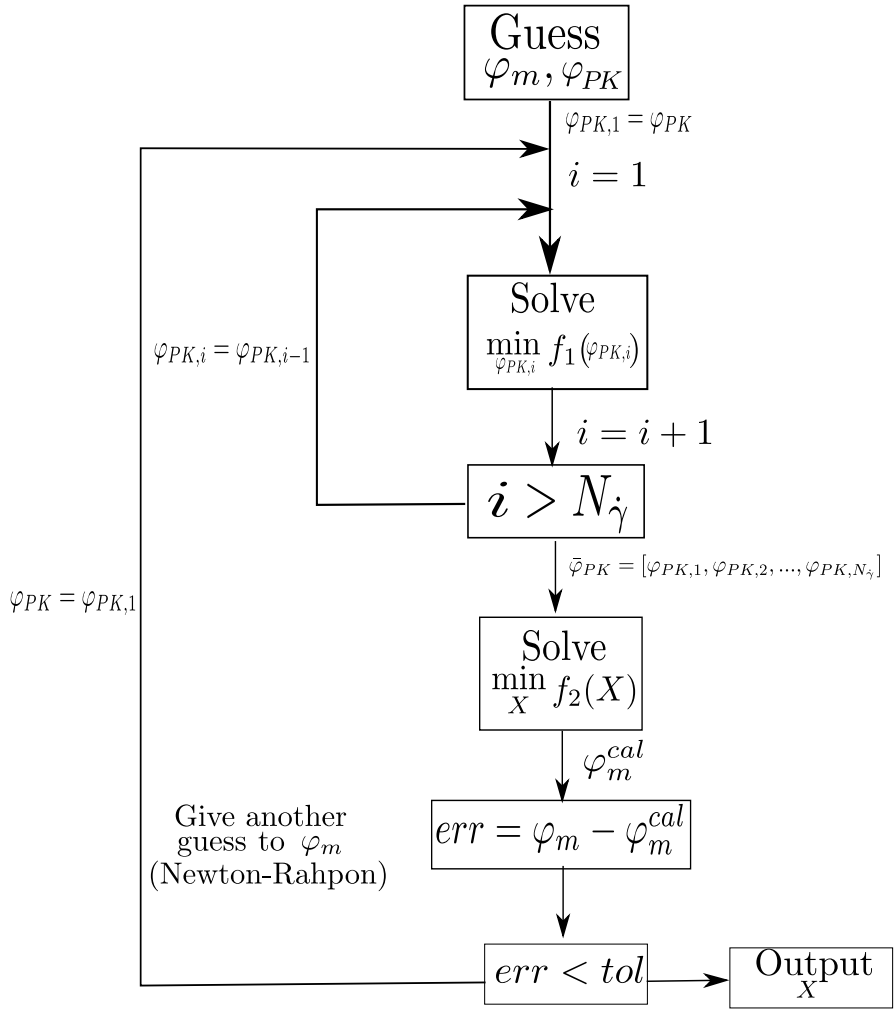

Figure E.1: Solution algorithm of KD equation by generalized methodology

Algorithm for Sudduth's equation

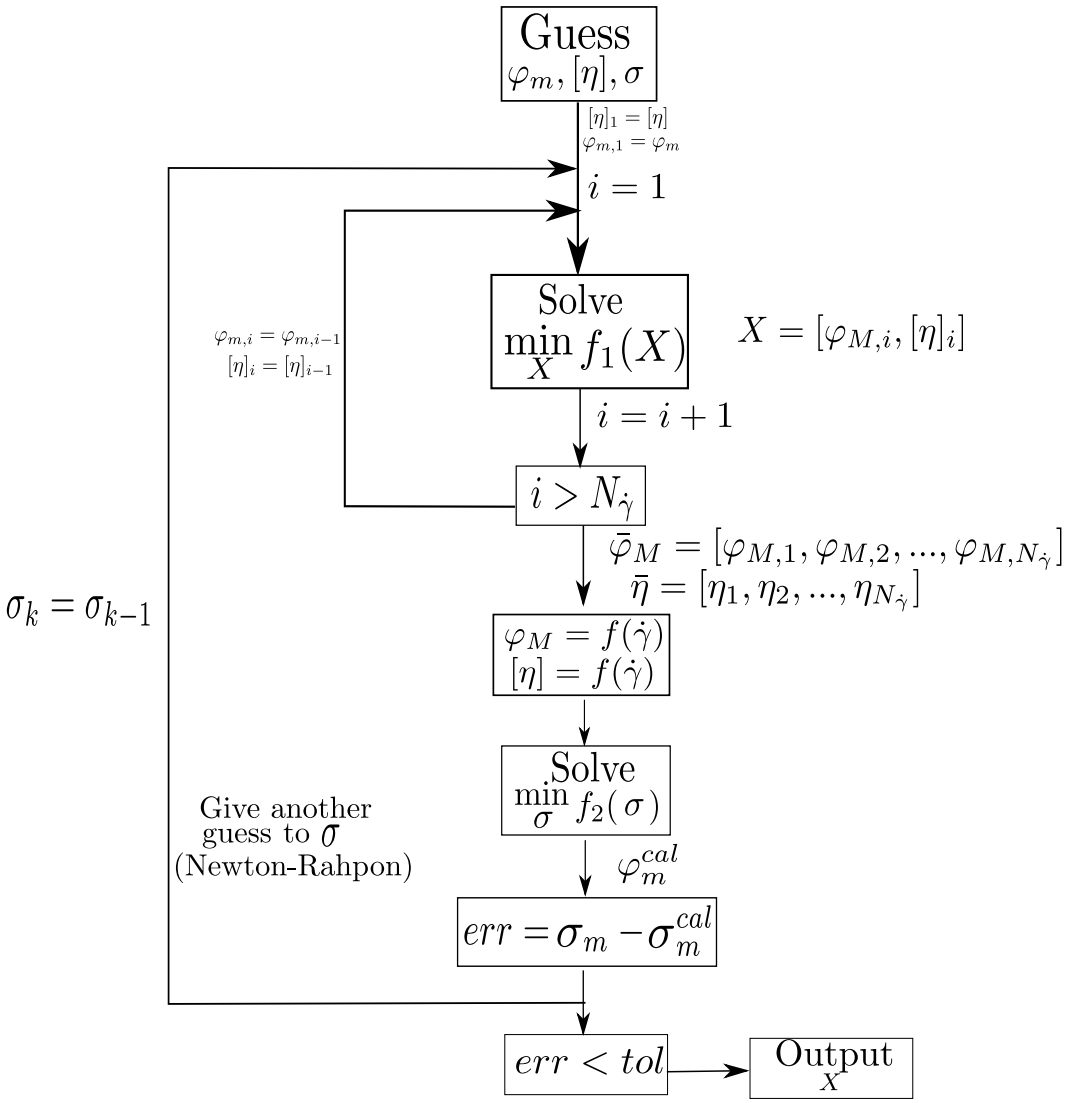

Figure E.2: Solution algorithm of KD equation by generalized methodology

Table E.1: Sudduth's fitting parameters

Emulsion	f^1			f^2			σ
	a	b	c	a	b	c	
A	-0.0219	0.2330	3.8847	0	0.0001	0.6891	0.45
B	0.0001	-0.0072	3.6417	0	0.0010	0.6389	0.36